Geochemistry, Geophysics, Geosystems

RESEARCH ARTICLE
10.1029/2018GC007863

Latitude Dependence of Geomagnetic Paleosecular Variation and its Relation to the Frequency of Magnetic Reversals: Observations From the Cretaceous and Jurassic

Pavel V. Doubrovine[1], Toni Veikkolainen[2], Lauri J. Pesonen[3], Elisa Piispa[4], Siim Ots[5], Aleksey V. Smirnov[6], Evgeniy V. Kulakov[1], and Andrew J. Biggin[7]

[1]Centre for Earth Evolution and Dynamics, University of Oslo, Norway, [2]Department of Geosciences and Geography, University of Helsinki, Finland, [3]Physics Department, University of Helsinki, Finland, [4]School of Geological Sciences and Engineering, Yachay Tech, Ibarra, Ecuador, [5]Department of Geology, University of Tartu, Estonia, [6]Department of Geological and Mining Engineering and Sciences, Michigan Technological University, Houghton, MI, USA, [7]Department of Earth, Ocean and Ecological Sciences, University of Liverpool, UK

Key Points:
- Estimates of geomagnetic paleosecular variation (PSV) in Cretaceous and Jurassic time were derived using a new paleomagnetic database
- Different PSV latitude patterns were observed for periods of stable geomagnetic polarity (84–126 Ma) and frequent reversals (126–198 Ma)
- Comparison with the PSV behavior for the last 10 Ma indicates that its latitude dependence is not a reliable proxy for reversal frequency

Supporting Information:
- Supporting Information S1
- Table S1
- Table S2
- Table S3
- Table S4
- Table S5

Correspondence to:
P. V. Doubrovine,
paveld@geo.uio.no

Citation:
Doubrovine, P. V., Veikkolainen, T., Pesonen, L. J., Piispa, E., Ots, S., Smirnov, A. V., et al. (2019). Latitude dependence of geomagnetic paleosecular variation and its relation to the frequency of magnetic reversals: Observations from the Cretaceous and Jurassic. *Geochemistry, Geophysics, Geosystems*, *20*, 1240–1279. https://doi.org/10.1029/2018GC007863

Received 27 JUL 2018
Accepted 29 JAN 2019
Accepted article online 31 JAN 2019
Published online 1 MAR 2019

Abstract Nearly three decades ago paleomagnetists suggested that there existed a clear link between latitude dependence of geomagnetic paleosecular variation (PSV) and reversal frequency. Here we compare the latitude behavior of PSV for the Cretaceous Normal Superchron (CNS, 84–126 Ma, stable normal polarity) and the preceding Early Cretaceous-Jurassic interval (pre-CNS, 126–198 Ma, average reversal rate of ~4.6 Myr^{-1}). We find that the CNS was characterized by a strong increase in the angular dispersion of virtual geomagnetic poles (VGPs) with latitude, which is consistent with the results of earlier studies, whereas the VGP dispersion for the pre-CNS period was nearly invariant with latitude. However, the PSV behavior for the last 5 or 10 million years (average reversal frequency of ~4.4–4.8 Myr^{-1}) shows that the latitude invariance of VGP scatter cannot be considered as a characteristic feature of a frequently reversing field and that a strong increase in VGP dispersion with latitude was not restricted to the long periods of stable polarity. We discuss models describing the latitude dependence of PSV and show that their parameters are not reliable proxies for reversal frequency and should not be used to make inferences about the geomagnetic field stability. During the pre-CNS interval, the geodynamo may have operated in a regime characterized by a high degree of equatorial symmetry. In contrast, more asymmetric geodynamos suggested for 0–10 Ma and the CNS were evidently capable of producing a very wide range of reversal frequencies.

Plain Language Summary In the geologic past, the changes in the Earth's magnetic field have led to numerous polarity reversals, causing the field directions over the entire Earth to be opposite to those observed today. More subtle changes during periods of stable field polarity are referred to as "secular variation." It is widely thought that the manner in which secular variation changes with geographic latitude provides an indirect way of assessing the field stability with regard to its propensity to reverse. Here we derived estimates of paleosecular variation (PSV) for a long interval of stable polarity in the Cretaceous (84–126 Ma) and the preceding Early Cretaceous-Jurassic interval (126–198 Ma), during which geomagnetic reversals were frequent. We found that the latitude behavior of PSV during these two intervals was significantly different, but the comparison with PSV estimates for the last 5 and 10 million years showed that a strong latitude dependence of PSV, or its invariance with latitude, cannot be considered as a characteristic feature of a stable or frequently reversing field. Our analysis suggests that models describing the latitude dependence of PSV do not provide reliable proxies for reversal frequency and should not be used to make inferences about the geomagnetic field stability.

1. Introduction

Paleosecular variation (PSV) of the geomagnetic field is a term broadly used to describe the temporal and spatial changes of the field taking place over time scales ranging from hundreds to millions of years. The main planetary magnetic field of the Earth is generated internally by convective motions in the outer liquid core, which are capable of acting as a self-exciting magnetic dynamo (e.g., Merrill et al., 1998)—a process commonly referred to as the geodynamo. It is well established from paleomagnetism, records of magnetic

stratigraphy, and analyses of marine magnetic anomalies that the dominantly dipolar magnetic field of the Earth has undergone numerous polarity reversals over the geologic past (e.g., Gradstein et al., 2012; Opdyke & Channell, 1996). While the dynamo theory has no difficulty in accommodating both the normal (similar to that observed today) and reverse (opposite) polarity states, and numerical simulations of Earth-like dynamos have been capable to reproduce field reversals and significant departures from axial dipolarity known as geomagnetic excursions (e.g., Glatzmaier et al., 1999; Glatzmaier & Roberts, 1995), the underlying dynamics is not yet clearly understood. Conceptually, geomagnetic reversals can be viewed as natural outgrowths of "runaway" secular variation (e.g., Biggin, van Hinsbergen, et al., 2008; Gubbins, 1994), although it cannot be ruled out that they may be related to some exceptional events triggered by internal instabilities in the fluid motion of the core. Nevertheless, there is a general consensus that the long-term trends in the occurrence of geomagnetic reversals, PSV behavior, and morphology and intensity of the field should be intrinsically linked as they originate from the same geodynamo process (e.g., Aubert et al., 2010; Tarduno et al., 2002).

One of the most interesting features of the reversal record is the observation that the frequency of polarity switches varied substantially on time scales of tens to hundreds of millions of years, with long periods of frequently reversing field sporadically punctuated by compatibly long intervals of stable polarity, where geomagnetic reversals were extremely rare or absent. Two periods of long-term stability of the geodynamo with regard to its propensity to reverse have been documented in the Phanerozoic: a long interval of normal polarity that spanned most of Cretaceous time named the Cretaceous Normal Superchron (CNS, 84–126 Ma; Ogg, 2012) and a similarly long period of dominantly reverse polarity in Late Carboniferous and Permian time (~262–318 Ma) known as the Permo-Carboniferous Reverse Superchron (PCRS), or the Kiaman Reverse Superchron (Opdyke & Channell, 1996). At the other extreme, field reversals were unusually frequent during the Jurassic interval of "magnetic hyperactivity" (~155–171 Ma) where the average reversal rate peaked at ~11 reversals per Myr (Myr^{-1}; Ogg, 2012). The remaining Cenozoic-Mesozoic times were characterized by less frequent reversals (generally, ~2–3 Myr^{-1}), which is still in a stark contrast with the "magnetically quiet" periods of the two superchrons.

Many attempts have been made to establish characteristic long-term signatures of the reversal frequency that could be observed in the paleomagnetic record, including variations in the field intensity and the behavior of PSV (e.g., Biggin, van Hinsbergen, et al., 2008; McFadden et al., 1991; Tarduno et al., 2001, 2002). The motivation behind these efforts has both pragmatic reasons and a fundamental value. On the one hand, if we would be able to define such signatures for the Cenozoic and Mesozoic, where the reversal chronology can be constrained with greater confidence from studies of magnetostratigraphy and patterns of marine magnetic anomalies (e.g., Ogg, 2012), these findings could be used to assess the stability of geodynamo during the earlier Paleozoic and Precambrian times where the reversal record is patchy, ambiguous, or lacking altogether (e.g., Biggin, Strik, et al., 2008; de Oliveira et al., 2018; Smirnov & Tarduno, 2004; Smirnov et al., 2011; Veikkolainen & Pesonen, 2014). On the other hand, the information about the field stability and its relations to paleomagnetic observables may provide us with deeper insights into the questions surrounding the long-term evolution of the geodynamo, changes in the thermal state of the mantle and the core, and the control of the lower mantle heterogeneities on the core-mantle heat flux (Aubert et al., 2010; Biggin et al., 2012, 2015; Smirnov et al., 2017). This has further implications for the future development of numerical models that would be capable to better reproduce the geodynamo process (e.g., Aubert et al., 2010).

Numerous studies have suggested a negative correlation between the average intensity of the geomagnetic field and the reversal frequency (e.g., Aubert et al., 2010; Biggin et al., 2012; Sprain et al., 2016; Tarduno et al., 2001, 2002; Tarduno & Cottrell, 2005; Tauxe & Staudigel, 2004). Yet, the implied relationship is subtle, allowing only very general conclusions about the tendency of the geodynamo to reverse during the periods of higher or lower field intensity (Kulakov et al., 2018).

Substantial efforts have also been put into investigating the potential link between PSV and the reversal frequency. Among those, the study of McFadden et al. (1991), who analyzed statistical properties of PSV derived from rapidly cooled igneous rocks (lavas) for the last 195 Ma, was the most influential and showed great promise in that it suggested a strong relationship between the reversal frequency and the dispersion of virtual geomagnetic poles (VGPs) derived from paleomagnetic directions and considered as a function of latitude. Later work by Tarduno et al. (2002), and most recently by Biggin, van Hinsbergen, et al. (2008), partly confirmed the findings of McFadden et al. (1991), and yet showed that a clear-cut relationship

suggested by the earlier study may not be as clear after all. Biggin, van Hinsbergen, et al. (2008) found that the low VGP dispersion at low latitudes and its strong increase with latitude during the CNS, which had been suggested to be a signature of long periods of stable polarity (Merrill & McFadden, 1988), were not as prominent as those observed in the PSV estimates of McFadden et al. (1991). Highly scattered PSV estimates for the Jurassic (145–200 Ma), a period during which the average frequency of geomagnetic reversals was high (~5 Myr^{-1}), did not allow Biggin, van Hinsbergen, et al. (2008) to establish whether the latitude dependence of VGP dispersion was distinctly different from that observed for the CNS as it was not clear what the latitude pattern of VGP dispersion in the Jurassic actually was. These results warrant obtaining better constraints on the PSV behavior in the Jurassic to test whether a consistent latitude pattern can be defined for this time interval.

In this study, we will present an updated database of paleomagnetic directions and VGPs for the Cretaceous and Jurassic that has been compiled from the literature (section 2) and use these data to define the patterns of latitude dependence of PSV for the two periods of dramatically different reversal frequency, namely, the CNS (84–126 Ma, average reversal frequency is ~0.05 Myr^{-1} according to the geomagnetic polarity time scale of Ogg, 2012, that includes one short reverse polarity interval [chron M-1r] within the CNS) and the preceding Early Cretaceous-Jurassic time interval (pre-CNS, 127–198 Ma, average reversal frequency of ~4.6 Myr^{-1}). In section 3, we will describe the methodology used in our analysis for estimating PSV and modeling its latitude dependence. In section 4, we will present the results and compare the latitude patterns of PSV for the CNS and pre-CNS periods. In section 5, we will compare our findings with the results of the earlier studies (Biggin, van Hinsbergen, et al., 2008; Cromwell et al., 2018; de Oliveira et al., 2018; Johnson et al., 2008; McFadden et al., 1991; Opdyke et al., 2015) and discuss how the latitude patterns of PSV relate to the average reversal frequency, what they can tell us about the morphology of the geomagnetic field in the past, and whether they can be considered as reliable indicators of the geodynamo stability. In section 6, we will provide a brief summary of our results and conclusions.

2. Sources of Data

Unlike nearly continuous records of secular variation provided by geomagnetic observatories for the last few hundred years, estimates of PSV for the geologic past rely on paleomagnetic analyses that most commonly yield temporally disjointed observations of the magnetic field. Rapidly cooled igneous rocks are typically considered to be the most reliable magnetic recorders (e.g., McFadden et al., 1988), but each individual cooling unit can only provide us with an instantaneous "spot reading" of the field. In contrast, sediments and slowly cooled plutonic rocks will tend to average out secular variation to some extent, and the PSV signal will be at least muted or at worst completely lost in the paleomagnetic data. This limits PSV analysis to the data obtained from extrusives and shallow intrusions, while those from sediments and deep intrusives are generally considered not suitable for it. The former, however, never provide uniform sampling of time, which further limits the analysis to the use of statistical measures of PSV that will be described in section 3.

In this study, we compiled an updated database of paleomagnetic directions from the literature published up to and including year 2017, covering the time interval from 198 to 74 Ma. Although the main focus of our analysis was a comparison between the CNS (84–126 Ma) and the preceding Early Cretaceous-Jurassic interval (127–198 Ma), we chose to complement our compilation with data from a younger time interval (74–84 Ma) to test whether there is a discernable change in the behavior of PSV that could signal the end of the CNS. This interval corresponds to the second and third longest polarity intervals in the Cenozoic and Mesozoic (chrons C33n and C33r, Ogg, 2012), which led Lowrie and Kent (2004) to suggest that they may have closer affinity to the CNS than to the rest of the polarity sequence.

Only data from igneous, rapidly cooled rocks (extrusive rocks and shallow intrusions, including lava flows, dykes, sills, and tuffs) were included in the database. Data from plutonic and sedimentary rocks were not considered because, as noted above, they are known to be prone to partial averaging of secular variation, and the data from sedimentary rocks can also be affected by inclination shallowing (e.g., Tauxe & Kent, 2004). Following the approach of Biggin, van Hinsbergen, et al. (2008), paleomagnetic data from rocks of similar age sampled at nearby geographic locations, which often belonged to the same rock formation, were combined into data sets (Figure 1). Each data set is a collection of site-mean directions of the characteristic

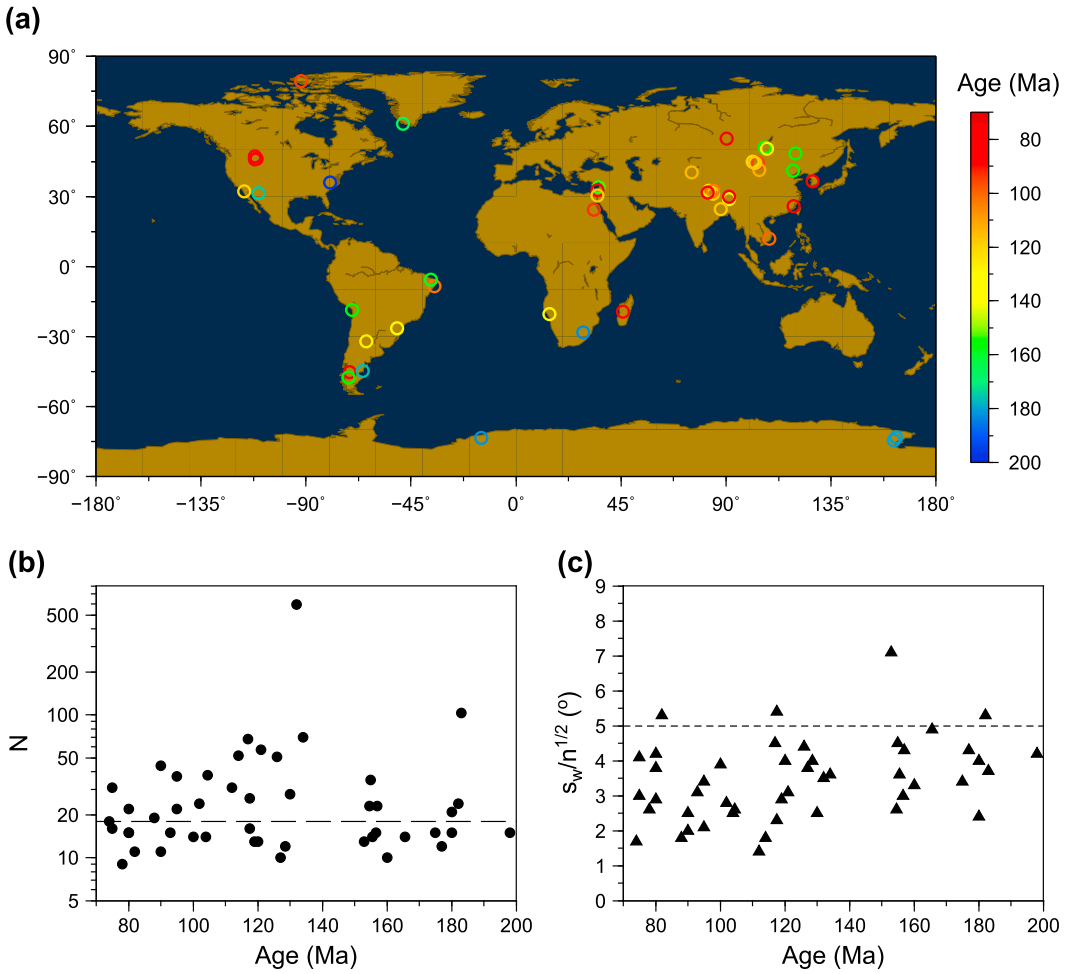

Figure 1. (a) Geographic locations of igneous formations from which the paleomagnetic data were collected; symbols are color-coded according to the nominal age (Table 1). (b) Number of individual site-mean data (N) for all data sets. The long-dashed line shows the median value of N. (c) Average values of within-site dispersion of paleomagnetic directions ($s_w/\sqrt{n}$). The short-dashed line corresponds to the upper limit (5°) for $s_w/\sqrt{n}$ below which the correction of robust paleosecular variation estimates (S') for within-site dispersion does not introduce a significant bias into the latitude dependence of S' (see section 3.1.5).

remanent magnetization (ChRM) and corresponding VGPs. The site-mean directions are Fisher averages (R. Fisher, 1953) of ChRM directions obtained from individual samples. From here on we will use the term "site" to refer to a single cooling unit rather than a distinct sampling location, so that each site-level datum can be treated as an instantaneous record of the geomagnetic field. In our nomenclature, the site stands either for a single igneous unit (e.g., a single lava flow), or several units formed over a short burst of magmatic activity and showing no discernable differences in paleomagnetic direction (e.g., several consecutive lava flows extruded so rapidly that they recorded essentially the same direction of the magnetic field). The collection of site-level data was necessary to ensure the internal consistency of the analysis, that is, it was our intention to derive PSV estimates using the same analytical procedures (section 3) for all individual data sets.

To ensure that low-quality data would not be included in our compilation, the papers that could be potentially used as data sources were carefully examined and all data sets were ranked according to the Van der Voo (1990) quality criteria. For a data set to be included in the compilation, we required the total Q score, based on the first six Van der Voo criteria (Q_{1-6}), to be equal to or greater than three. The seventh criterion (dissimilarity of the mean pole with poles of younger age) was not used for the reasons discussed by Veikkolainen et al. (2014) and Pivarunas et al. (2018). We further applied the following selection criteria:

1. The age of the rock formation must be reasonably well constrained, preferably by radiometric dates, so that the data set can be unambiguously allocated as representing the magnetic field during the CNS or the intervals with higher reversal rates preceding or following the superchron.
2. There must be no evidence that the ChRM directions record secondary magnetic overprints. No data from rocks suspected to be remagnetized were included.
3. Data from igneous formations that were tectonically folded or tilted after their emplacement must be structurally corrected (restored to paleohorizontal). Data from areas that may have been affected by uncertain post-emplacement tilting and those showing evidence for local block rotations between the sampling sites were not used.
4. Following the earlier studies of PSV for the Mesozoic, Paleozoic, and Precambrian (Biggin, van Hinsbergen, et al., 2008; Biggin, Strik, et al., 2008; de Oliveira et al., 2018; Smirnov et al., 2011; Veikkolainen & Pesonen, 2014), we required each data set to comprise paleomagnetic directions from at least nine sites ($N \geq 9$ independent spot readings of the magnetic field), and each site-mean direction to be based on ChRM directions from at least three independent samples ($n \geq 3$). We will discuss the influence of imposing stricter criteria (higher minimum values of N and n) on the estimates of latitude dependence of PSV in section 4.
5. The ChRM components must have been isolated using stepwise demagnetization techniques. Unlike Smirnov et al. (2011), we did not enforce a strict rule that all sample-level data must have been processed using the principal component analysis (Kirschvink, 1980), but we required that the stepwise demagnetization and isolation of ChRM directions using orthogonal vector plots must have been done for at least a pilot specimen collection. This corresponds to selecting data with a "demagnetization code" (DC) of three or higher (McElhinny & McFadden, 2000).
6. The uncertainties of the site-mean directions of ChRM must be estimated and presented in the original study/studies, as either the Fisher concentration parameter (k) or the angle of 95% confidence about the mean direction (α_{95}) (R. Fisher, 1953), to allow the estimation of within-site scatter (section 3).

The data sets that satisfied our selection criteria are listed in Table 1. The table also provides background information on the geographic location and age of the rock formation, the number of individual site-mean directions/VGPs in the data set, the Van der Voo (1990) quality ranking, and references. Each data set was assigned a unique identification number (DSID) for cross-referencing these metadata with the site-level data, which are presented in the supporting information Table S1. In addition to the site-mean directions, VGPs, and their relevant statistical summaries, this table lists the geographic coordinates for the sites (where these were not available the average study location was used), nominal ages assigned to the data, DCs, rock types and lithologies, and digital object identifiers for the papers from which the data were collected. For the site-level data from the formations that were demonstrably affected by short bursts of eruptive activity (e.g., sequences of lava flows recording indistinguishable directions of the magnetic field), we used the "direction groups" as they were defined in the original studies for the site-level entries (e.g., Butler et al., 1991; Kosterov & Perrin, 1996; Tarduno et al., 2001); otherwise, each site-level entry in Table S1 represents a single igneous unit. The statistical properties of the site-level database are illustrated in Figure S1, which shows the distributions of the number of samples per site, DC, α_{95}, and the Fisher precision parameter k for the site-mean ChRM directions.

Overall, our compilation contains data from 47 igneous formations (Figure 1), comprising ca. 1,770 site-mean directions and corresponding VGPs. For each individual data set, we assigned a nominal age based on available radiometric dates and/or upper and lower age constraints from biostratigraphy, geologic correlation, and considerations of geomagnetic polarity (using the geomagnetic polarity time scale of Ogg, 2012). In cases when the age is not constrained by high-quality U/Pb or Ar/Ar isotopic dates, or when the available radiometric dates show a broad range of possible ages, these assignments can be somewhat subjective and should be viewed with caution. Nevertheless, since our main objective was to relate the data sets either to the nonreversing field in the Cretaceous (the CNS), or to the reversing field during Jurassic-Early Cretaceous time, we consider these assignments adequate for the purpose of our analysis.

We did not apply site selection criteria based on the value of α_{95} for the mean direction. This approach is similar to that used by Smirnov et al. (2011), and we note that for most sites (84%) the α_{95} values do not exceed 10° and are greater than or equal to 20° for only 1.7% of sites. Biggin, van Hinsbergen, et al. (2008)

Table 1
Sources of Data and Background Information for Paleomagnetic Data Sets

DSID	Rock formation	Country	Lat (°N)	Lon (°E)	Age (Ma)	N	n_{tot}	Q	References
NPW17-44	Patagonian Plateau basalts	Chile, Argentina	−45.3	288.7	74	18	248	5	Butler et al. (1991)
NPW17-41	Adel Mountains volcanics	USA	47.2	248.1	75	31	232	5	Gunderson and Sheriff (1991) Harlan et al. (2005)
NPW17-43	Minusa Trough intrusions	Russia	54.9	90.3	75	16	249	6	Metelkin, Kazansky, et al. (2007)
NPW17-39	Gongju Basin volcanics	South Korea	36.5	127.1	78	9	102	5	Doh et al. (2002)
NPW17-37	Elkhorn Mountains volcanics	USA	46.0	248.1	80	15	112	5	Diehl (1991)
NPW17-38	Shexing Formation lavas	China	29.9	91.3	80	22	132	3	Tan et al. (2010)
NPW17-63	Yare Basin volcanics	China	31.6	82.2	80	15	136	5	Yi et al. (2015)
NPW17-40	Maudlow Formation	USA	46.1	248.9	82	11	55	5	Swenson and McWilliams (1989)
NPW17-35	Yongtai volcanics	China	25.7	119.0	88	19	343	4	Huang et al. (2013)
NPW17-36	Madagascar flood basalts	Madagascar	−19.5	45.9	90	44	273	4	Riisager et al. (2001) Cucciniello et al. (2010)
NPW17-57	Mount Carmel volcanics	Israel	32.7	35.0	90	11	67	3	Ron et al. (1990) Segev et al. (2002)
NPW17-58	Wadi Natash volcanics	Egypt	24.4	33.4	93	15	248	3	Schult et al. (1981)
NPW17-29	Arctic Canada lavas	Canada	79.4	267.8	95	37	286	5	Tarduno et al. (2002)
NPW17-31	Shovon and Khurmen-Uul volcanics (non-SEAB)	Mongolia	44.3	103.6	95	22	139	4	Hankard et al. (2007)
NPW17-27	South Vietnam volcanics	Vietnam	11.9	108.6	100	14	85	3	Chi and Dorobek (2004)
NPW17-53	Cabo Magmatic Province	Brazil	−8.4	325.1	102	24	220	4	Font et al. (2009), Schult and Guerreiro (1980)
NPW17-26	Qiangtang Terrane lavas	China	32.5	84.3	104	14	91	5	Chen et al. (2017)
NPW17-25	Artz-Bogd volcanics (non-SEAB)	Mongolia	44.3	102.2	104.5	38	211	4	Hankard et al. (2007), van Hinsbergen et al. (2008)
NPW17-61	Suhongtu volcanics	China	41.2	104.1	112	31	424	5	Zhu et al. (2008)
NPW17-24	Tuoyun lavas	China	40.2	75.3	114	52	356	4	Lhuillier et al. (2016)
NPW17-22	Rajmahal traps	India	24.6	87.6	117.5	68	315	5	Klootwijk (1971), Poornachandra Rao and Mallikharjuna Rao (1996), Tarduno et al. (2001) Coffin et al. (2002)
NPW17-67	Israeli alkali basalts	Israel	30.5	34.8	117.5	16	96	4	Sherwood et al. (1993)
NPW17-71	South East Artz Bogd lavas (SEAB)	Mongolia	44.4	102.5	117.5	26	167	5	van Hinsbergen et al. (2008)
NPW17-20	Dianzhong Formation volcanics	China	31.1	84.4	119	13	126	4	Yang et al. (2015)
NPW17-21	San Marcos dyke swarm	Mexico	32.1	243.6	120	13	84	4	Böhnel et al. (2002)
NPW17-69	South East Ih Bogd and Baga Bogd lavas (non-SEAB)	Mongolia	44.8	101.5	121	56	340	6	van Hinsbergen et al. (2008)
NPW17-16	Qushenla formation lavas	China	32.4	82.7	126	51	444	5	Ma et al. (2014)
NPW17-15	El Salto-Almafuerte lavas	Argentina	−32.2	295.7	127	10	53	3	Mendía (1978)
NPW17-42	Transbaikal basalts (Chikoy-Khilok)	Russia	50.5	107.5	128.5	12	87	5	Metelkin et al. (2010)
NPW17-14	Sangxui Formation lavas	China	28.8	91.2	130	28	230	6	Ma et al. (2016)
NPW17-12	Parana Magmatic Province	Brazil, Argentina Uruguay	−26.4	309.0	132	594	3587	6	Solano et al. (2010), Raposo and Ernesto (1995), Raposo et al. (1998), Ernesto et al. (1990, 1999), Mena et al. (2011) Moreira Florisbal et al. (2014)
NPW17-10	Etendeka traps	Namibia	−20.5	14.2	134	70	529	6	Dodd et al. (2015)
NPW17-51	Lebanon volcanics	Lebanon	34.0	35.5	153	13	76	3	Gregor et al. (1974), van Dongen et al. (1967)
NPW17-59	Inner Mongolia igneous units	China	48.5	119.6	154.5	23	172	4	Zhao et al. (1990)
NPW17-07	Tiaojishan Formation	China	41.1	118.6	155.0	35	255	5	Ren et al. (2016)
NPW17-17	Transbaikal basalts (Tugnui, Margintui)	Russia	50.9	106.5	155.5	14	112	6	Metelkin, Gordienko, et al. (2007)
NPW17-49	El Quemado complex	Argentina	−47.5	288.2	156.5	15	137	5	Iglesia Llanos et al. (2003)
NPW17-06	Camaraca Formation	Chile	−18.6	289.7	157	23	115	3	Palmer et al. (1980)
NPW17-05	Rio Grande do Norte dykes	Brazil	−5.7	323.4	160	10	77	3	Bucker et al. (1986)

Table 1 *(continued)*

DSID	Rock formation	Country	Lat (°N)	Lon (°E)	Age (Ma)	N	n_{tot}	Q	References
NPW17-66	Southern Greenland dykes	Denmark	61.2	311.5	165.5	14	74	4	Piper (1975)
NPW17-08	Canelo Hills volcanics	USA	31.5	249.5	175	15	117	5	Kluth et al. (1982) Gilbert and Lawton (2012)
NPW17-48	Marifil Formation	Argentina	−44.8	294.4	177	12	87	5	Iglesia Llanos et al. (2003)
NPW17-03	Kirkpatrick basalts	Antarctica	−73.3	162.9	180	21	156	5	Lemna et al. (2016)
NPW17-68	Ferrar dolerites	Antarctica	−74.5	162.0	180	15	242	4	Lanza and Zanella (1993) Riley and Knight (2001)
NPW17-02	Vestfjella dykes	Antarctica	−73.5	345.0	182	24	109	4	Løvlie (1979) Luttinen et al. (2015)
NPW17-47	Karoo Magmatic Province	Africa	−28.4	28.8	183	103	549	6	Kosterov and Perrin (1996), Henthorn (1981), Hargraves et al. (1997) Duncan et al. (1997), Riley et al. (2004)
NPW17-01	Piedmont mafic dykes	USA	35.9	280.3	198	15	100	3	Smith (1987) Beutel et al. (2005)

Note. DSID is the data set identification number. Lat and Lon are the geographic latitude and longitude for the average site location. Age is the nominal age assigned to the data set. N is the number of site-level data. n_{tot} is the total number of samples per data set. Q is the quality score based on the first six Van der Voo (1990) criteria. The "References" column lists studies from which paleomagnetic data were compiled. Extra references for radiometric ages are given in the square brackets.

used additional site selection criteria ($n \geq 5$ and $k \geq 50$) to isolate subsets of higher technical data quality (which they referred to as Group 1 data sets) from their compilation of the CNS and Jurassic data. We will examine how this restriction affects the estimates of latitude dependence of PSV in section 4. Compared to the study of Biggin, van Hinsbergen, et al. (2008), our database contains more individual data sets because we sampled a slightly broader age interval and included the data published after 2008. Furthermore, since we used stricter selection criteria, 11 out of 28 data sets used by Biggin, van Hinsbergen, et al. (2008) were excluded from our compilation because of the lack of uncertainty estimates for the site-mean directions (criterion 6), a small ($n \leq 2$) number of samples per site (criterion 4), and/or evidence for local block rotation or remagnetization (criterion 2). Examples of the accepted data sets are shown in Figure 2.

3. Methodology

3.1. Measures of PSV

In PSV studies, the geomagnetic field variability is typically described by the scatter of VGPs or, alternatively, by the scatter of paleomagnetic directions. In our analysis, we used two alternative approaches for quantifying this scatter.

3.1.1. The Traditional Approach: Angular Dispersion

The first approach uses a familiar measure of VGP scatter, which is often referred to as the "angular dispersion" or "angular standard deviation" in the paleomagnetic literature (e.g., Cox, 1970; McFadden et al., 1991). The angular dispersion of VGPs (S) was calculated using the equation (Cox, 1970)

$$S^2 = \frac{1}{N-1}\sum_{i=1}^{N}\Delta_i^2, \quad (1)$$

where N is the number of VGPs comprising a paleomagnetic data set and Δ_i is the angular deviation of the ith VGP from the mean paleomagnetic pole. The mean pole was computed as a Fisher average of the VGPs included in the data set (R. Fisher, 1953). Before calculating the mean pole and the angular dispersion, the VGPs corresponding to the site-mean directions of reverse polarity (if they were present in the data set) were replaced by the antipodal VGPs, and the angular distances between each VGP and the mean pole were checked to ensure that no VGP in the data set deviated by more than 90° from the mean. Note that all VGPs given in Table S1 conform to this convention, that is, each VGP data set is confined to the hemisphere centered on the mean pole (e.g., Figure 2).

Under the assumption that the geomagnetic field averaged over a sufficiently long time interval equates the field of a geocentric axial dipole (GAD), the mean of a VGP distribution is expected to coincide with the

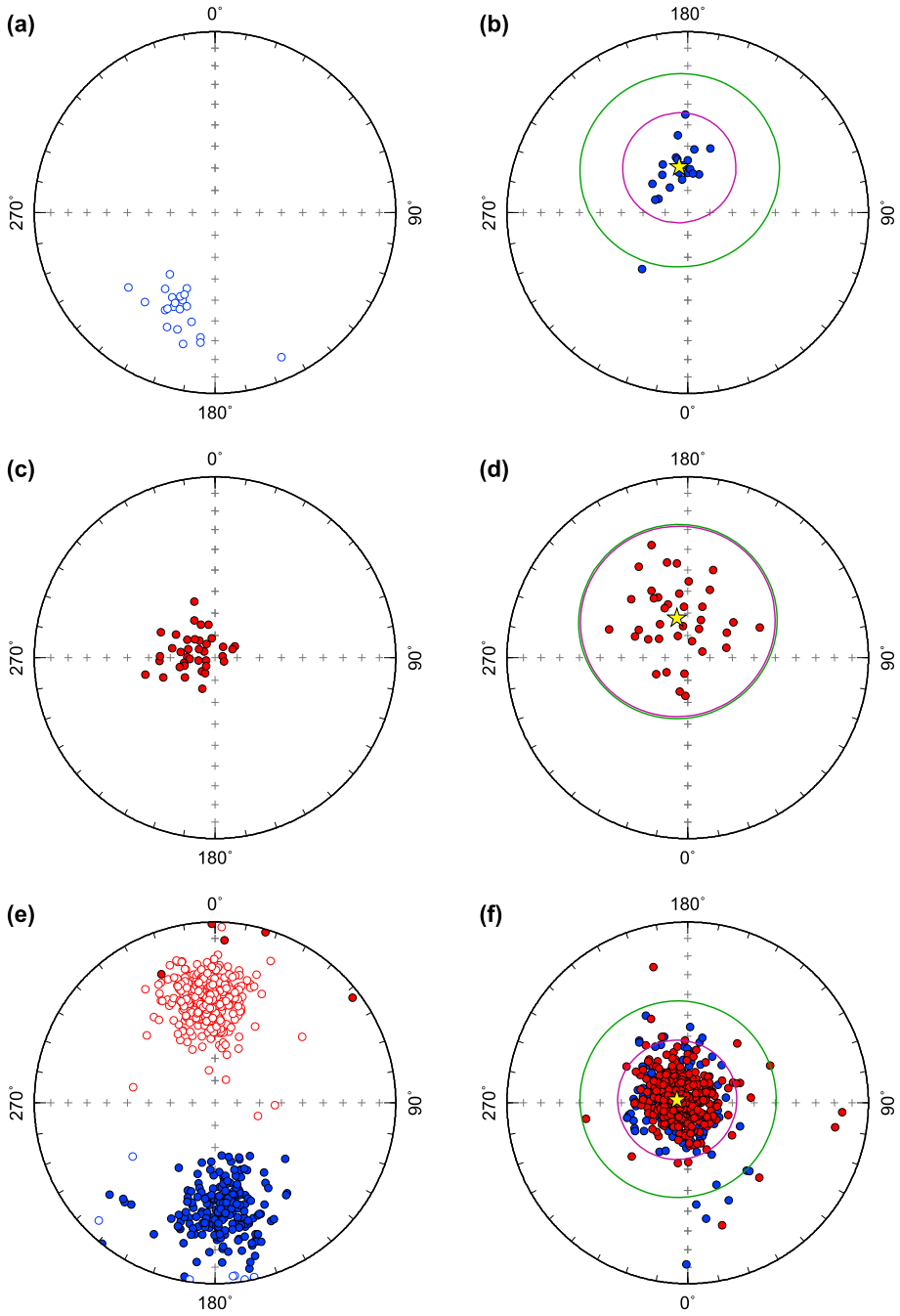

Figure 2. Equal-area plots showing examples of site-mean characteristic remanent magnetization directions (a, c, e) and virtual geomagnetic poles (b, d, f). The data are from (a, b) the Shexing Formation lavas (~80 Ma, DSID = NPW17–38), (c, d) Arctic Canada lavas (95 Ma, DSID = NPW17–29), and (e, f) the Parana Magmatic Province (132 Ma, DSID = NPW17–12); see Table 1 for references. The white and color-filled circles in (a), (c), and (e) show the directions with negative and positive inclinations, respectively. The red and blue colors indicate the normal and reverse polarities. Virtual geomagnetic poles are plotted in the northern hemisphere. The yellow star symbols in (b), (d), and (f) show the mean poles calculated after removing the outliers according to the Vandamme (1994) criterion. The purple circles show the Vandamme (1994) cutoff angles; the green circles show the 45° cutoff angle.

geographic pole (Merrill et al., 1998). Hence, the mean pole can be viewed as an estimate of the position of the paleogeographic north pole with respect to the location of the source rocks in present geographic coordinates. Note that this approach differs from that used to produce values of *S* for recent time periods (e.g., Cromwell et al., 2018; Johnson et al., 2008; Opdyke et al., 2015) where the scatter is measured about

the actual geographic pole. Notwithstanding critical failure to average secular variation by individual data sets or significant departures from GAD morphology, the two approaches should give similar values.

The angular dispersion of paleomagnetic directions (s) was calculated using the equation (Cox, 1970)

$$s^2 = \frac{1}{N-1}\sum_{i=1}^{N}\delta_i^2, \tag{2}$$

where δ_i denotes the angle between the ith site-mean ChRM direction and the Fisher mean direction of N site-means. The site-mean directions corresponding to the reverse polarity were inverted to the antipodal directions before calculating the mean direction and the angular dispersion. In the remainder of this chapter, we will focus on the analysis of VGP data; the analysis of directional data is completely analogous, except for several instances that will be explicitly discussed. As a convention, we will use capital letters (e.g., S, Δ_i) for VGP data and lowercase letters (e.g., s, δ_i) for directional data.

The angular dispersion of VGPs given by equation (1) includes two sources of scatter—a typically dominant contribution caused by the secular variation of the field ("between-site dispersion", S_b) and a minor contribution arising from random errors related to the uncertainties of ChRM directions due to measurement errors ("within-site dispersion", S_w). To estimate the scatter caused by PSV, S_b was calculated using the approximation given by McFadden et al. (1991):

$$S_b^2 = S^2 - \frac{S_w^2}{n} = S^2 - \frac{1}{N}\sum_{i=1}^{N}\frac{S_{wi}^2}{n_i}, \tag{3}$$

where S_w^2/n denotes the contribution from within-site dispersion, S_{wi} is the within-site dispersion associated with the ith site, and n_i is the number of individual paleomagnetic sample directions used to obtain the ith site-mean direction and the corresponding VGP.

Assuming that at each site the sample ChRM directions are Fisher-distributed, which is reasonable given the random nature of measurement errors, we estimated the concentration parameters of within-site ChRM directions (k_{wi}) using Fisher statistics and then transferred these estimates to VGP space using the equation (Cox, 1970)

$$K_{wi} = k_{wi}\left[\frac{1}{8}\left(5 + 18\sin^2\lambda + 9\sin^4\lambda\right)\right]^{-1}, \tag{4}$$

where λ is the paleolatitude of the sampling site computed as 90° minus the angular distance between the site and the mean pole. The values of within-site dispersion contributing to the VGP scatter were approximated by

$$S_{wi} = \left(\frac{180^\circ}{\pi}\right)\sqrt{\frac{2}{K_{wi}}} \cong \frac{81^\circ}{\sqrt{K_{wi}}}, \tag{5}$$

and used in equation (3) to calculate S_b. For the analysis in direction space, k_{wi} values were substituted for K_{wi} in equation (5) to estimate the within-site dispersion s_{wi}.

3.1.2. Treatment of Outliers

The angular dispersion S is a direct analogy of standard deviation as estimated from a sample of random observations in univariate analysis. When paleomagnetic directions and VGPs derived from them are treated as random observations, and it is assumed that random sampling of the field produces a population of VGPs that is described by a Fisher distribution with a precision parameter K, the choice of this metric comes naturally because the Fisherian mean of the VGP positions provides the maximum likelihood estimate of the population mean, whereas the value of S^2 is the unbiased estimate of $2/K$ for a concentrated distribution (i.e., when $K \gg 1$; Cox, 1969; R. Fisher, 1953; McFadden, 1980).

In paleomagnetic studies, however, a situation commonly arises when the majority of VGPs cluster around the mean pole and can be fit by a Fisher distribution reasonably well (although this is not always the case), whereas some VGPs lie far from the mean, resulting in a longer tail of the observed distribution compared to that expected from the Fisher model (e.g., Harrison, 2009; Shibuya et al., 1995; Suttie et al., 2015). These "outlier" VGPs are usually interpreted as representing the field undergoing geomagnetic excursions or

polarity reversals, and the common practice is to remove them from the calculation of the VGP mean and dispersion, because it is considered desirable to focus on the field behavior away from times of excursions and polarity transitions. Technically, this is done by applying some maximum threshold value for Δ_i, which we will refer to as the "cutoff angle," to select VGPs and directions corresponding to these VGPs that should be excluded from a data set. Similarly to Biggin, van Hinsbergen, et al. (2008), we used two approaches for defining the cutoff angle (Δ_{max}): one that uses a fixed value of 45° (which is intermediate between the values used by previous studies of PSV, 35°–55°) and the second that assigns the "optimum" Δ_{max} value based on the procedure of Vandamme (1994) for estimating the angular dispersion of the population that can be reasonably assumed to represent nontransitional data:

$$\Delta_{max} = 1.8 \cdot S + 5^{\circ}. \quad (6)$$

In this equation Δ_{max} is calculated iteratively whereby S is first estimated for the whole data set using equation (1), and if there are VGPs that deviate from the mean pole by more than Δ_{max} degrees, the VGP with the largest deviation is removed and the calculation is repeated until all VGPs retained in the data set satisfy the condition $\Delta_i \leq \Delta_{max}$. To test how these two trimming options affected the estimated values of VGP scatter, we also calculated the values of S and S_b retaining all VGPs in the data sets, that is, without imposing any cutoff angle.

3.1.3. A less Orthodox Approach: Mean Angular Deviation

Although it has become routine in studies of PSV to discard the outliers from VGP data sets, this is not universally accepted in the community (e.g., Tauxe et al., 2003) because it is generally not possible to separate VGPs corresponding to the "normal secular variation" (i.e., periods of stable geomagnetic polarity) from those representing polarity transitions and excursions if the data do not provide a temporally dense and stratigraphically ordered record of changes in the field direction. The trimming procedures whereby a data set is truncated by Δ_{max} have been designed to remove most of the transitional and excursional data without cutting off a statistically significant fraction of the main VGP distribution (Vandamme, 1994). McElhinny and McFadden (1997) showed that for Fisher distributions, less than 4% of probability mass in the distribution tail is truncated by the Vandamme (1994) cutoff angle (equation (6)), introducing a negligible bias to the estimated VGP scatter. However, when applying the Vandamme (1994) or fixed cutoff, there are no guarantees that all transitional and excursional data have been removed from the truncated data set or that the removed VGPs uniquely represent polarity transitions and excursions. There also exists a further argument that, since the distinction between "transitional" data and normal secular variation is not grounded in any understanding of the physical processes responsible for the variability, the entire distribution should be considered.

Instead of relying on trimming techniques, it is preferable to treat the transitional and excursional data as an integral part of secular variation, without any arbitrary separation of the field behavior into the "normal" and "exotic" states. That said, the presence or absence of occasional VGP outliers due to polarity transitions or excursions strongly influences S and S_b (as they are sensitive to Δ_i^2), especially for small data sets, which may result in unrecognized biases in the latitudinal dependence of VGP scatter. Consequently, if all available data are retained, it is desirable to use a metric of VGP scatter that would be more robust to (less influenced by) outliers than the angular dispersion.

Suttie et al. (2015) developed a new statistical technique for quantifying the scatter of paleomagnetic directions and VGPs and introduced a new measure (denoted S'), which is arguably robust to outliers. We used this technique as an alternative way of measuring PSV in our analysis. The method of Suttie et al. (2015) is based on the use of the spherical exponential (SE) distribution as a sampling distribution (in the sense of assessing the likelihood of observations given a probability model) for obtaining the estimates of central location and scatter of a VGP population. Here we will briefly recount their methodology; the details can be found in the original publication (Suttie et al., 2015).

The SE distribution is defined as

$$dP(\theta,\varphi) = p(\theta,\varphi)d\Omega = \frac{K_E^2 + 1}{2\pi(1 + \exp(-K_E\pi))} \exp(-K_E\theta)d\Omega, \quad (7)$$

where θ and φ are, respectively, the colatitude and azimuthal angle relative to the central location (taken as the geographic pole in the case of VGP distribution), $dP(\theta,\varphi)$ is the probability of the observation within the

elementary area on the unit sphere $d\Omega = \sin\theta d\theta d\varphi$ bound by the limits $[\theta, \theta + d\theta]$ and $[\varphi, \varphi + d\varphi]$, $p(\theta, \varphi)$ is the probability density function, and K_E (>0) is the concentration parameter that characterizes the spread of the distribution about the central location.

The choice of the SE distribution as a sampling distribution is sensible in the context of PSV analysis because it is the maximum entropy distribution (i.e., the least informative) among those having a specified expectation for the VGP colatitude ($E(\theta) \equiv \langle\theta\rangle$):

$$\langle\theta\rangle = \frac{2K_E}{K_E^2+1} + \frac{\pi\exp(-K_E\pi)}{1+\exp(-K_E\pi)} \cong \frac{2K_E}{K_E^2+1} \cong \frac{2}{K_E} \quad \text{when } K_E \gg 1. \tag{8}$$

Hence, by assigning the SE distribution to VGPs, we essentially state that we do not want to assume any prior knowledge about secular variation other than it produces a distribution of VGPs about the geographic pole with some expected value of colatitude, which we would like to estimate and use as a measure of secular variation.

Compared to the Fisher distribution, the SE distribution has a longer tail and may thus provide a more accurate statistical description for data sets containing VGPs far away from the central location. Indeed, Suttie et al. (2015) showed that several data sets from Cenozoic large igneous provinces, unmutilated by truncation of outliers, can be fit by the SE distribution better than by the Fisher model. A drawback in using the SE distribution is that there is no explicit formulation for the estimate of central location and its confidence region. From equation (7), it is evident that the likelihood of a point with coordinates (θ, φ) to be the central location, given the observations of N VGPs with coordinates (θ_i, φ_i), is maximized when the sum of angular deviations $\Delta_i^{(\theta,\varphi)}$ from that point is the minimum. Thus, the maximum likelihood estimate for the central location $\left(\widehat{\theta}, \widehat{\varphi}\right)$ is given by the equation

$$\sum_{i=1}^{N} \Delta_i^{\left(\widehat{\theta},\widehat{\varphi}\right)} = \min_{(\theta,\varphi)} \sum_{i=1}^{N} \Delta_i^{(\theta,\varphi)}. \tag{9}$$

This estimate has a character of a median-type estimator on the sphere (N. I. Fisher, 1985), which is less sensitive to outliers than the mean estimated using the Fisher statistics, since the latter minimizes the sum of squared deviations. The spherical median $\left(\widehat{\theta}, \widehat{\varphi}\right)$ can be found by straightforward numerical minimization, and its distribution (and hence confidence limits) can be evaluated using the Bayesian approach described by Suttie et al. (2015).

The SE distribution naturally leads to the choice of the mean angular deviation from the central location as a measure of VGP scatter:

$$S' = \frac{1}{N}\sum_{i=1}^{N} \Delta_i. \tag{10}$$

Being the arithmetic mean rather than a "root-mean-square" (RMS) deviation (equation (1)), S' is less affected by occasional outliers than S and hence can be considered a more robust measure of PSV. If the central location is known (e.g., the geographic pole for paleomagnetic data from recent times), equation (10) gives us the unbiased estimate of the expected VGP colatitude $\langle\theta\rangle$, that is, $\langle S'\rangle = \langle\theta\rangle$. However, when we do not know where the "true" center of the distribution is and use the spherical median $\left(\widehat{\theta}, \widehat{\varphi}\right)$ estimated from the data to calculate deviations Δ_i, this introduces a negative bias into S' as a measure of $\langle\theta\rangle$. The reason is that $\left(\widehat{\theta}, \widehat{\varphi}\right)$ minimizes the total angular deviation for a finite number of observations (equation (9)), and any other point on the sphere, including the true distribution center, will produce a larger mean deviation than S'. Hence, generally $\langle S'\rangle < \langle\theta\rangle$, with the difference diminishing to zero as the number of observations becomes infinitely large.

3.1.4. Correcting Bias in S' Due to Finite Sample Size

To investigate the bias we performed numerical simulations in which 1,000 samples of size N were drawn from the SE distribution with a specified $\langle\theta\rangle$ (given by equation (8)). For each sample, the spherical

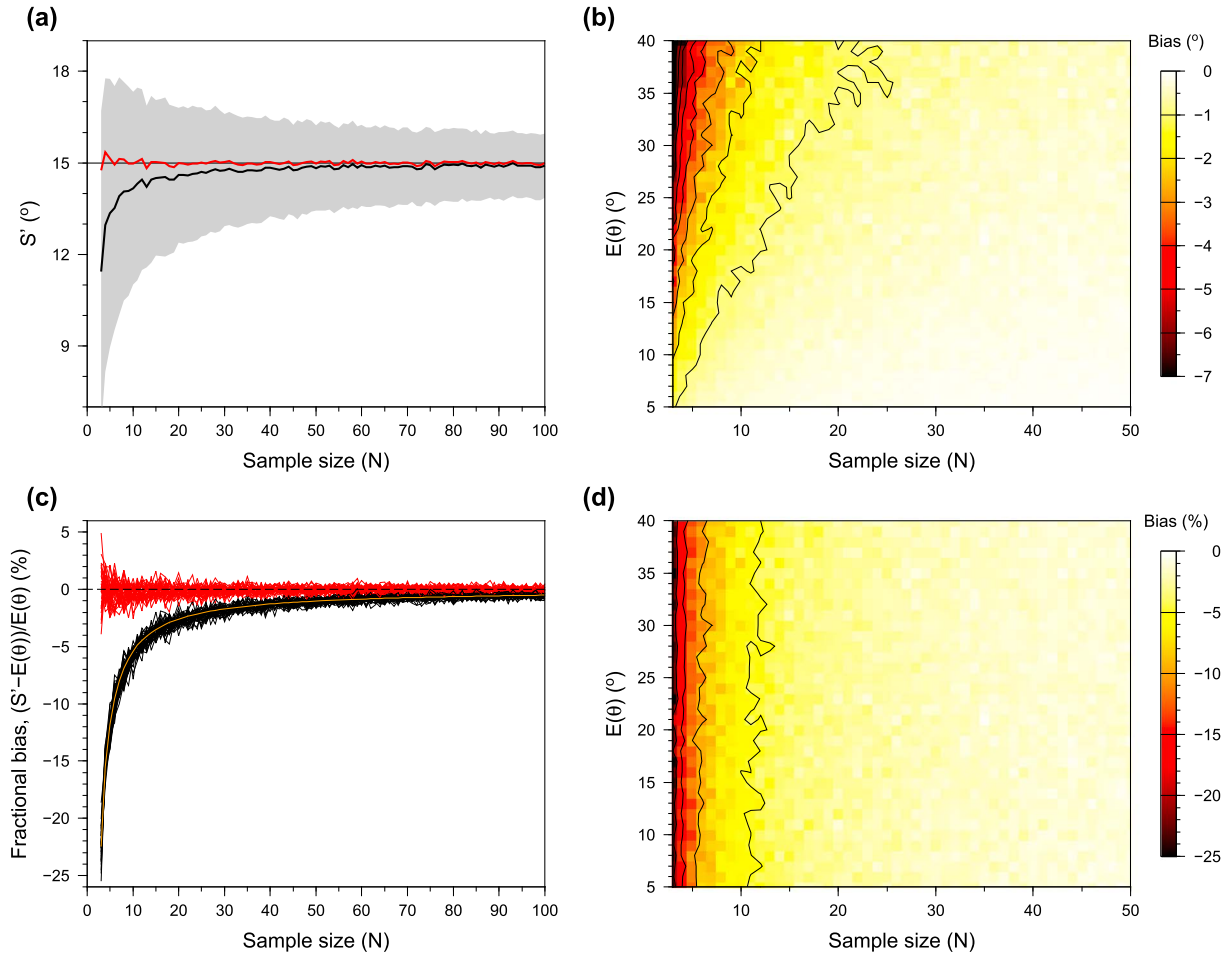

Figure 3. (a) An example of negative bias in $S^{'}$ introduced by the finite sample size (N). The black line shows the mean value of $S^{'}$ calculated using equation (10) for 1,000 random draws of N virtual geomagnetic poles from the SE distribution with the expected angular distance from the central location $\langle\theta\rangle = 15^{\circ}$. The gray envelope shows the range of the $S^{'}$ values corresponding to 95% of resamplings. The red line shows the mean of $S^{'}$ values corrected for the sample-size bias using equation (12). (b) Bias of the mean of uncorrected $S^{'}$ values as a function of sample size and expected angular distance. (c) Fractional bias $\left(\overline{S^{'}}-\theta\right)/\theta$ of the uncorrected and corrected $S^{'}$ values for the values of expected angular distance ranging from 5° to 40° (black and red lines as in Figure 2a, respectively). Orange line shows the functional relationship given by equation (11). (d) Bias of the uncorrected mean $S^{'}$ expressed as a percentage of the expected angular distance.

median location and $S^{'}$ were calculated from equations (9) and (10), and then the mean value $\overline{S^{'}}$ was calculated for all resamplings. The procedure was repeated for different N and $\langle\theta\rangle$, with the sample size ranging from 3 to 100, and the expected colatitude from 5° to 40°. The results of this experiment are shown in Figure 3.

As expected, the bias is small for large values of N (<1° for $N > 30$), but becomes substantial for small samples (Figures 3a and 3b), reaching about 9° in the "worst case" encountered ($N = 3$, $\langle\theta\rangle = 40°$). Another observation is that the bias expressed as a percentage of the expected value $\langle\theta\rangle$ is not sensitive to $\langle\theta\rangle$ and follows a rather simple functional relationship with respect to N (Figures 3c and 3d):

$$\frac{\overline{S^{'}}-\langle\theta\rangle}{\langle\theta\rangle} = 1-\frac{N}{\sqrt{N(N-1)}}. \tag{11}$$

This suggests that the unbiased estimate of $\langle\theta\rangle$ can be obtained by simply "upscaling" $S^{'}$ with a factor that depends on N only, so it becomes

$$S' = \frac{1}{2-\frac{N}{\sqrt{N(N-1)}}} \cdot \frac{1}{N} \sum_{i=1}^{N} \Delta_i. \quad (12)$$

It is not trivial why the unbiased estimate should have this form, but from the practical point of view, the use of equation (12) instead of (10) evidently makes the bias negligible (Figure 3c), even for small samples. Hence, we adopted this formulation in our analysis.

3.1.5. Correcting S' for Within-Site Dispersion

Another point that was not addressed in the original work of Suttie et al. (2015) is how the within-site dispersion affects S'. Similarly to the traditional approach described above, it is desirable to separate its contribution from that caused by PSV and derive an estimate analogous to the between-site dispersion S_b. A simple approximation can be obtained as follows.

If there is a distribution of colatitudes with the expected value $\langle\theta\rangle$, the variance of θ can be expressed as

$$\mathrm{var}(\theta) \equiv \left\langle (\theta - \langle\theta\rangle)^2 \right\rangle = \left\langle \theta^2 \right\rangle - \langle\theta\rangle^2 \cong V' \cdot \langle\theta\rangle^2, \quad (13)$$

where V' is the distribution shape parameter defined by Suttie et al. (2015). For an SE distribution with a large concentration parameter ($K_E \gg 1$), V' is a constant equal to 1/2. For a concentrated Fisher distribution, V' is also largely independent of the precision parameter K and is approximately two times smaller than that for the SE distribution.

For an observed sample of VGPs, we can define the shape parameter by replacing the expected values in equation (13) with their estimates (S^2 and S'):

$$V' = \frac{S^2 - S'^2}{S'^2} = \frac{S^2}{S'^2} - 1, \quad (14)$$

and similarly for the sample that would be observed in the absence of within-site errors:

$$V'_b = \frac{S_b^2 - S_b'^2}{S_b'^2} = \frac{S_b^2}{S_b'^2} - 1. \quad (15)$$

If we assume that the contribution from the within-site errors to the total VGP scatter is small compared to that caused by secular variation, which is typical for paleomagnetic data sets, we would not expect the shape of the distribution to be significantly changed by the within-site errors, so that it is reasonable to approximate V'_b by V'. Thus, assuming that $V'_b \cong V'$ and combining equations (14) and (15), we obtain

$$S'_b \cong \frac{S' S_b}{S} = \frac{S'}{S} \sqrt{S^2 - \frac{S_w^2}{n}} = S' \sqrt{1 - \frac{1}{NS^2} \sum_{i=1}^{N} \frac{S_{wi}^2}{n_i}}, \quad (16)$$

where we used the approximation for S_b^2 given by equation (3), which is valid for any concentrated distribution and large N (McElhinny & McFadden, 1997; McFadden et al., 1991). We stress that when applying the S_w correction to S' (equation (16)), both the S' and S^2 values should be calculated with respect to the same central location, estimated by the spherical median, although using the Fisher mean instead would typically make very little difference.

Given the approximate nature of the solution for S'_b (equation (16)), we should also consider the possible bias in S'_b estimates. The approximation based on the assumption that the shape of the distribution is not influenced by the measurement errors ($V'_b \cong V'$) will not be valid when the within-site dispersion is comparable to that caused by PSV. Another complication arises from the need to transfer the within-site dispersion into pole space, which may lead to extra bias because the transfer function given by equation (4) is also an approximation valid only asymptotically in the limit of large k_w (Cox, 1970).

To investigate the magnitude of these biases, we performed two sets of numerical simulations. In the first experiment, we simulated s' for paleomagnetic directions without transferring them into VGPs. One thousand random samples of 50 directions were generated from the SE distribution with a specified mean

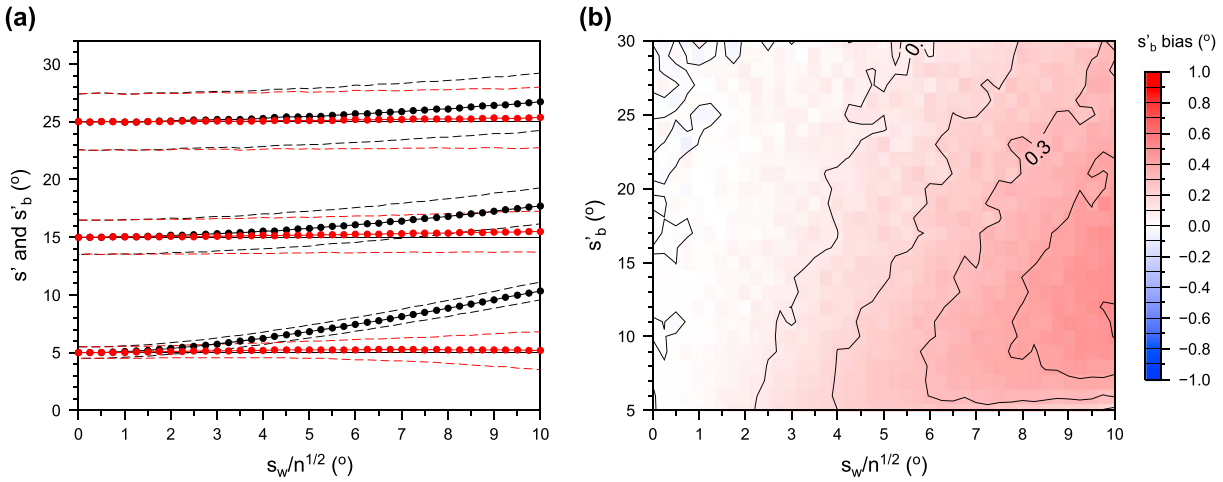

Figure 4. (a) Examples of bias in s' (direction space) introduced by the uncorrected within-site dispersion ($s_w/\sqrt{n}$). Black circles show the average values of s' obtained from numerical simulations with the expected between-site angular deviation of directions $\langle\theta\rangle$= 5°, 15°, and 25° that were not corrected for the within-site dispersion (see text). Red circles show the corresponding values with the within-site correction applied (s'_b, equation (16)). (b) Bias of the mean values of s'_b as a function of the true s'_b ($\langle\theta\rangle$) and within-site dispersion ($s_w/\sqrt{n}$).

angular deviation (the expected value of s'_b), which was varied from 5° to 30°. In each sample, the directions were perturbed by random errors drawn from the Fisher distribution with a specified value of $k_w = (180°/\pi)^2 \cdot 2n/s_w^2$ (cf. equation (5)), with $s_w/\sqrt{n}$ ranging from 0° to 10°. From the perturbed sample directions, we calculated s' and s'_b using equations (12) and (16), respectively, and their respective mean values based on 1,000 resamplings for all combinations of the true s'_b and $s_w/\sqrt{n}$. The results of this experiment (Figure 4) show that the correction given by equation (16) works well in removing the contribution from the within-site dispersion, even when it is comparable with or larger than the between-site scatter. It is apparent that the correction introduces a small positive bias that becomes progressively larger at higher levels of within-site noise. Yet, the bias does not exceed 0.5°, and for $s_w/\sqrt{n} \leq 5^\circ$ it is less than ~0.2°, which we consider negligible.

The second experiment was similar in design, except this time we simulated samples of VGPs from the SE distribution with a predefined expected colatitude (true S'_b) and calculated field directions corresponding to these VGPs at different latitudes (from 0° to 90°). The directions were then perturbed with Fisherian errors and converted back to VGPs. The within-site dispersion was transferred to pole space using equation (4), and the mean values of estimated S' and S'_b were calculated for each combination of the true S'_b, $s_w/\sqrt{n}$ and latitude. The results are illustrated in Figure 5.

First, we note that the contribution from the within-site errors not only increases S' in comparison with the true value, but also introduces a positive latitude dependence of S' (Figure 5a). This is analogous to the bias in angular dispersion (S) caused by uncorrected contribution from within-site scatter and stems from the fact that a latitude-independent dispersion of directions translates into a latitude-dependent dispersion of VGPs (Biggin, van Hinsbergen, et al., 2008; Cox, 1970; Linder & Gilder, 2012). The correction for the within-site dispersion removes the latitude dependence and correctly restores S' to the expected value of S'_b value when $s_w/\sqrt{n}$ is smaller than ~5°, but tends to underestimate S'_b at high latitudes for higher within-site dispersions. This introduces negative latitude dependence at high latitudes, which is especially prominent for low values of S'_b (Figure 5b). The reason for that is the use of the Cox (1970) approximation when transferring the directional dispersion into pole space (equation (5)), which overestimates S_w^2/n at high latitudes (and to a lesser degree underestimates it at low latitudes) when the dispersion of directions is high. For $s_w/\sqrt{n}$ not exceeding 5°, the bias in estimated S'_b is positive and smaller than 0.3° for all latitudes (Figures 5c–5f), and we conclude that in this case the correction can be used safely. However, for higher values of within-site dispersion and latitudes above ~60°, it can lead to significant underestimation of S'_b and should not be used blindly.

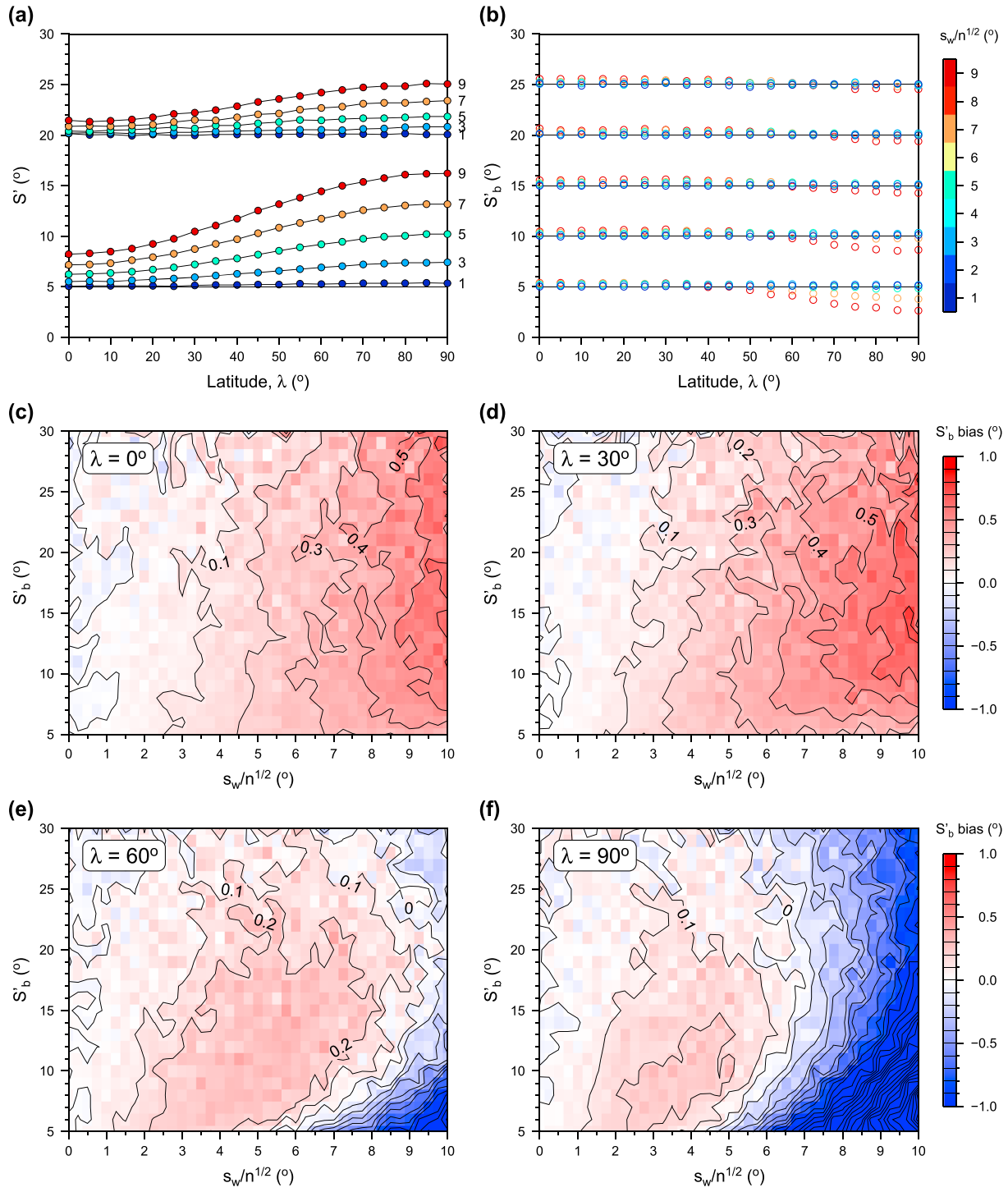

Figure 5. (a) Examples of bias in $S^{'}$ (virtual geomagnetic pole space) due to the uncorrected within-site dispersion, which introduces artificial latitude dependence of $S^{'}$. Circles, which are color-coded according to the level of within-site dispersion (note that $s_w/\sqrt{n}$ is the dispersion in direction space), show the average values of uncorrected $S^{'}$ obtained in numerical simulations with the expected between-site virtual geomagnetic pole colatitudes $\langle\theta\rangle$= 5° and 20° (see text). (b) Mean values of corrected $S^{'}$ ($S_b^{'}$, equation (16)) obtained in the same numerical experiment for the values of $\langle\theta\rangle$= 5°, 10°, 15°, 20°, and 25°. (c–f) Bias of the mean values of $S_b^{'}$ as a function of the true $S_b^{'}$ ($\langle\theta\rangle$) and within-site dispersion ($s_w/\sqrt{n}$) at different latitudes. Note that the negative bias below the −1° level is shown by the uniform blue color in (e) and (f).

We note that for almost all data sets included in our compilation (43 of 47), the average value of $s_w/\sqrt{n}$ was below 5°, and only slightly higher for the remaining four data sets (Figure 1c). Thus, we considered that the correction for within-site scatter derived above is not likely to impart any substantial bias and applied it to S' estimates derived from our Cretaceous and Jurassic data.

3.2. Modeling the Latitude Dependence of PSV

In this study, we analyzed the latitude dependence of secular variation in both pole (VGP) space and direction space. The analysis of field variability in direction space is rarely included in PSV studies but was performed here in order to test the hypothesis of Linder and Gilder (2012), who suggested that the latitude dependence of VGP angular dispersion is a mathematical artifact originating from the conversion of paleomagnetic directions to VGPs (see section 5 for relevant discussion).

To describe the dispersion of VGPs as a function of paleolatitude (λ), we used Model G of McFadden et al. (1988):

$$S_b(\lambda) = \sqrt{S_s^2 + S_p^2} = \sqrt{a^2 + (b\lambda)^2}. \tag{17}$$

This model assumes that the angular dispersion of VGPs can be represented by the quadrature sum of the contributions from two independent dynamo families (S_s and S_p). S_s, which was argued to be latitude-invariant ($S_s = a$; McFadden et al., 1988, 1991), corresponds to the variation in equatorially symmetric terms of the spherical harmonic expansion of the field, that is, the variation of the Gauss coefficients g_l^m and h_l^m with $l - m$ even (e.g., g_1^1, h_1^1, g_2^0) with respect to the axial dipole term (g_1^0). S_p represents the variation in antisymmetric terms ($l - m$ odd: g_2^1, h_2^1, g_3^0, ...), argued to vary as a linear function of latitude ($S_p = b\lambda$). Although the complete separation of the symmetric and antisymmetric families is unlikely, we consider Model G to be a useful framework for comparisons with the results of the earlier studies (Biggin, van Hinsbergen, et al., 2008; de Oliveira et al., 2018; McFadden et al., 1991). For each data set, the paleolatitude (λ) was estimated using angular distance between the mean VGP and the average site location. The shape parameters of Model G (a and b) were calculated by minimizing the sum of squared deviations between S_b data and the model.

The same procedure was applied to S_b' data, despite the fact that it is a different measure of PSV and there is no theoretical justification for Model G-type behavior for the latitudinal variation of S_b'. From a practical point of view, however, the use of the same functional form for the relationship between S_b' and λ provided us a straightforward way of comparing the results based on the two alternative approaches for quantifying PSV.

The confidence intervals for a and b were estimated through simple, nonparametric bootstrap with replacement of the S_b and S_b' data that were used as input for defining the models (cf. Biggin, van Hinsbergen, et al., 2008). We stress that at this point we consider a and b only as shape parameters of a descriptive model (for both S_b and S_b' data) without attaching any physical meaning to them. A more detailed discussion of Model G will be provided in section 5.

For the analysis in direction space, we chose to fit the data with Model A of Irving and Ward (1964):

$$s_b(\lambda) = s_0\left(1 + 3\sin^2\lambda\right)^{-1/2}, \tag{18}$$

where s_0 is the model parameter corresponding to the angular dispersion at the equator. This simple phenomenological model assumes that the total magnetic field can be represented by the field of a GAD (varying with latitude) and a perturbing field of constant magnitude (independent of latitude) and randomly distributed direction, statistically describing secular variation. Similarly to the analysis in VGP space, we use this model in a purely descriptive sense. Model A was also fitted to s_b' data for the purpose of comparison. The paleolatitude was calculated from the inclination (I) of the mean direction for each data set using the dipole equation, that is, $\tan(\lambda) = ½ \tan(I)$ (McElhinny & McFadden, 2000). The confidence interval for s_0 was estimated using the bootstrap technique.

4. Results

4.1. Latitude Dependence of PSV

The values of angular dispersion and mean angular deviation for all data sets included in our compilation are presented in Tables S2.1–S2.4. Table S2.1 lists the angular dispersions (S_b and s_b) calculated after excluding the outlier VGPs (and directions corresponding to these VGPs) according to the Vandamme (1994) criterion (section 3.1.2). The estimates of S_b and s_b obtained using the fixed 45° cutoff angle and without exclusion of outliers are given in Tables S2.2 and S2.3, respectively. These tables also provide relevant statistical summaries, including Fisher mean directions and VGP locations, their uncertainties, paleolatitudes derived from these estimates, and the 95% confidence regions for the values of angular dispersion. The corresponding estimates based on the use of SE distribution (S_b' and s_b', section 3.1.3) are given in Table S2.4.

Figure 6 illustrates the distribution of PSV estimates as a function of paleolatitude for the entire database. Overall, the data show general tendencies for the estimates in pole space (S_b and S_b', Figures 6a and 6c) to increase with the increasing absolute values of latitude and for the estimates in direction space (s_b and s_b', Figures 6b and 6d) to decrease. This behavior is consistent with the results of the earlier studies (e.g., Biggin, van Hinsbergen, et al., 2008; Irving & Ward, 1964; McFadden et al., 1991; McElhinny & McFadden, 1997; Smirnov & Tarduno, 2004; Smirnov et al., 2011; Veikkolainen & Pesonen, 2014). The trends are similar for both the northern- and southern-hemisphere locations, showing no obvious equatorial asymmetry.

For the analysis of latitude dependence of secular variation, we split our Cretaceous-Jurassic database into three age groups corresponding to the intervals (1) preceding the CNS ("pre-CNS", 127–198 Ma, 20 data sets), (2) the CNS (84–126 Ma, 19 data sets), and (3) postdating the CNS ("post-CNS", 74–83 Ma, 8 data sets). Because of the scarcity of data for the times preceding the CNS, we did not attempt to further subdivide the pre-CNS interval into shorter segments according to variation in the reversal rate and will examine only the long-term signal for the entire interval to make a first-order comparison between the PSV behavior of the reversing and nonreversing field.

The values of symmetric (a) and antisymmetric (b) terms of Model G and the equatorial dispersion of Model A (s_0) for the three intervals are presented in Tables 2 and 3. The fits of Model G (McFadden et al., 1988, 1991) and Model A (Irving & Ward, 1964) to the CNS and pre-CNS subsets are shown in Figures 7–12. Because of the limited number of data sets, substantial scatter of PSV estimates, and no clear indication for distinct latitude patterns in the northern and southern hemisphere for both periods, we did not attempt to test for possible equatorial asymmetry of PSV. Because both Model G and A are symmetric with respect to the equator (equations (17) and (18)), we plotted the PSV estimates versus the absolute values of paleolatitude in Figures 7b–7d (and similarly for Figures 8–12), but indicated the estimates corresponding to the northern and southern paleolatitudes by solid and open symbols, respectively.

Figures 7 and 8 show that applying the variable cutoff for VGP outliers (Vandamme, 1994) to the CNS data had little influence on the estimated model parameters. For the fit of Model G (Figure 7), the exclusion of outliers reduces the values of the symmetric term of the model (a) from 12.3° to 10.7°, and the antisymmetric term (b) from 0.24 to 0.21, but the differences are smaller than the 95% uncertainties of these parameters, and hence are not significant at the 95% confidence level. However, the scatter of S_b estimates relative to the model curve gets noticeably smaller when the outliers are excluded, with the RMS deviation decreasing from 5.1° to 2.8°. Similarly, for the fit of Model A in direction space (Figure 8), the exclusion of outlier data reduces the s_0 parameter from 17.9° to 15.0°, which is not significant given the estimated uncertainties, and lowers the RMS deviation from 6.3° to 3.2°. The case when the outlier data were excluded using the fixed 45° cutoff for VGPs (Figures 7c and 8c) produced Models G and A ($a = 11.1° \pm 2.6°$, $b = 0.21 + 0.06/-0.19$, $s_0 = 15.4° \pm 2.1°$) that were not distinguishable from those obtained with the variable cutoff or no cutoff.

The model fits for the Early Cretaceous-Jurassic (pre-CNS, 127–198 Ma) were more sensitive to the exclusion of outliers (Figures 9 and 10). When the Vandamme (1994) cutoff was applied, we observed a weak dependence of S_b values on latitude (Figure 9b), which is best fit by Model G with the parameters $a = 12.7° + 1.9°/-2.7°$ and $b = 0.13 \pm 0.13$. Although these values are not statistically distinguishable from the corresponding parameters for the CNS ($a = 10.7° + 2.2°/-2.4°$, $b = 0.21 + 0.05/-0.17$, Figure 6b), the difference suggests a

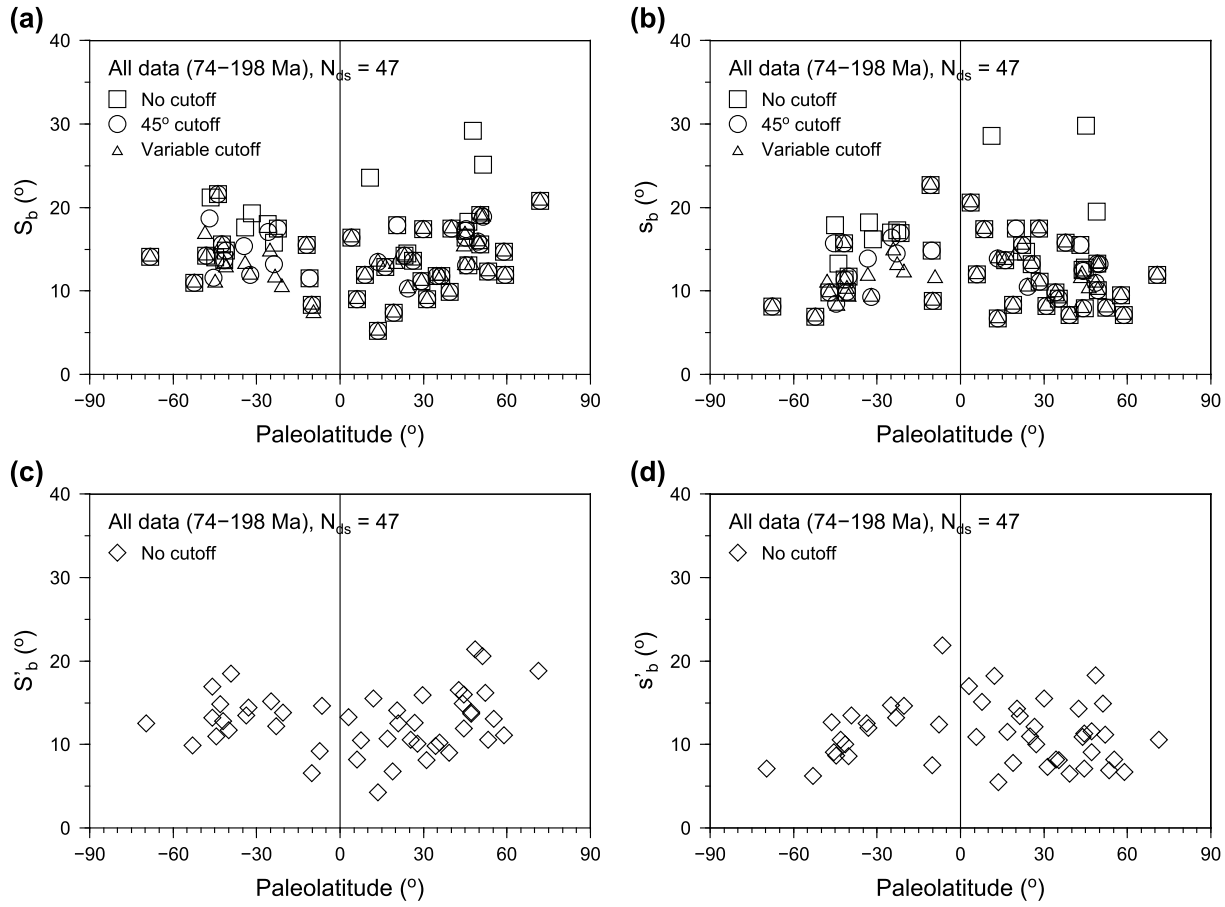

Figure 6. Paleosecular variation estimates versus paleolatitude for the entire Cretaceous-Jurassic database, which were obtained through calculations of the angular dispersion (a, b) and mean angular deviation (c, d) of virtual geomagnetic poles (a, c) and paleomagnetic directions (b, d). All estimates were corrected for within-site dispersion. The effects of applying three different cutoffs are shown in (a) and (b) (see text).

larger contribution of equatorially symmetric terms and a lower contribution of antisymmetric terms into the secular variation during the time interval preceding the CNS, which is qualitatively consistent with the results of earlier studies (Biggin, van Hinsbergen, et al., 2008; McFadden et al., 1991; Tarduno et al., 2002). In contrast, when the 45° cutoff was used (Figure 9c), or no outliers were excluded (Figure 9d), the S_b values did not show any noticeable increase with latitude, resulting in flat Model G curves ($b = 0$). The values of parameter a (14.9° for the 45° cutoff, and 15.7° for no cutoff applied) were significantly higher than the corresponding value obtained using the Vandamme (1994) cutoff. Furthermore, unlike the CNS case, the RMS misfit of the estimated S_b relative to the model did not show a systematic reduction after exclusion of outliers, being 2.9° for variable cutoff, 2.7° for the 45° cutoff, and 3.0° for no cutoff (Table 2). These observations suggest that the application of the Vandamme (1994) variable cutoff to pre-CNS data sets may have removed some scatter arising from secular variation rather than transitional or excursional fields (cf. Smirnov et al., 2011), and the most reliable estimates of the Model G parameters were obtained with the fixed cutoff (45°) applied to the data sets. The weak latitude dependence of S_b or the lack of thereof is reflected by a stronger tendency of the directional angular dispersion (s_b) to decrease with latitude, signified by higher values of the s_0 parameter compared to the corresponding values for the CNS (Figures 8 and 10). The significance of this result will be discussed in section 5.

Given the observation of a weaker latitude dependence of angular dispersion of VGPs during the Early Cretaceous-Jurassic (pre-CNS) interval compared to the superchron (Figures 7 and 9), and a correspondingly stronger latitude variation for the dispersion of field directions (Figures 8 and 10), it is interesting to see whether this result is supported by the analysis of robust estimates of PSV based on the SE distribution

Table 2
Parameters of Model G for the Latitude Dependence of PSV in Pole Space

PSV estimates	N_{ds}	a (°)	b	RMS (°)	χ^2	χ^2_{95}	$P(\chi^2_{sim} \geq \chi^2)$
Pre-CNS (127–198 Ma)							
S_b, variable cutoff	20	12.7 + 1.9/−2.7	0.13 + 0.13/−0.13	2.86	76.9	37.6	3.2E-04
S_b, fixed cutoff	20	14.9 + 1.0/−2.0	0.00 + 0.22/−0.00	2.68	53.4	35.5	3.2E-03
S_b, no cutoff	20	15.7 + 1.1/−1.9	0.00 + 0.23/−0.00	2.97	40.0	32.5	9.7E-03
S'_b no cutoff	20	13.3 + 1.0/−1.9	0.01 + 0.19/−0.01	2.37	40.4	36.6	2.8E-02
S_b, variable cutoff	9[a]	12.4 + 2.4/−4.3	0.15 + 0.17/−0.15	2.04	43.3	22.6	2.5E-03
S_b, fixed cutoff	9[a]	15.6 + 1.1/−4.2	0.00 + 0.29/−0.00	2.17	50.4	24.9	2.8E-03
S_b, no cutoff	9[a]	16.5 + 1.2/−3.4	0.00 + 0.30/−0.00	2.56	19.1	17.9	3.8E-02
S'_b, no cutoff	9[a]	13.7 + 1.1/−3.6	0.00 + 0.27/−0.00	2.03	31.4	21.9	1.1E-02
CNS (84–126 Ma)							
S_b, variable cutoff	19	10.7 + 2.2/−2.4	0.21 + 0.05/−0.16	2.79	168.0	30.2	0.0
S_b, fixed cutoff	19	11.1 + 2.6/−2.6	0.21 + 0.06/−0.19	3.16	192.1	32.3	0.0
S_b, no cutoff	19	12.3 + 3.4/−4.0	0.24 + 0.12/−0.24	5.08	295.9	45.1	0.0
S'_b, no cutoff	19	9.8 + 2.3/−2.6	0.22 + 0.07/−0.13	3.30	155.8	35.7	0.0
S_b, variable cutoff	11[a]	8.1 + 5.4/−4.7	0.26 + 0.04/−0.16	2.58	95.3	19.5	0.0
S_b, fixed cutoff	11[a]	8.2 + 5.6/−4.6	0.27 + 0.05/−0.14	2.68	98.9	19.7	0.0
S_b, no cutoff	11[a]	8.1 + 6.3/−8.1	0.32 + 0.12/−0.12	4.66	131.0	22.6	0.0
S'_b, no cutoff	11[a]	6.8 + 5.4/−6.8	0.27 + 0.08/−0.09	3.17	79.5	19.9	0.0
Post-CNS (74–83 Ma)							
S_b, variable cutoff	8	7.4 + 7.4/−4.2	0.27 + 0.09/−0.25	2.90	24.4	14.9	2.8E-03
S_b, fixed cutoff	8	7.4 + 7.4/−4.2	0.27 + 0.09/−0.24	2.90	24.4	14.9	3.1E-03
S_b, no cutoff	8	9.0 + 7.3/−6.9	0.28 + 0.14/−0.28	4.39	43.2	18.8	2.9E-04
S'_b, no cutoff	8	6.5 + 6.7/−5.9	0.26 + 0.10/−0.26	3.26	24.3	15.7	4.5E-03
S_b, variable cutoff	7[b]	11.2 + 5.2/−4.0	0.21 + 0.12/−0.21	2.60	12.1	12.8	6.3E-02
S_b, fixed cutoff	7[b]	11.2 + 5.2/−4.0	0.21 + 0.12/−0.21	2.60	12.1	12.8	6.3E-02
S_b, no cutoff	7[b]	13.9 + 4.0/−4.3	0.18 + 0.19/−0.18	3.99	19.6	14.5	1.2E-02
S'_b, no cutoff	7[b]	10.7 + 4.3/−3.9	0.19 + 0.13/−0.19	3.00	11.4	12.5	7.2E-02

Note. N_{ds} is the number of data sets used to fit the model. a and b are the Model G parameters and their uncertainties (95% confidence intervals). RMS is the root-mean-square misfit between the S_b or S'_b data and the model curve. χ^2 is the statistic for the goodness of model fit. χ^2_{95} is the upper 5% critical value for χ^2. $P(\chi^2_{sim} \geq \chi^2)$ is the probability for χ^2 to be as large or larger than the actually observed value. The values of χ^2_{95} and $P(\chi^2_{sim} \geq \chi^2)$ were estimated using Monte Carlo simulations with 10^5 synthetic data sets, zero probability values indicate that all simulations yielded $\chi^2_{sim} < \chi^2$ (see text). PSV = paleosecular variation.
[a]Only data sets with $N \geq 20$ site-mean data were used to fit the model. [b]The data set from the Yare basalts (Yi et al., 2015) suspect for undersampling of PSV was excluded.

(S'_b and s'_b), where data sets are not truncated by arbitrary cutoff angles and outlier data are treated as an integral part of secular variation (section 3.1.3). Because both angular dispersion and mean angular deviation quantify the same scatter of VGPs or field directions, we should expect them to produce similar patterns of variation with latitude, and the consistency of observed patterns based on the two alternative measures of PSV would give us higher confidence in the robustness of the obtained result.

The values of S'_b and s'_b for the CNS and pre-CNS time intervals are plotted in Figures 11 and 12, and the parameters for Models G and A fit to these data are presented in Tables 2 and 3. The S'_b estimates for the CNS show a clear increase with latitude, which is fit by Model G with the parameters $a = 9.8° + 2.3°/-2.6°$ and $b = 0.22 + 0.07/-0.13$ (Figure 11). In contrast, the S'_b values for the pre-CNS time interval do not indicate a systematic variation with latitude, resulting in a nearly flat model curve ($a = 13.3° + 1.0°/-1.9°$, $b = 0.01 + 0.19/-0.01$). The estimates of s'_b in direction space for the pre-CNS interval show a more pronounced decrease with latitude than those for the CNS (Figure 12). Overall, the model curves fit to the S'_b and s'_b data have very similar shapes compared to the curves for the angular dispersion for the two respective age intervals (CNS and pre-CNS, Figures 7–10). This consistency indicates that the difference in the patterns of latitude behavior of secular variation during the CNS (84–126 Ma) and the Early Cretaceous-Jurassic interval preceding the superchron (127–198 Ma) is a robust result and supports our suggestion that the application of the Vandamme (1994) variable cutoff has partly removed some of the signal related to normal

Table 3
Parameters of Model A for the Latitude Dependence of PSV in Direction Space

PSV estimates	N_{ds}	s_0 (°)	RMS (°)	χ^2	χ^2_{95}	$P(\chi^2_{sim} \geq \chi^2)$	r
Pre-CNS (127–198 Ma)							
s_b, variable cutoff	20	16.6 + 1.9/−1.7	2.76	67.3	33.9	2.0E-05	**−0.655 + 0.303/−0.187**
s_b, fixed cutoff	20	18.3 + 1.8/−1.7	2.87	76.4	34.3	5.0E-05	**−0.694 + 0.307/−0.164**
s_b, no cutoff	20	19.4 + 1.9/−1.8	3.10	90.2	33.8	0.0	**−0.698 + 0.322/−0.178**
S'_b, no cutoff	20	16.4 + 1.6/−1.6	2.46	57.1	35.4	1.3E-03	**−0.731 + 0.281/−0.156**
s_b, variable cutoff	9[a]	16.5 + 1.9/−1.6	1.95	28.1	17.5	2.3E-03	**−0.620 + 0.617/−0.314**
s_b, fixed cutoff	9[a]	19.0 + 2.0/−2.1	2.32	36.1	21.4	3.8E-03	−0.673 + 0.724/−0.279
s_b, no cutoff	9[a]	20.6 + 2.5/−2.7	2.96	41.9	19.9	5.4E-04	−0.644 + 0.749/−0.301
S'_b, no cutoff	9[a]	16.8 + 1.7/−1.8	2.02	31.3	18.7	2.2E-03	**−0.688 + 0.654/−0.268**
CNS (84–126 Ma)							
s_b, variable cutoff	19	15.0 + 2.0/−1.9	3.18	237.8	32.4	0.0	**−0.445 + 0.431/−0.318**
s_b, fixed cutoff	19	15.4 + 2.1/−2.1	3.37	264.4	33.2	0.0	**−0.430 + 0.415/−0.312**
s_b, no cutoff	19	17.9 + 3.8/−3.4	6.30	479.7	58.7	0.0	−0.221 + 0.440/−0.426
S'_b, no cutoff	19	14.4 + 2.2/−2.1	3.76	231.0	40.1	0.0	−0.280 + 0.455/−0.402
s_b, variable cutoff	11[a]	14.4 + 3.4/−2.8	3.43	190.9	19.3	0.0	0.110 + 0.624/−0.623
s_b, fixed cutoff	11[a]	14.7 + 3.5/−2.9	3.53	207.3	19.4	0.0	0.125 + 0.584/−0.637
s_b, no cutoff	11[a]	17.4 + 7.0/−4.7	6.94	384.2	35.7	0.0	0.192 + 0.433/−0.443
S'_b, no cutoff	11[a]	14.2 + 4.3/−3.3	4.33	196.6	23.1	0.0	0.253 + 0.433/−0.523
Post-CNS (74–83 Ma)							
s_b, variable cutoff	8	14.6 + 3.9/−3.5	3.41	47.2	14.7	0.0	0.210 + 0.602/−0.95
s_b, fixed cutoff	8	14.6 + 3.9/−3.4	3.41	47.2	14.7	0.0	0.210 + 0.604/−0.949
s_b, no cutoff	8	16.4 + 5.4/−4.5	4.73	57.1	17.3	0.0	0.101 + 0.618/−0.977
S'_b, no cutoff	8	13.7 + 4.2/−3.7	3.71	42.3	15.4	1.0E-05	0.208 + 0.574/−1.062
s_b, variable cutoff	7[b]	16.6 + 2.8/−2.2	2.19	17.0	13.5	1.5E-02	−0.319 + 0.790/−0.552
s_b, fixed cutoff	7[b]	16.6 + 2.8/−2.2	2.19	17.0	13.5	1.5E-02	−0.319 + 0.796/−0.542
s_b, no cutoff	7[b]	18.9 + 4.5/−2.9	3.52	22.6	16.7	1.2E-02	−0.338 + 0.641/−0.632
S'_b, no cutoff	7[b]	15.9 + 3.2/−2.2	2.50	12.3	14.1	9.0E-02	−0.301 + 0.694/−0.663

Note. s_0 is the Model A parameter and its uncertainty (95% confidence limits). RMS is the root-mean-square misfit between the s_b or s'_b data and the model curve. r is the Pearson correlation coefficient and its 95% uncertainties. The values of r indicating significant negative correlation between s_b or s'_b and latitude are highlighted by bold typesetting. Other parameters are as in Table 1. PSV = paleosecular variation.
[a]Only data sets with $N \geq 20$ site-mean data were used to fit the model. [b]The data set from the Yare basalts (Yi et al., 2015) suspect for undersampling of PSV was excluded.

secular variation from low-latitude to midlatitude data sets for the pre-CNS interval, producing an artificial increase of S_b values with latitude.

A small number of data sets for the Late Cretaceous interval postdating the CNS (74–84 Ma, eight data sets) and a limited distribution of paleolatitudes for these data sets resulted in large uncertainties for the model parameters that characterize the latitude variation of PSV (Figures S2–S4). These limitations make the comparison between the CNS and post-CNS intervals ambiguous. Nevertheless, we note that the apparent increase of S_b and S'_b with latitude is similar to that observed for the CNS (Figures 7 and 11). We further note that the fit of Model G is strongly influenced by a single low-latitude data set from the ~80-Ma-old basalts sampled in the Yare basin of the southern Tibet (Yi et al., 2015). This data set comprising 15 VGPs produced very low values of the angular dispersion and mean angular deviation ($S_b = 5.2°$, $S'_b = 4.3°$), which are the lowest values in the entire database, suggesting that PSV may not be fully represented in the data. The possibility that the Yare basalts have undersampled secular variation was also noted by Yi et al. (2015). If this data set is excluded, the Model G curve becomes noticeably flatter, and the parameters a and b become nearly identical to those characterizing the latitude dependence of S_b and S'_b for the CNS (red curves in Figures S2 and S4 and Table 2). Overall, our limited subset of PSV estimates does not provide evidence for any substantial difference in the behavior of secular variation during the CNS and the time interval immediately following the CNS. However, we stress that the latitude dependence suggested by our models for the post-CNS interval is not a robust result.

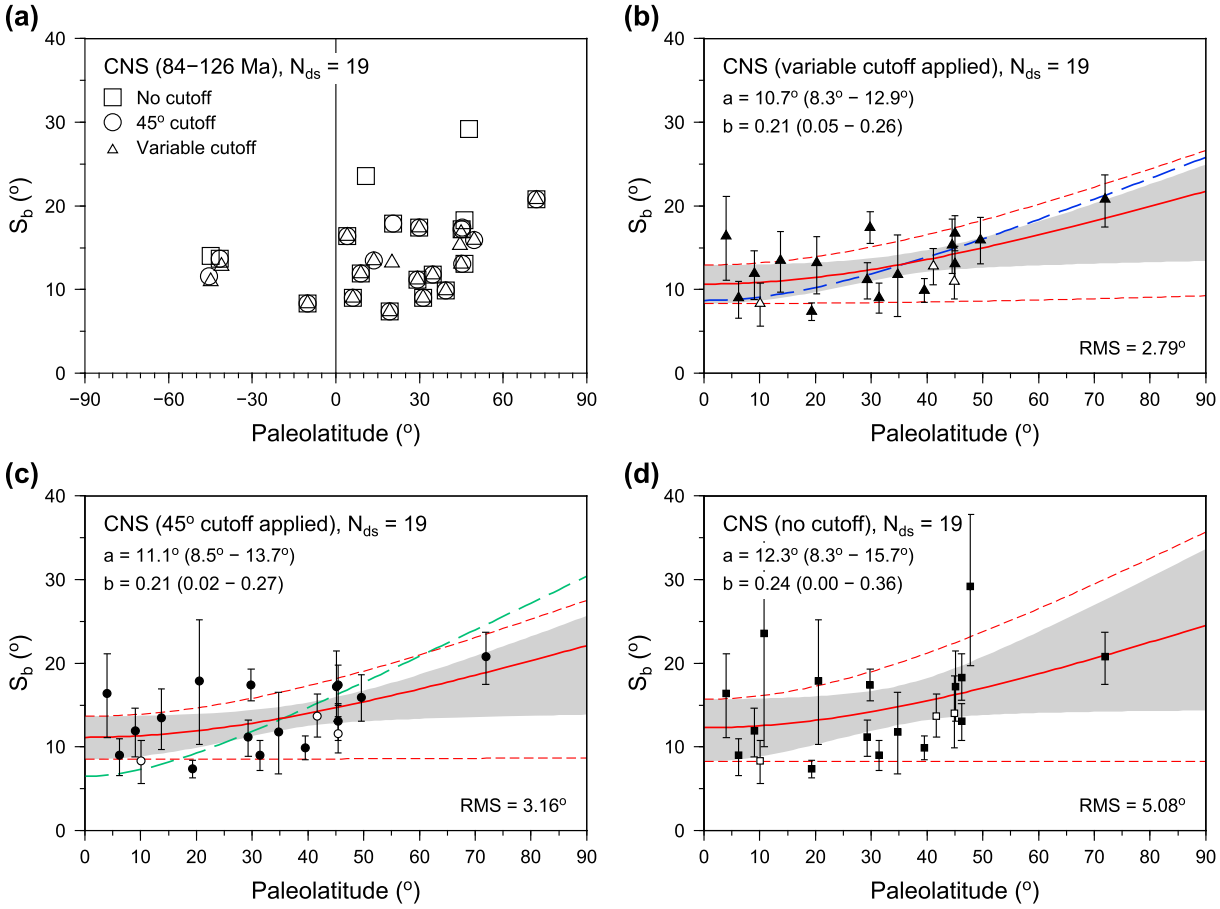

Figure 7. Latitude dependence of virtual geomagnetic pole dispersion in the CNS (84–126 Ma). The effects of three different cutoffs are shown in (a). In (b)–(d), the S_b values for the northern and southern paleolatitudes are shown by black and white symbols, respectively; the error bars show their 95% confidence intervals. Red curves are the fits of Model G (McFadden et al., 1988) to S_b data. Thin dashed red lines correspond to 95% uncertainties of the model parameters (a and b) estimated using the bootstrap method. These do not take into account the covariance of a and b and hence overestimate the 95% confidence region for the model, which is shown by the gray-shaded fields in (b)–(d) and was estimated numerically from bootstrap realizations of the model at each specific latitude. The blue dashed curve in (b) shows the Model G fit of Biggin, van Hinsbergen, et al. (2008) for their Group 1 data; the emerald green dashed curve in (c) is the Model G fit of McFadden et al. (1991) for 80–110 Ma (see text). CNS = Cretaceous Normal Superchron; RMS = root-mean-square.

4.2. Sensitivity Tests

PSV estimates derived from small data sets, and those relying on data of low technical quality, are often considered to be prone to unrecognized biases that can potentially affect the inferred patterns of latitude dependence (e.g., Biggin, van Hinsbergen, et al., 2008; Cromwell et al., 2018; Johnson et al., 2008; Tauxe et al., 2003). Here we examine whether such biases have possibly influenced the results presented in section 4.1.

An important source of bias may be related to undersampling of secular variation by data sets comprising small numbers of individual site-mean directions. The effect of the number of individual site-mean data (N) on the accuracy of S_b estimates was studied by Biggin, van Hinsbergen, et al. (2008), who showed that the errors associated with undersampling of PSV can be on the order of ±5° for data sets containing less than $N = 18$ site-means and that the confidence intervals produced for these estimates using the bootstrap method tend to be underestimated. In our compilation, approximately half of data sets contain less than 20 individual site-mean directions (the median value of N is 18 for the entire database, Figure 1b), and the S_b values derived from these data sets can be prone to the effect of undersampling. To test how these estimates influence our results, we fitted Model G curves using only S_b and S_b' estimates obtained from data sets with $N \geq 20$ (11 data sets for the CNS and 9 data sets for the pre-CNS interval; Figure 13 and Table 2). The exclusion of data sets with $N < 20$ for the CNS resulted in model curves that were steeper than the curves obtained with

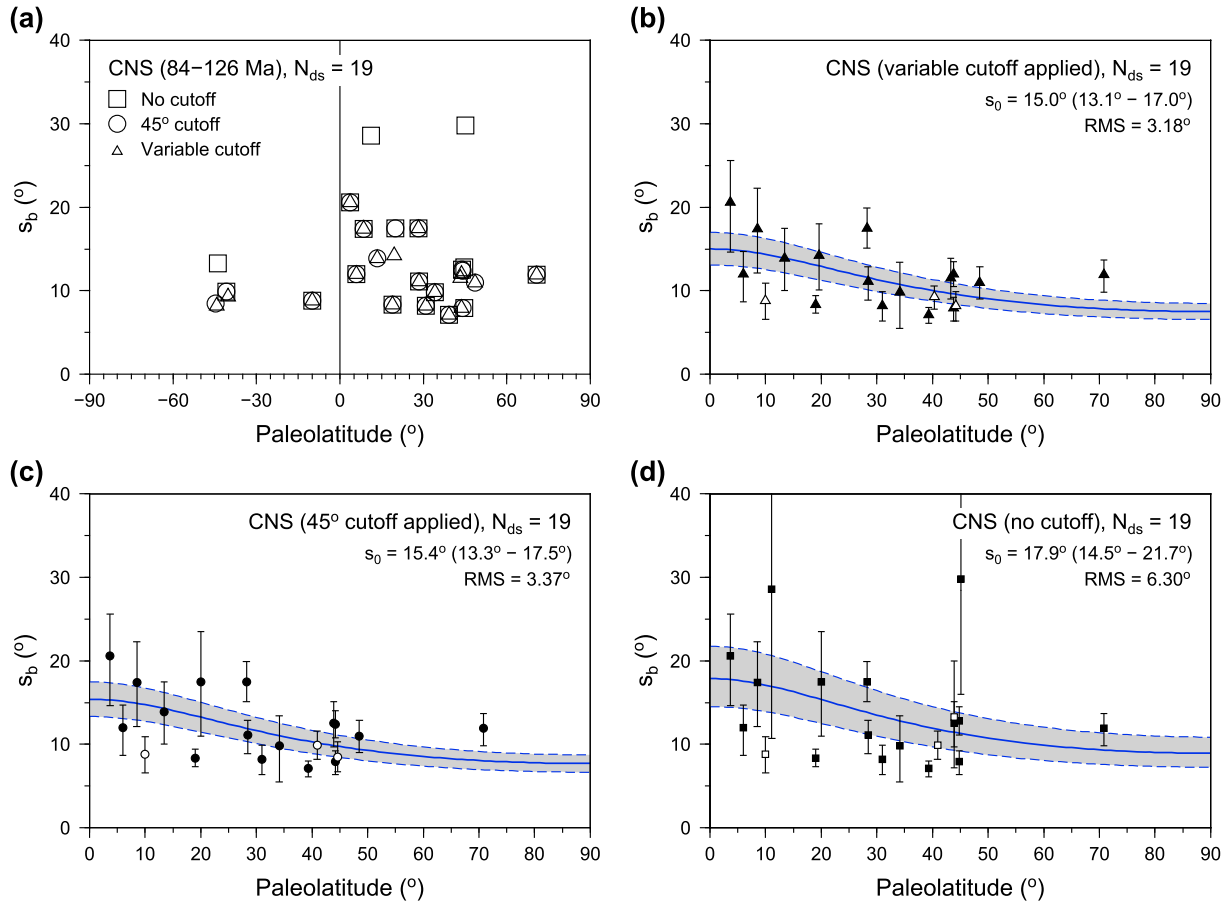

Figure 8. Latitude dependence of angular dispersion of paleomagnetic directions in the CNS (84–126 Ma). The effects of three different cutoffs are shown in (a). In (b)–(d), the s_b values for the northern and southern paleolatitudes are shown by black and white symbols, respectively; the error bars show their 95% confidence intervals. Blue curves are the fits of Model A (Irving & Ward, 1964) to s_b data. Thin dashed blue lines show the 95% confidence region for the model. CNS = Cretaceous Normal Superchron; RMS = root-mean-square.

all data sets retained, but the latter (shown by black curves in Figure 13) lie entirely within the 95% confidence limits of the models (gray-shaded envelopes in Figure 13), indicating that the exclusion of low-N data sets did not introduce a statistically significant change in model parameters. The model curves for the pre-CNS interval showed negligible changes after the exclusion of low-N data sets (Figures 13b, 13d, and 13f and Table 2). This suggests that the observed weak dependence or invariance of S_b and S_b' with paleolatitude is not an artifact of the inclusion of data sets that are more likely to have undersampled secular variation.

A further consideration is the influence of technical data quality. Studies of PSV behavior for the last 5–10 Ma (Cromwell et al., 2018; Johnson et al., 2008; Tauxe et al., 2003) applied more stringent data quality requirements than those adopted in our study (section 2). Specifically, they excluded data derived from blanket demagnetization of specimen collections (DC = 3, see Table 6.2 of McElhinny & McFadden, 2000, for definitions of DC values), site-mean directions based on measurements of less than four or five independent samples per site (n), and site-mean directions with associated values of within-site precision $k_w < 50$ or 100. To investigate how these additional site selection criteria influence our results, we performed the following tests.

First, we isolated the data sets based on stepwise demagnetization and the use of principal component analysis for defining ChRM directions (DC = 4 or 5) and fitted Model G curves to S_b and S_b' estimates derived from these data sets. Restricting the data to DC ≥ 4 reduced the number of data sets for the CNS and pre-

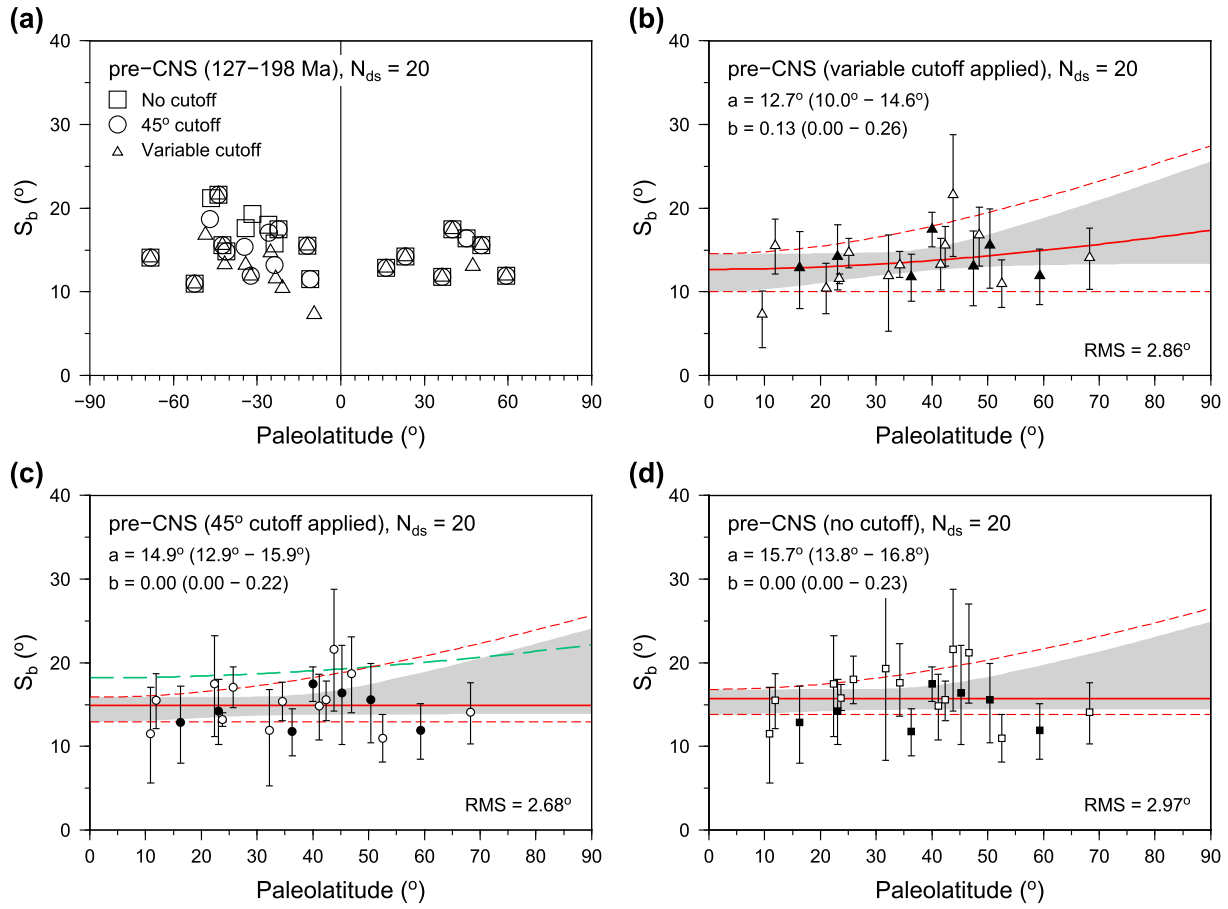

Figure 9. Latitude dependence of virtual geomagnetic pole dispersion and Model G curves for the pre-CNS interval (127–198 Ma). See the caption of Figure 7 for description. The emerald green dashed curve in (c) is the Model G fit of McFadden et al. (1991) for 110–195 Ma. CNS = Cretaceous Normal Superchron; RMS = root-mean-square.

CNS intervals from 19 to 18 and from 20 to 11, respectively. For the CNS, the changes introduced into the Model G curves by the exclusion of data with DC = 3 were negligible (Figure S5). Minor differences were observed for the pre-CNS interval, but these were not significant given the 95% confidence regions of the models. These comparisons indicate that the results of our analysis were not sensitive to the inclusion of data based on blanket demagnetization methods.

In the second experiment, we filtered the database, retaining only the site-mean data based on $n \geq 5$ individual samples, or by selecting data with $n \geq 5$ and $k_w \geq 50$ (these criteria were used by Biggin, van Hinsbergen, et al., 2008, for defining their high quality, Group 1 data sets, see section 5.1). Filtering by the value of n eliminated one data set for the pre-CNS interval and resulted in Model G curves that were similar to those obtained using all available data (Figure S6). Applying the additional requirement for within-site precision ($k_w \geq 50$) further eliminated three data sets for the CNS and five data sets for the pre-CNS interval, which resulted in slightly steeper Model G curves for the CNS and consistently flat curves for the pre-CNS period (Figure S7). However, in all cases (Figures S6 and S7), the Model G curves obtained using all available data were within the 95% confidence limits of the models constrained using more stringent site selection criteria ($n \geq 5$, or $n \geq 5$ and $k_w \geq 50$), and hence the differences between them are not statistically significant.

On the basis of these results, we conclude that the use of data sets comprising small numbers of site-level data and the inclusion of data of low technical quality have not introduced significant biases in the estimates of latitude dependence of PSV for the CNS pre-CNS intervals. Comparing the latitude patterns of S_b and S_b' for the CNS and pre-CNS intervals shown in Figures 13 and S5–S7, the difference between the two periods

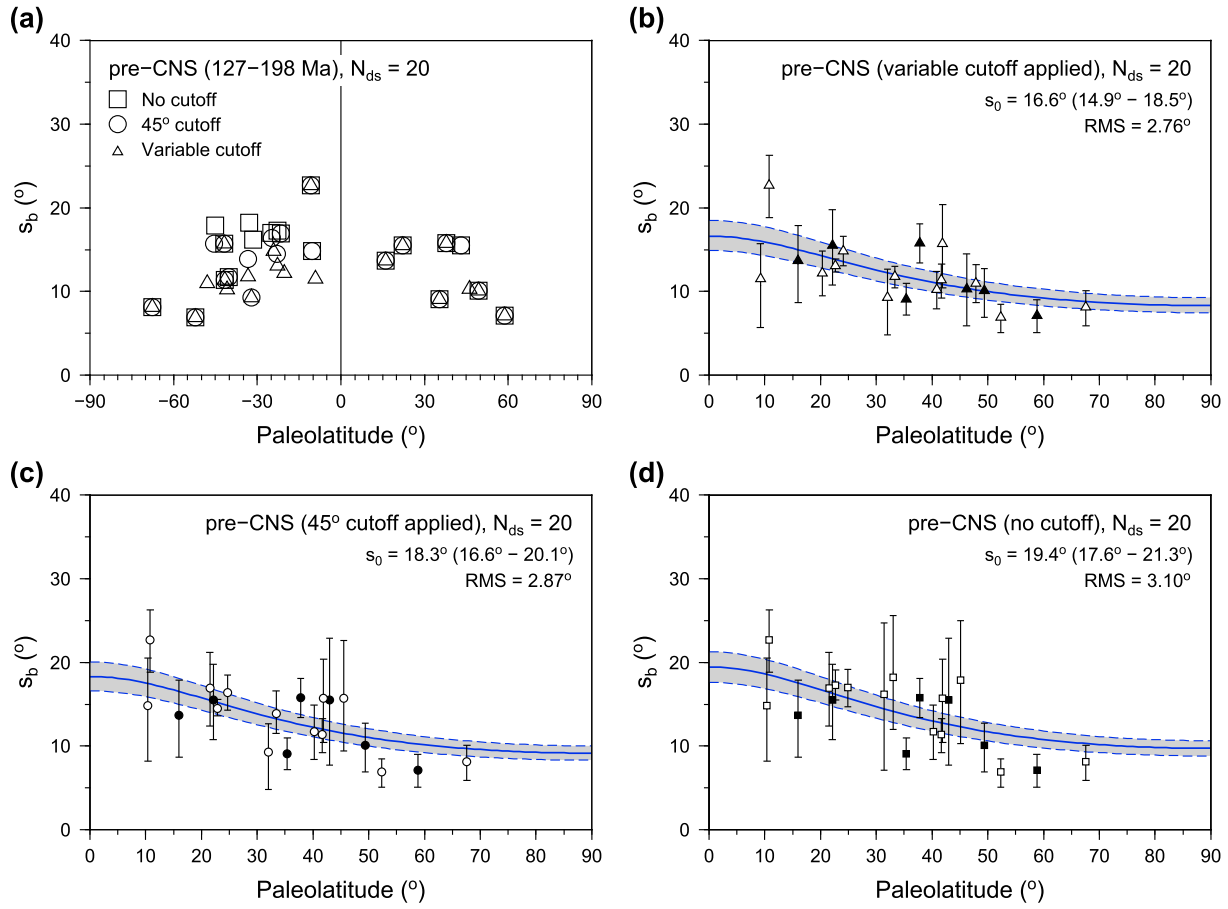

Figure 10. Latitude dependence of angular dispersion of paleomagnetic directions and fits of Model A for pre-CNS interval (127–198 Ma). See the caption of Figure 8 for description. CNS = Cretaceous Normal Superchron; RMS = root-mean-square.

comes out even more clearly than in the similar comparisons between the PSV models constrained by all available data (Figures 7 and 9). This further strengthens our conclusion that the different behavior of PSV as a function of latitude during the CNS and the preceding interval of high reversal frequency in Early Cretaceous-Jurassic time is a real geomagnetic phenomenon rather than an artifact of data selection.

5. Discussion

5.1. Comparison With Earlier PSV Studies for the Cretaceous and Jurassic

Biggin, van Hinsbergen, et al. (2008) studied PSV using data from 11 rock units formed during the CNS (84–126 Ma) and from 17 units of Jurassic age (145–200 Ma). Based on reliability, their data were divided into high (Group 1) and low (Group 2) quality data sets. Group 1 data indicated a strong latitudinal dependence of VGP dispersion for the CNS, but were inconclusive for the Jurassic, hinting at a weak, nearly latitude-invariant behavior. For the Group 2 data, both CNS and Jurassic subsets featured an increase of VGP dispersion with latitude in a nearly similar manner, which increased the authors' confidence in the results for CNS but decreased it for the Jurassic results. The highly scattered values of S_b for the Jurassic, limited to low and intermediate latitudes ($\lambda \leq 50°$), essentially preclude any meaningful definition of the latitude pattern of VGP dispersion from the Biggin, van Hinsbergen, et al. (2008) data.

When compared to the results of Biggin, van Hinsbergen, et al. (2008), our estimates for the CNS produced a somewhat weaker latitude variation of S_b (Figure 7b). Specifically, the value of parameter $b = 0.21 + 0.05/-0.17$ for Model G obtained in this study (with the variable cutoff applied, Table 2) is lower than the corresponding values of Biggin, van Hinsbergen, et al. (2008; $b = 0.27 + 0.04/-0.05$ and $b = 0.26 + 0.03/-0.04$ for

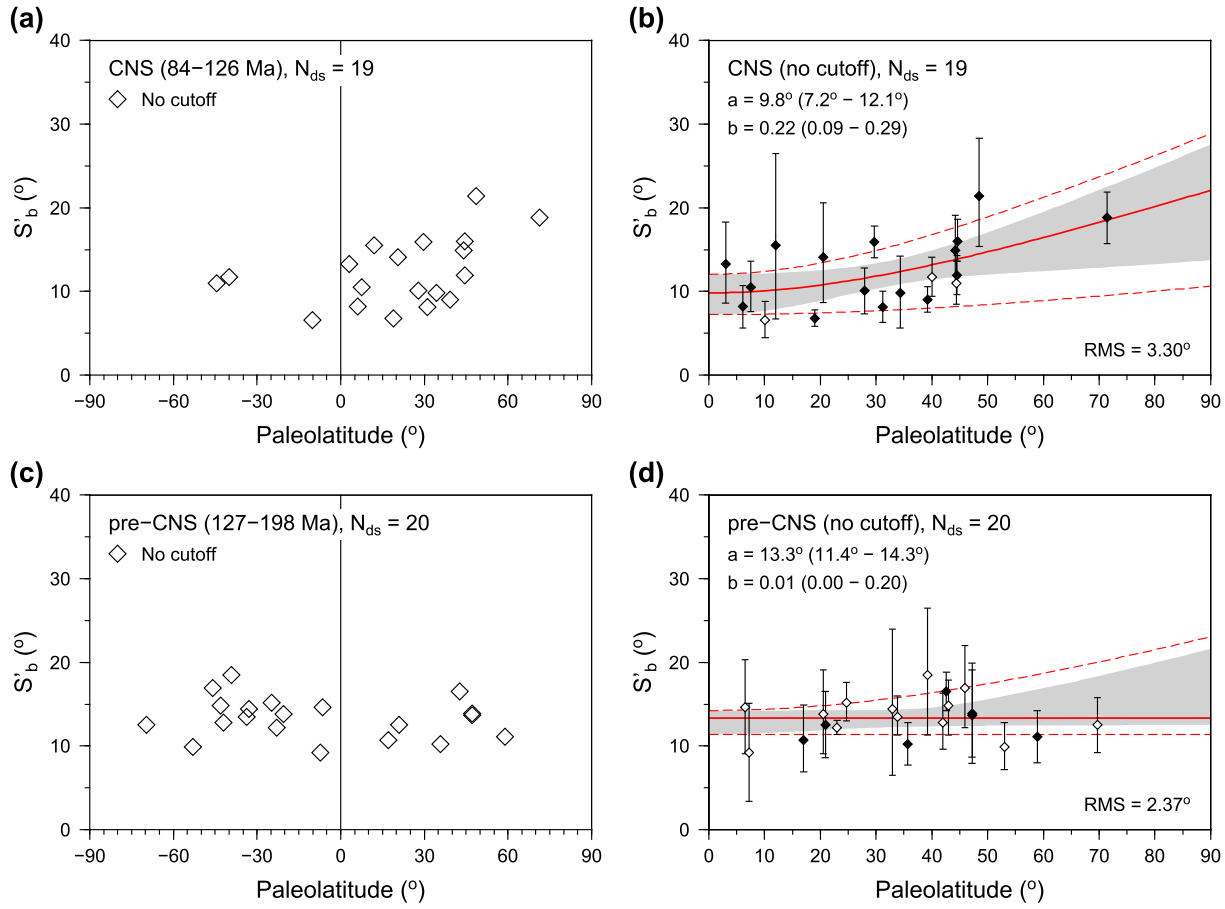

Figure 11. Latitude dependences of the mean angular deviation of virtual geomagnetic poles (S_b') for the CNS (a, b) and pre-CNS (c, d) time intervals. See the caption of Figure 7 for description. CNS = Cretaceous Normal Superchron; RMS = root-mean-square.

the Groups 1 and 2 data sets, respectively), whereas $a = 10.7° + 2.2°/-2.4°$ is slightly higher ($a = 8.7° + 2.0°/-2.4°$ for Group1 and $a = 9.9° + 1.4°/-2.1°$ for Group 2), but the differences are not statistically significant at the 95% confidence level. Because both studies used similar analytical techniques, the difference reflects the data selection criteria used (section 2) and the addition of new data that were not available to Biggin, van Hinsbergen, et al. (2008). Our database included several CNS data sets that suggest higher values of VGP dispersion at low latitudes compared to the estimates of Biggin, van Hinsbergen, et al. (2008), pulling the fit of Model G toward higher a and lower b values. Most of these low-latitude estimates come from data sets comprising $N < 20$ individual site-mean data and hence are less reliable than the estimates based on larger data sets. When these low-N data sets are excluded from the analysis, the fit of Model G ($a = 8.1° + 5.4°/-4.7°$, $b = 0.26 + 0.04/-0.17$, variable cutoff) becomes nearly identical to that obtained by Biggin, van Hinsbergen, et al. (2008) from the Group 1 CNS data sets (Figure 13a). Similarly, when the site selection criteria for the Group 1 data sets ($n \geq 5$, $k_w \geq 50$, section 4.2) are applied to our data, two low-latitude data sets are eliminated and the model fit ($a = 9.0° \pm 2.5°$, $b = 0.26 + 0.03/-0.09$, Figure S7a) becomes indistinguishable from that obtained by Biggin, van Hinsbergen, et al. (2008). The agreement between the results of our study and Biggin, van Hinsbergen, et al. (2008) suggests that the overall pattern of latitude behavior of PSV have been reliably established for the CNS.

Because Biggin, van Hinsbergen, et al. (2008) were not able to establish a clear pattern of PSV variation with latitude in the Jurassic, we cannot provide a meaningful comparison with our results for the pre-CNS interval. Yet, we point out that the scatter of our PSV estimates about the model curves for the pre-CNS interval is not higher than that for the CNS data (in fact, the RMS misfits for the pre-CNS models are slightly lower than those for the CNS, Table 2). This contrasts with the observations of Biggin, van Hinsbergen, et al. (2008) who suggested that PSV in the Jurassic could have been inherently more variable than during the CNS. Our pre-

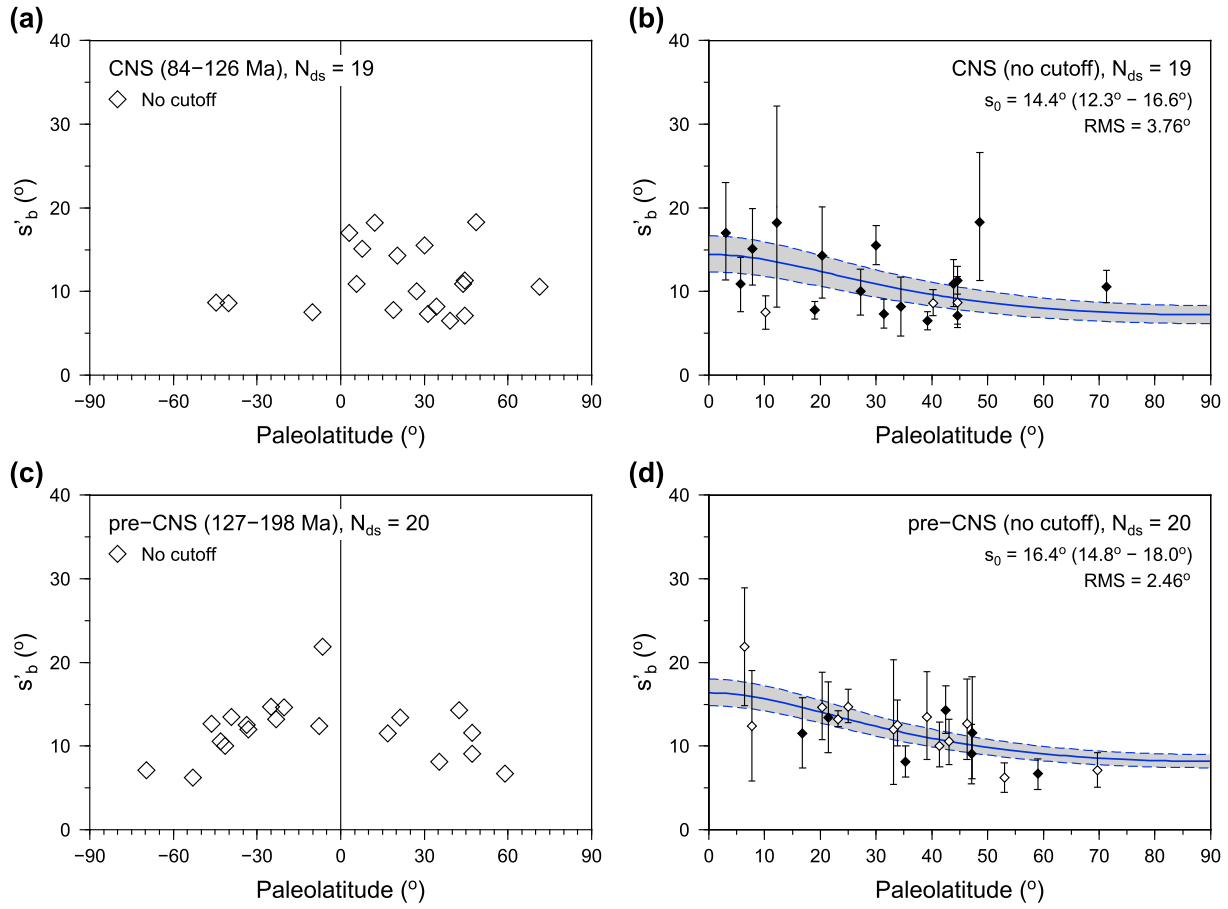

Figure 12. Latitude dependences of the mean angular deviation of paleomagnetic directions (s_b') for the CNS (a, b) and pre-CNS (c, d) time intervals. See the caption of Figure 8 for description. CNS = Cretaceous Normal Superchron; RMS = root-mean-square.

CNS data do not support this suggestion. We suspect that the stricter data selection criteria used in our study were effective in eliminating much of the noise. For information, 11 of 28 data sets used by Biggin, van Hinsbergen, et al. (2008) did not satisfy these criteria and were excluded from the analysis (section 2).

The findings of our study are in good qualitative agreement with the results of McFadden et al. (1991), which suggest a prominent increase of S_b as a function of latitude for the 80–110 Ma period and a nearly latitude-invariant behavior for the 110–195 Ma interval. However, the Model G parameters estimated by McFadden et al. (1991) for these two time intervals (a = 6.5° + 2.9°/−4.2°, b = 0.33 ± 0.05 for 80–110 Ma, and a = 18.2° ± 1.7°, b = 0.14 + 0.10/−0.14 for 110–195 Ma) differ significantly from our estimates for the CNS and pre-CNS intervals (Figures 7c and 9c). Although McFadden et al. (1991) used different age bins, we can roughly relate their 80–110 Ma fit to the CNS, and the 110–195 Ma fit to the pre-CNS interval, and the most appropriate comparison would be with the results obtained using the data set trimmed by the 45° cutoff angle since McFadden et al. (1991) applied a 40° cutoff to their VGP data. For the 80–100 Ma, the model of McFadden et al. (1991) suggests a much sharper increase of S_b from the equator to the pole than observed in our CNS data (Figure 7c), and also in the data of Biggin, van Hinsbergen, et al. (2008).

A probable source for this discrepancy was discussed by Biggin, van Hinsbergen, et al. (2008), who suggested that a stronger latitude variation of the McFadden et al. (1991) S_b estimates for 80–110 Ma may be an artifact of using a constant value for the S_w correction in pole space (see section 3) that has resulted in underestimated S_b values at low latitudes and overestimated values at high latitudes. However, this bias cannot explain the discrepancy for the pre-CNS interval, where our S_b values consistently fall below the Model G curve of McFadden et al. (1991), being lower by ~4° on average (Figure 9c). This result suggests that either our estimates of S_b were systematically biased to lower values or that the values of McFadden et al. (1991) are

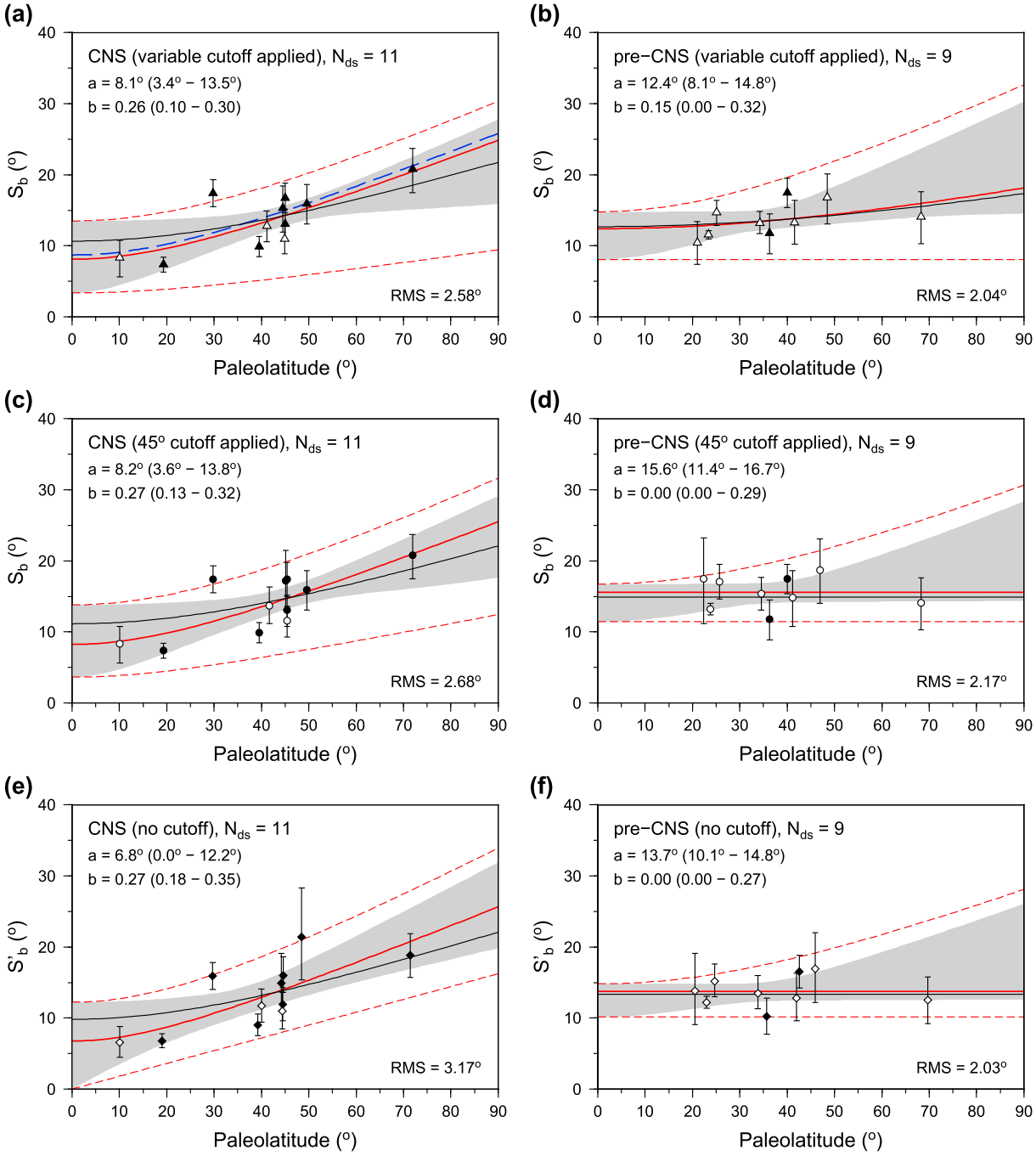

Figure 13. Model G curves for the CNS (a, c, e) and pre-CNS (b, d, f) time intervals based on virtual geomagnetic pole dispersions estimated from data sets with $N \geq 20$ individual site-mean data are shown by the red lines. Black solid curves show the fits of Model G based on all available data (i.e., including the estimates obtained from data sets with $N \geq 20$ and with $N < 20$, as in Figures 7b, 7c, 9b, 9c, 11b, and 11d). The blue dashed curve in (a) shows the Model G fit of Biggin, van Hinsbergen, et al. (2008) for their Group 1 data (see text). CNS = Cretaceous Normal Superchron; RMS = root-mean-square.

overestimates. We consider the former possibility unlikely since both the high-N and low-N pre-CNS data sets show similar values of S_b and the persistent negative bias due to undersampling of PSV can be ruled out. Other potential biases, which will be discussed in section 5.3, will tend to increase estimated S_b values, so they are not likely to impart a systematic negative bias. Thus, we argue that secular variation during the pre-CNS interval was lower than that suggested by the estimates of McFadden et al. (1991), and the overall level of PSV was compatible with the field variability in the CNS.

5.2. Is the Latitude Dependence of PSV a Mathematical Artifact?

Linder and Gilder (2012) suggested that the latitude dependence of angular dispersion of VGPs originates from a geometrical aberration of the conversion of paleomagnetic directions to poles. This suggestion was based on the analysis of secular variation recorded by geomagnetic observatories over 26 years (from 1981 to 2006), which showed that the Fisher precision parameter for directions (k), and hence the angular dispersion (s) for these historical data, do not show a clear dependence on geomagnetic latitude. However, a 26-year record is substantially shorter than typical time scales for the analysis of PSV, and it remains unclear whether the implied invariance of angular dispersion in direction space is a viable hypothesis for describing the long-term signal of secular variation. If it were the case, we would always expect the dispersion of VGPs to increase with latitude in the manner approximated by equation (4) (Cox, 1970), that is, for any time interval we would expect a ~2.5-fold increase of S_b from the equator to the pole. This is not supported by the comparison of S_b estimates for the CNS and pre-CNS time intervals (Figures 7 and 9).

The patterns of angular dispersion in direction space (Figures 8 and 10) suggest a decrease of s_b with the increasing latitude, which is qualitatively consistent with Model A of Irving and Ward (1964). The decrease is prominent in the data for the pre-CNS interval (127–198 Ma), but less clear for the CNS (84–126 Ma). To test whether this decrease is significant, we calculated values of Pearson correlation coefficient, defined as

$$r = \frac{\sum_{i=1}^{N_{ds}} \left(\lambda_i - \overline{\lambda}\right)\left(s_{bi} - \overline{s_b}\right)}{\sqrt{\sum_{i=1}^{N_{ds}} \left(\lambda_i - \overline{\lambda}\right)^2} \sqrt{\sum_{i=1}^{N_{ds}} \left(s_{bi} - \overline{s_b}\right)^2}}, \tag{19}$$

where N_{ds} denotes the number of s_{bi} estimates for the selected time interval (number of data sets), λ_i is the paleolatitude, and $\overline{s_b}$ and $\overline{\lambda}$ are the mean values of s_{bi} and λ_i, respectively. The distribution for r was estimated by resampling the (λ_i, s_{bi}) data using nonparametric bootstrap with replacement, and its 95% confidence limits were calculated as the 2.5th and 97.5th percentiles of the resampled r values. When the value of $r = 0$ was within the 95% confidence interval, we concluded that the correlation between s_b and latitude was not significant. Otherwise, we deemed the correlation significant, indicating that the hypothesis of latitude invariance of s_b should be rejected at the 5% probability level. Similar tests were made for s_b' estimates. The values of correlation coefficient are given in Table 3.

As we expected, the r values for the pre-CNS time interval indicated a strong ($r \approx -0.7$) and statistically significant negative correlation between s_b and s_b' and latitude. Similar values were obtained in tests where we excluded the estimates based on data sets with $N < 20$ site-mean directions. In this case, the significance of correlation could be established only for s_b estimates obtained from data sets trimmed with the variable cutoff angle (Vandamme, 1994) and s_b' values due to a smaller number of data sets resulting in wider confidence intervals for r (Table 2). Nevertheless, we consider that the consistency of results and preponderance of statistically significant tests provide strong evidence against the latitude invariance of PSV in direction space. In contrast, the r values for the CNS (84–126 Ma), ranging from approximately −0.2 to −0.4, suggested only a weak negative correlation and were more sensitive to the treatment of outliers. A significant negative correlation was observed for the s_b estimates from data sets in which the site-mean directions corresponding to VGPs outside the Vandamme (1994) or fixed cutoff angles were excluded (Table 2), whereas the s_b and s_b' data based on untrimmed data sets showed weaker correlation that was not significant at the 5% level. When the small-sample data sets ($N < 20$) were removed from computation, the r values suggested a very weak positive correlation, but the implied increase of s_b and s_b' with latitude was clearly not significant and is likely to be an artifact of the small number of data sets used in calculation. Similarly, the tests for the post-CNS interval were not conclusive, suggesting insignificant correlation, with the nominal r values being low in absolute value and either positive or negative, depending on whether the s_b and s_b' estimate from the Yare basalts suspect to be biased by undersampling of secular variation (see discussion in section 4.1) was included or not.

Given a weak latitude dependence of secular variation in direction space during the CNS, the increase of S_b and S_b' in pole space (Figures 7 and 11b) could be considered to result from the conversion of paleomagnetic directions to VGPs, as was suggested by Linder and Gilder (2012). But this is not the case for the pre-CNS interval where the strong decrease of s_b and s_b' with latitude is counterbalanced by the modulation arising from the direction-to-pole conversion, resulting in S_b and S_b' values that are nearly invariant with latitude

(Figures 9 and 11d). Thus, we conclude that while it may be reasonable to describe secular variation as latitude-invariant scatter of field directions for some intervals in the geologic past, this invariance is not a universal property of the geomagnetic field, and treating the latitude dependency of VGP dispersion as a pure mathematical artifact is an oversimplification. A similar conclusion was reached by Veikkolainen and Pesonen (2014), who showed that the latitude invariance of angular dispersion in direction space is not supported by PSV data for the Precambrian.

On a more general note, the analysis of PSV in direction space has a clear advantage in that it does not introduce any artificial latitude dependence resulting from the conversion of directions to VGPs. Yet, if the modulation of angular dispersion by this geometric transformation is clearly understood and taken into consideration, it would be unreasonable to argue that the analysis of PSV in direction space could offer us better insights into the underlying geodynamo processes. Historically, the choice of using the dispersion of VGPs rather than directions was motivated by the property of the VGP scatter arising from variations in degree-1 terms of geomagnetic potential (dipole wobble) to be latitude invariant. Early PSV models that sought to separate the contributions from dipole and nondipole fields made use of this property (a brief discussion of these models is provided by McFadden & McElhinny, 1984). Later models (e.g., Model G of McFadden et al., 1988) followed the approach and were designed to parameterize the latitude dependency of PSV measured by the angular dispersion of VGPs, linking the latitude patterns to the properties of geodynamo. To make use of these developments, we will now turn to the discussion of the latitude patterns of PSV in pole space.

5.3. Applicability of Model G for Describing the Latitude Behavior of PSV

The results presented in section 4 suggest that secular variation of the geomagnetic field during the CNS (84–126 Ma) and the preceding pre-CNS interval (127–198 Ma) produced different patterns of VGP dispersion as a function of latitude. For the CNS, we observed a distinctly stronger tendency for S_b to increase with increasing latitude (Figure 7), as compared to the pre-CNS estimates, which showed a much weaker or insignificant increase depending on the applied cutoff (Figure 9). This result was further supported by the analysis of robust estimates of PSV ($S_b^{'}$) that showed a similar difference (Figure 11). In terms of the shape parameters of Model G of McFadden et al. (1988), the disparity between the CNS and pre-CNS intervals suggests higher variability of equatorially symmetric spherical harmonics of the geomagnetic potential (a) and lower variability of antisymmetric terms (b) during the pre-CNS interval, which is qualitatively consistent with the results of McFadden et al. (1991). However, very low values of b for the pre-CNS subset (nominally, $b = 0$ when the 45° cutoff or no cutoff was applied to the data, Figures 8c and 8d) are conceptually inconceivable as this would imply the lack of variation in antisymmetric terms. This may point to the inadequacy of Model G for explaining the latitude dependence of VGP dispersion.

In that regard we recall that the simple functional form of Model G (equation (17)) was suggested by McFadden et al. (1988) from the analysis of the "equivalent" VGP dispersion of the present geomagnetic field, which reflects the departures of the instantaneous field from that of the GAD along a line of geographic latitude. After computing equivalent VGP dispersions from the IGRF65 model (the International Reference Geomagnetic Field model for the epoch of 1965) for different latitude bands and splitting them into the contributions associated with the equatorially symmetric and antisymmetric terms (S_s and S_p, respectively), they observed that the S_s term was nearly constant ($S_s \approx a$), whereas S_p could be well approximated by a linear function ($S_p = b\lambda$). A close similarity between the latitude dependence of VGP dispersion for the past 5 Ma and that observed for the equivalent VGP scatter led McFadden et al. (1988) to suggest that the latitude variation deduced from the present field may be typical for the behavior of PSV in the geologic past. This is how Model G was born, and the validity of its underlying assumptions (the invariance of S_s and the linearity of S_p with latitude) received little attention in the following work (e.g., McElhinny & McFadden, 1997; McFadden et al., 1991). However, neither the latitude invariance of S_s nor the linearity of S_p is a general property related to the symmetry of the spherical harmonics forming the two families; the only symmetry constraint is that $S_p = 0$ at the equator. Hulot and Gallet (1996) showed that the equivalent VGP scatter curves for earlier historical epochs (1800 and 1900) were significantly different from the curve for the 1965 or 1980 field models. They also showed that interactions between different spherical harmonics may lead to VGP dispersion curves with shapes that do not conform to that implied by Model G, including the curves that do not show an appreciable latitude increase of VGP dispersion, or even decreasing dispersion

at high and intermediate latitudes. We also note that some numerical geodynamo models operating in a regime of high reversal frequency (e.g., Glatzmaier et al., 1999) produced VGP dispersion curves that were nearly invariant with latitude (see Figure 1 of Biggin, van Hinsbergen, et al., 2008, and discussion therein), which is in qualitative agreement with our results for the pre-CNS interval.

It should be clear from the preceding discussion that one should be cautious when interpreting the parameters of Model G in terms of contributions arising from variations in equatorially symmetric and antisymmetric spherical harmonics, and even greater care should be taken when expressing findings in terms of partitioning between the corresponding dynamo families. Although theoretically plausible, the separation or independence of the symmetric and antisymmetric dynamo families requires specific symmetry conditions (see Merrill & McFadden, 1988, for discussion) and is not likely in strong-field Earth-like dynamos because the coupling between the convective motions in the liquid core and magnetic field would necessarily result in members of one family affecting members of the other family (McFadden et al., 1991). That said, from the modeling perspective, there is nothing wrong with using Model G in a descriptive sense unless the data clearly suggest a pattern of latitude variation precluded by the model (e.g. a decrease of S_b with latitude), which is not the case for our estimates of VGP dispersion in the Cretaceous and Jurassic.

This brings us to the question of how well Model G fits the data. The PSV estimates for the CNS and pre-CNS intervals show a considerable scatter about the model curves, with many estimates significantly departing from model predictions (Figures 7 and 9). If the model provides an accurate description of the latitude dependency of PSV, we would expect the mismatches between the model curve and the individual estimates of VGP dispersion to have the character of random noise that could be explained by uncertainties in the data. To test this, we evaluated the goodness of fit by calculating values of χ^2 statistic, defined as

$$\chi^2 = \sum_{i=1}^{N_{ds}} \frac{(S_{bi} - S_b(\lambda_i))^2}{\sigma_i^2}, \tag{20}$$

where N_{ds} denotes the number of individual S_{bi} estimates used to fit the model, $S_b(\lambda_i)$ is the model prediction, and σ_i^2 is the variance for S_{bi} estimated using the bootstrap method (given in Tables S2.1–S2.3). The distribution of χ^2 under the hypothesis that the model is correct and the observed misfits originate solely from random data errors was estimated using Monte Carlo simulations (Press et al., 1992), in which we generated 10^5 synthetic samples of (λ_i, S_{bi}) data by randomly drawing S_{bi} values at each latitude λ_i from a normal distribution with the mean prescribed by the model ($S_b(\lambda_i)$) and the variance equal to σ_i^2. For each simulation, we fitted a Model G curve to the synthetic data and calculated the χ^2 statistic relative to that curve, which we will denote as χ^2_{sim} to avoid confusion with χ^2 for the model fitted to the original data. The upper critical value for χ^2 (χ^2_{95}, 5% significance level) was calculated as the 95th percentile of the χ^2_{sim} distribution, and the probability of obtaining χ^2 equal to or greater than the observed value was estimated as the number of simulations with $\chi^2_{sim} \geq \chi^2$ divided by the total number of simulations. In cases when χ^2 exceeded the critical value, or, equivalently, the probability was less than 0.05, we concluded that the model did not provide a statistically acceptable fit to the data.

In all tests for the CNS and pre-CNS intervals, the χ^2 values were substantially larger than the corresponding critical values (χ^2_{95}) and the estimated probabilities were below the 5% threshold (Table 2), indicating significant misfits that cannot be explained by the uncertainties of PSV estimates. These results, however, do not necessarily invalidate Model G because we should take into account the possibility that the latitude patterns of PSV can vary over time when analyzing data that cover periods of several tens of millions of years, such as the CNS and pre-CNS intervals. If temporal variations are substantial, the model should no longer be expected to provide an adequate description of the observations. In addition, we should also allow for possible systematic biases in PSV estimates that are not reflected in their confidence intervals.

The possible bias related to undersampling of secular variation by data sets comprising small numbers of individual site-mean data has already been discussed in section 4.2. The goodness of fit tests for the models constrained by data sets with $N \geq 20$ (Figure 13), which are not likely to suffer from undersampling of PSV, showed the χ^2 values exceeding the critical values (Table 2), suggesting that the use of PSV estimates derived from small data sets is not a likely cause for the unacceptable misfits of Model G for the CNS and pre-CNS intervals. Other possibilities for abnormally high variability of the PSV estimates with respect to the model may include systematic errors in measurements of the paleohorizontal at sampling sites (these are generally

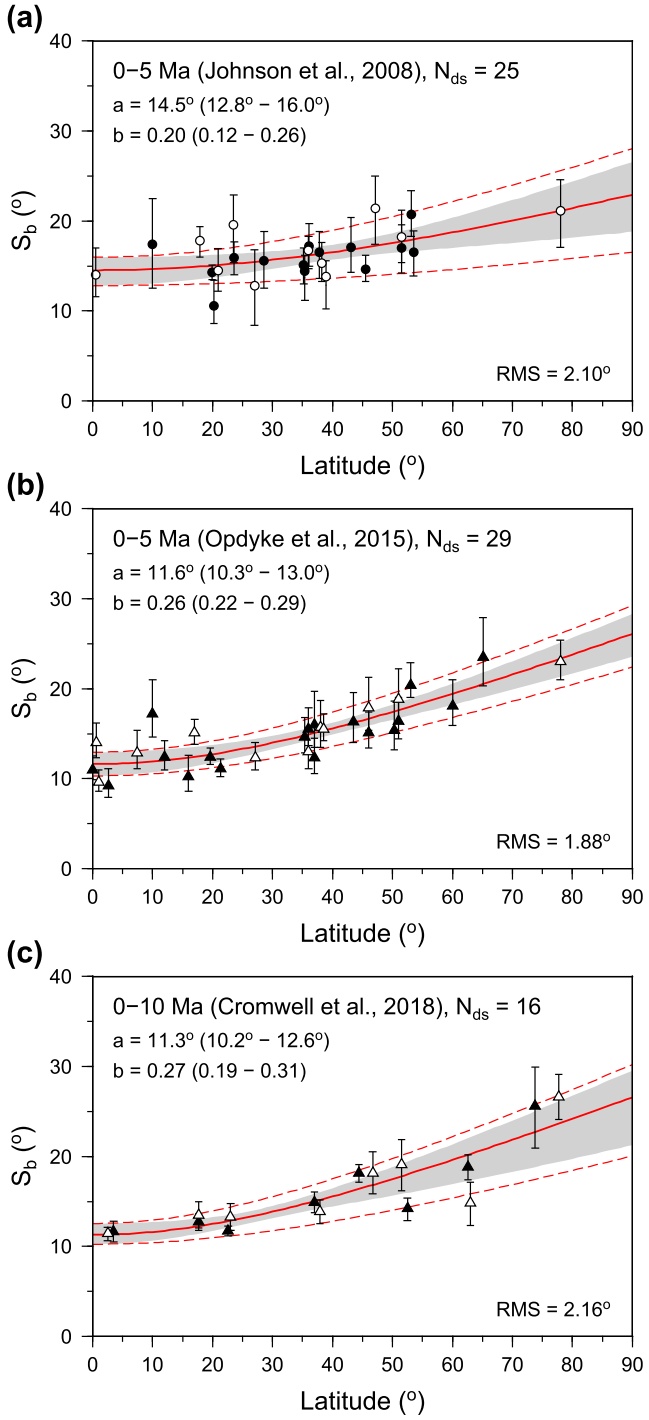

Figure 14. Latitude dependence of virtual geomagnetic pole dispersion and Model G curves for 0–5 Ma and 0–10 Ma. The S_b estimates are from the compilations of (a) Johnson et al. (2008), (b) Opdyke et al. (2015), and (c) Cromwell et al. (2018). RMS = root-mean-square.

considered to be small and not likely to bias S_b values by more than 1–2°, see discussion in Biggin, van Hinsbergen, et al., 2008), and the original dips of volcanic rocks (e.g., lava flows) deposited on geographic slopes that were mistakenly treated as post-emplacement tectonic tilts. Although we made a considerable effort to exclude the data sets that could have been affected by these biases, we cannot guarantee that our PSV estimates for the Cretaceous and Jurassic are completely free of these errors. Given this uncertainty, it is instructive to consider whether Model G provides an accurate description for the high-quality PSV estimates derived from geologically recent lavas (e.g., 0–5 Ma), which are not likely to be affected by these biases.

In Figure 14, we plot the Model G curves fitted to the S_b estimates from three recent compilations of paleomagnetic data for 0–5 Ma lavas (Johnson et al., 2008; Opdyke et al., 2015) and 0–10 Ma lavas (Cromwell et al., 2018). These S_b values are unlikely to be affected by undersampling of PSV because they were derived from large data sets (the median values of N are 43 for the compilation of Johnson et al., 2008, 53 for Opdyke et al., 2015, and 121 for Cromwell et al., 2018). Johnson et al. (2008) and Opdyke et al. (2015) obtained their estimates from VGP data sets corresponding to separate localities, using the fixed (45°) and variable (Vandamme, 1994) VGP cutoffs, respectively. Cromwell et al. (2018) calculated VGP dispersions from data sets that combined VGPs from sites located in 10° latitude bands, which was similar to the approach of McElhinny and McFadden (1997). For the purpose of comparison, we chose to use the S_b values derived from the PSV10$_{vcut}$ subset of the Cromwell et al. (2018) database (Figure 14c), in which the outlier VGPs were removed using the variable cutoff.

The parameters of Model G and the χ^2 statistics for the goodness of model fit are presented in Table 4. Although the scatter of the S_b estimates about the model curves (RMS values in Table 4) was notably smaller than for the CNS and pre-CNS data sets, the values of χ^2 were greater than χ^2_{95} for all models, indicating that Model G does not provide a statistically acceptable fit to the S_b data for 0–5 Ma (Johnson et al., 2008; Opdyke et al., 2015) and for 0–10 Ma (Cromwell et al., 2018). Furthermore, because 93% of data in the PSV10 database of Cromwell et al. (2018) come from rocks that are not older than 5 Ma, we should expect similar patterns of latitude dependence for the three S_b data sets. However, while the models based on the estimates of Opdyke et al. (2015) and Cromwell et al. (2018) are in agreement, the model based on the Johnson et al. (2008) data suggests a weaker latitude dependence, and the difference is significant, at least with regard to the parameter a (Figure 14 and Table 4). The difference can be partly explained by the different cutoffs applied to the VGP data sets, and is likely related to the paucity of low-latitude data sets in the compilation of Johnson et al. (2008). The equatorial intercept (a) of the model curve for the Johnson et al. (2008) data (Figure 14a) is essentially controlled by the two low-latitude PSV estimates from Costa Rica (S_b = 14°, Cromwell et al., 2013; Johnson et al., 2008) and Ecuador (S_b = 17.2°, Opdyke et al., 2006). Data subsequently collected from other localities within 10° of the equator (Gromme et al., 2010; Kent et al., 2010; Opdyke et al., 2010, 2015) showed somewhat lower values of VGP dispersion (S_b < 13°, Figure 14b), which led Opdyke et al. (2015) to suggest that the results from Costa Rica and Ecuador may have been affected by unrecognized tectonic disturbances (tilting) in these actively deforming regions, resulting in artificially higher dispersion than expected on the basis

Table 4
Parameters of Model G for 0–5 and 0–10 Ma

PSV estimates	N_{ds}	a (°)	b	RMS (°)	χ^2	χ^2_{95}	$P(\chi^2_{sim} \geq \chi^2)$
S_b, fixed cutoff, 0–5 Ma (Johnson et al., 2008)	25	14.5 + 1.5/−1.7	0.20 + 0.06/−0.08	2.10	69.4	38.1	6.0E-05
S_b, variable cutoff, 0–5 Ma (Opdyke et al., 2015)	29	11.6 + 1.4/−1.3	0.26 + 0.03/−0.04	1.88	103.5	41.3	0.0
S_b, variable cutoff, 0–10 Ma (Cromwell et al., 2018)	16	11.3 + 1.3/−1.1	0.27 + 0.04/−0.08	2.16	107.6	27.6	0.0

Note. PSV = paleosecular variation; RMS = root-mean-square.

of the results from tectonically quiescent low-latitude sites. Because Opdyke et al. (2015) and Cromwell et al. (2018) included the Johnson et al. (2008) data in their compilations, and because their results suggest very similar patterns for the latitude behavior of PSV, we consider that the work of Opdyke et al. (2015) and Cromwell et al. (2018) supersedes the results of Johnson et al. (2008).

The statistically unacceptable misfits suggest that the VGP dispersion during the last 5–10 Ma was inherently more variable compared to the smooth latitude trend implied by Model G. Nevertheless, we can treat Model G as a useful approximation for the overall trend of latitude dependence in VGP scatter over the considered time interval, even though the model does not provide an accurate description for the data in the statistical sense. From this perspective, the scatter about the model curve unexplained by the data uncertainties can be considered to reflect the variability in the latitude pattern of PSV within the time interval for which the model was defined and its possible variations with longitude that Model G is not capable to capture. The same philosophy can be equally applied to the interpretation of Model G curves derived from the analysis of our Cretaceous and Jurassic PSV estimates.

With this caveat in mind, and clearly recognizing the limitations of Model G, we will now discuss how the long-term temporal changes in latitude signatures of PSV could relate to the stability of the geomagnetic field manifested by changes in frequency of magnetic reversals.

5.4. Latitude Behavior of PSV and the Stability of Geodynamo

In Figure 15, we compare the estimates of Model G parameters (a, b, and their ratio b/a) available from the literature for different intervals from Carboniferous to recent time (Biggin, van Hinsbergen, et al., 2008; Cromwell et al., 2018; de Oliveira et al., 2018; Johnson et al., 2008; McFadden et al., 1991; Opdyke et al., 2015) with the results obtained here. Among these studies, only the recent work of de Oliveira et al. (2018) has not been already discussed. This study provided estimates of VGP dispersion for the long interval of dominantly reverse geomagnetic polarity spanning Late Carboniferous through Late Permian time, the PCRS (~262–318 Ma). The results suggested that secular variation during the PCRS was characterized by a strong increase of VGP scatter with latitude, which can be described by a Model G curve with the parameters $a = 9.4° + 1.5°/-1.9°$ and $b = 0.27 + 0.02/-0.05$ (based on nine data sets from igneous rocks that de Oliveira et al., 2018, considered the most reliable). These values are similar to those obtained by Biggin, van Hinsbergen, et al. (2008) and are compatible with our estimates for the CNS. We note that de Oliveira et al. (2018) did not correct the S values for the within-site scatter. After correcting their values for S_w (available for eight of nine data sets), we obtained $a = 9.3°$ and $b = 0.21$, which are close to our estimates for the CNS.

The consistent behavior of PSV during the CNS and PCRS suggests that a strong increase of VGP dispersion with latitude may be a characteristic feature of a geodynamo operating in a regime when geomagnetic reversals are suppressed. By the same rationale, it may be tempting to assume that a weak or absent latitude dependence observed for the pre-CNS interval is a fingerprint of a frequently reversing field, but this is not supported by the PSV estimates for 0–5 and 0–10 Ma (Figure 14). The average reversal rate over the last 5–10 Ma (4.4–4.8 Myr^{-1} according to the polarity time scale of Ogg, 2012) was similar to that during the pre-CNS interval (~4.6 Myr^{-1}), and yet the PSV data from most recent compilations of Opdyke et al. (2015) and Cromwell et al. (2018) show a clear increase of VGP dispersion with latitude (Figures 14b–14c). Furthermore, given the uncertainties of model parameters and the scatter of S_b values, we cannot say that the latitude patterns for the last 5–10 Ma and for the CNS differ significantly (Figures 7 and 14b–14c). Thus, we conclude that a latitude-invariant VGP dispersion curve is not a reliable indicator of a

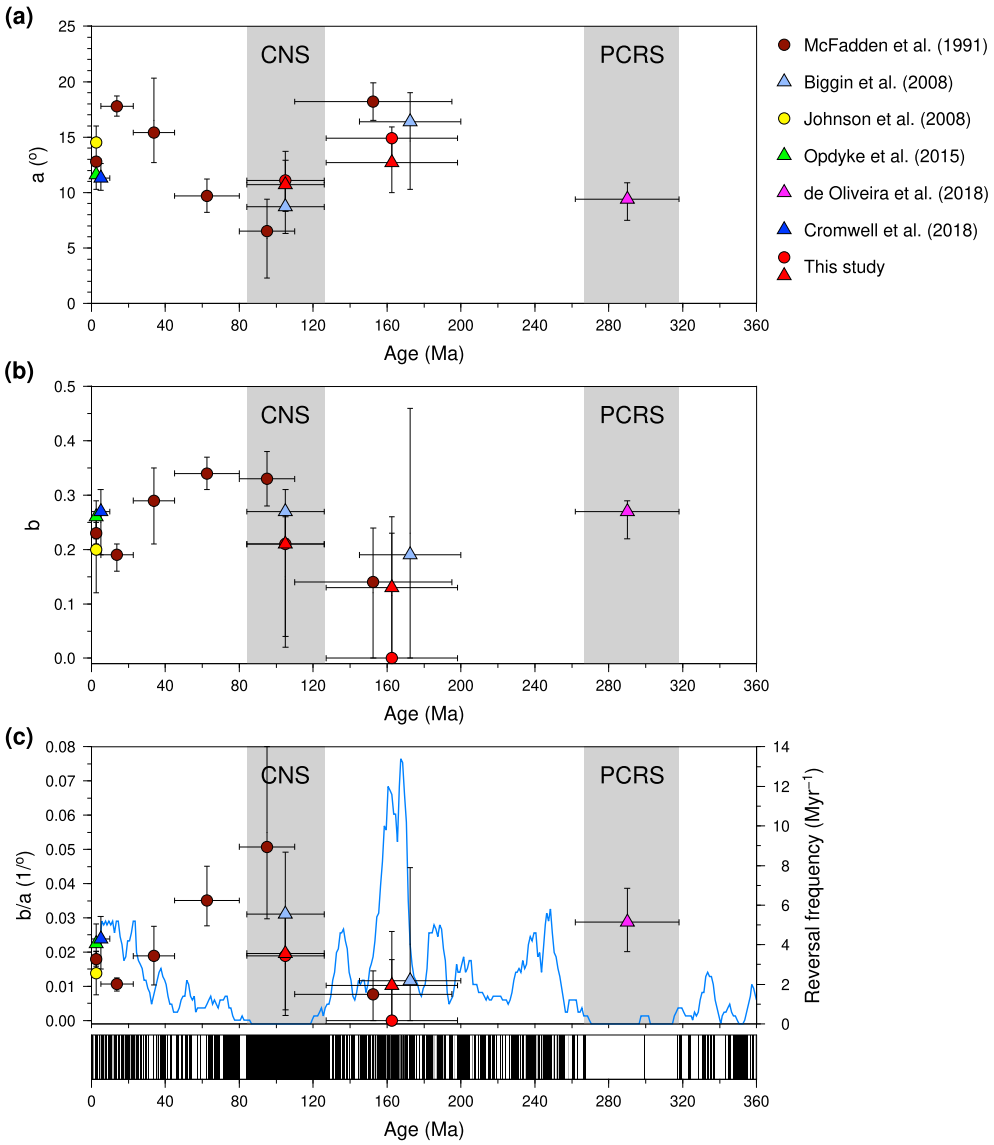

Figure 15. Variations in Model G parameters estimated in this study and previously published studies of paleosecular variation for Carboniferous through 0–5 Ma (Biggin, van Hinsbergen, et al., 2008; Cromwell et al., 2018; de Oliveira et al., 2018; Johnson et al., 2008; McFadden et al., 1991; Opdyke et al., 2015). Triangles show the parameters obtained by fitting paleosecular variation estimates derived from virtual geomagnetic pole data sets truncated by the variable cutoff angle (Vandamme, 1994); circles show the corresponding estimates based on data sets trimmed by a fixed (40° or 45°) cutoff angle. The "barcode" diagram below (c) shows the geomagnetic polarity time scale (Gradstein et al., 2012), black bars corresponding to the normal polarity, and white bars corresponding to the reverse polarity. The blue curve in (c) shows the average reversal frequency calculated with a 5 Ma sliding window. CNS = Cretaceous Normal Superchron; PCRS = Permo-Carboniferous Reverse Superchron.

frequently reversing field, and similarly, a prominent increase of VGP dispersion with latitude is not restricted to the time intervals when geomagnetic reversals are rare or absent.

Merrill and McFadden (1988) developed a conceptual model for the origin of geomagnetic reversals (model M^2) that implied a causal relationship between the reversal frequency and the relative contributions from the primary dynamo family (antisymmetric, dominated by the axial dipole, g_1^0) and the secondary family (symmetric, mostly dominated by the equatorial dipole, g_1^1, h_1^1, and the axial quadrupole, g_2^0). The model stipulates that during the periods of stable polarity the axial dipole term of the primary family dominates the field and the two families are largely independent, whereas the polarity transitions are initiated at times

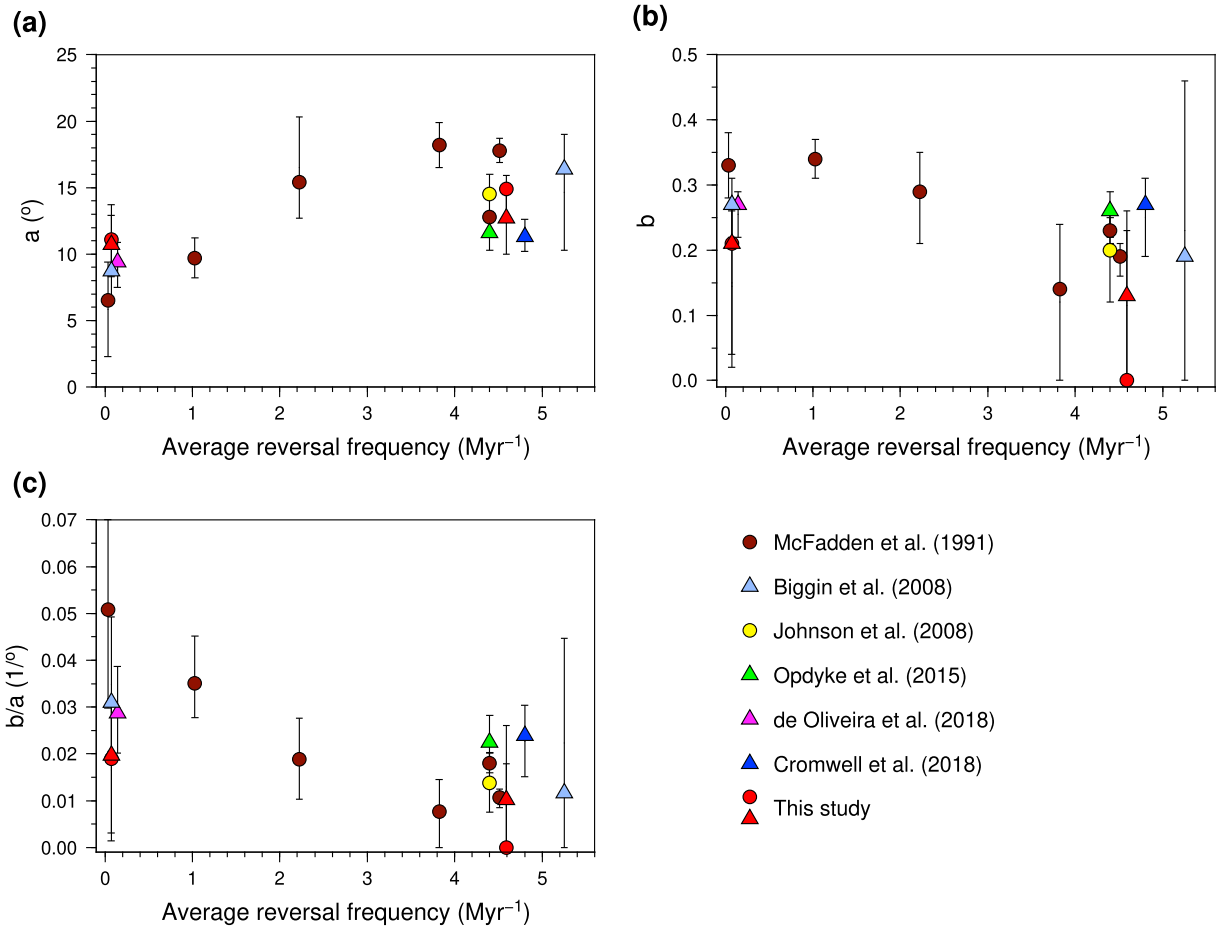

Figure 16. Relationships between the Model G parameters (a, b, and a/b) and the average reversal frequency. Triangles show the parameters obtained by fitting paleosecular variation estimates derived from virtual geomagnetic pole data sets truncated by the variable cutoff angle (Vandamme, 1994); circles show the corresponding estimates based on data sets trimmed by a fixed cutoff angle.

when the contribution from the secondary family becomes comparable to that of the primary family and the two families become critically coupled, possibly due to instabilities in the convective motions of the liquid core producing high degrees of equatorial asymmetry of the velocity field. Assuming that the magnitude of field variation associated with each family is proportional to their overall contributions to the field, this leads to the following predictions for the latitudinal behavior of PSV in terms of Model G parameters. During the intervals of dominantly stable polarity (such as the CNS and PCRS), the values of a should be lower than those for the periods of frequently reversing field (e.g., the Early Cretaceous-Jurassic), and the relative contribution of the primary family (b/a) should be higher. Additional support for the expected negative correlation between b/a and the reversal frequency comes from magnetohydrodynamic dynamo simulations. Coe and Glatzmaier (2006) showed that the magnetic energy in a model of Glatzmaier et al. (1999; their model E) that did not produce reversals was preferentially partitioned into the equatorially antisymmetric spherical harmonics. The variation of these terms would result in a strong latitude dependence of VGP scatter corresponding to a high b/a ratio. In contrast, the models that generated magnetic reversals showed a more even distribution between the symmetric and antisymmetric harmonics across the energy spectrum, for which we would expect flatter VGP dispersion curves and lower b/a values.

The variations of a, b, and b/a as a function of time (Figure 15) and reversal frequency (Figure 16) seem to exhibit the relationships predicted by model M^2 for Late Carboniferous through Cretaceous time. Notwithstanding considerable uncertainties of estimated parameters, we observe that the value of parameter a peaked during the Early Cretaceous and Jurassic (average reversal rate of ~5 Myr^{-1}), while b and b/a were

consistently lower than those for the CNS and PCRS (average reversal rates of 0.05 and 0.14 Myr^{-1}, respectively). During the time interval that followed the CNS (0–84 Ma), the frequency of reversals has been gradually ramping up (Figure 15c), and an increase observed in the a values estimated by McFadden et al. (1991), and a corresponding decrease in b and b/a, fit well with the predictions of model M^2. However, PSV analyses for the last 5–10 Ma (Figure 14) when the reversal rate (4.4–4.8 Myr^{-1}) was comparable to the average reversal frequency for the pre-CNS interval (4.6 Myr^{-1}) show that the values of a for 0–5 and 0–10 Ma are similar to that characterizing the latitudinal dependence of PSV during the pre-CNS interval (Figure 16a), but the values of b and b/a are actually closer to the values obtained for the CNS and PCRS (Figures 16b–16c). Furthermore, the values of a for the models based on the data of Opdyke et al. (2015) and Cromwell et al. (2018; Figures 14b–14c) do not significantly differ from that for the CNS (Figure 7b). Thus, it appears that neither a nor b/a is a reliable proxy for the reversal frequency. The relationship between the Model G parameters and the reversal frequency may exist, but a straightforward correlation of a or anticorrelation of b/a with the reversal rate suggested by the analysis of McFadden et al. (1991) is not supported by these comparisons.

A latitude-invariant behavior of VGP dispersion cannot be explained within the framework of Model G separating the geodynamo into the symmetric and antisymmetric families as it would imply invariability of all antisymmetric terms. A better insight into how the latitude-invariant behavior of VGP scatter relates to the harmonic content of the field can be offered by statistical models of PSV describing it as a "giant Gaussian process" (Constable & Parker, 1988). In this approach, the statistical properties of the field (such as the dispersion of VGPs or paleomagnetic directions) are modeled by random variations in the coefficients of the spherical harmonic expansion of the geomagnetic potential (g_l^m and h_l^m). In the statistical PSV models (e.g., Constable & Johnson, 1999; Constable & Parker, 1988; Johnson & Constable, 1996; Tauxe & Kent, 2004), g_l^m and h_l^m are assumed to have Gaussian distributions, whereas the time-averaged field is assumed to have the GAD structure, often with a small axial quadrupole component superimposed. These models suggest that higher variability in antisymmetric harmonics, and hence the magnetic energy preferentially partitioned into antisymmetric terms in the time-average sense, results in stronger latitude dependences of VGP dispersion (corresponding to higher b/a ratios for Model G).

In the end-member isotropic model of Constable and Parker (1988), equal variances were assigned to all coefficients for the same spherical harmonic degree (l) regardless of the symmetry of each particular degree-and-order term (l and m), and the variances for the nondipole terms ($l \geq 2$) were set to the values that produce a flat power spectrum at the core-mantle boundary similar to that of the present nondipole field. The model produced VGP scatter that was nearly invariant with latitude and the average level of S_b was remarkably similar to that observed in our data for pre-CNS time interval (~15°). This similarity suggests that during the Early Cretaceous-Jurassic interval of frequent geomagnetic reversals the geodynamo may have operated in a regime where the magnetic energy was more evenly partitioned between the equatorially symmetric and antisymmetric spherical harmonics than during the superchrons (CNS, PCRS) and recent time (0–10 Ma). Conversely, geodynamos with lower degrees of equatorial symmetry (i.e., more energy partitioned into the antisymmetric harmonics), as suggested by strong latitudinal increases of VGP dispersion for the last 5–10 Ma, the CNS and PCRS intervals, are evidently capable of producing both frequent geomagnetic reversals and long periods of stable polarity, which is not consistent with the findings of Coe and Glatzmaier (2006). Future work on numerical simulations of the geodynamo will help to elucidate this issue.

6. Summary and Conclusions

We have compiled an updated paleomagnetic database from rapidly cooled igneous rocks that were specifically selected to obtain reliable estimates of PSV of geomagnetic field in the Late Cretaceous through Jurassic, allowing us to compare the latitude dependence of PSV during time intervals characterized by drastically different frequencies of geomagnetic reversals. The main result of our analysis is the observation of distinctly different latitude variations of PSV for the Early Cretaceous-Jurassic time interval when the field reversed frequently (127–198 Ma) and the period of stable geomagnetic polarity in the Cretaceous (the CNS, 84–126 Ma). For the CNS, the VGP dispersion was found to show a strong increase from the equator to the pole, which is consistent with the earlier results of Biggin, van Hinsbergen, et al. (2008). The observed latitude behavior of PSV is also consistent with that during the PCRS (~262–318 Ma; de Oliveira et al., 2018). In

contrast, the intervening Early Cretaceous-Jurassic period of frequent geomagnetic reversals (pre-CNS, 127–198 Ma) was characterized by a nearly latitude-invariant dispersion of VGPs, with the average level of VGP scatter similar to that observed for the CNS. This result was further validated by the analysis of robust PSV estimates based on the methodology originally developed by Suttie et al. (2015) and supplemented by the corrections for biases due to finite sample size and within-site dispersion of paleomagnetic directions developed in this study (section 3).

Our PSV estimates for the Early Cretaceous-Jurassic do not support the hypothesis of Linder and Gilder (2012) that the latitudinal variation of VGP dispersion is a mathematical artifact arising from the transformation of paleomagnetic directions to poles and that PSV is best described by latitude-invariant dispersion of directions. We also showed that the commonly used Model G of McFadden et al. (1988) does not provide a statistically acceptable fit even for the most reliable PSV data for the last 5–10 Ma, and hence, can be used only in a strictly descriptive sense as an approximation for the latitude dependency of VGP dispersion. Furthermore, the comparison between the Model G fits for the CNS, pre-CNS, and recent (0–10 Ma) PSV data cast doubt on the validity of links between the model parameters and the reversal frequency suggested by McFadden et al. (1991). In particular, the equatorial intercept of the model curve (a) and the magnitude of increase in VGP dispersion with latitude (b/a ratio) do not appear to be reliable indicators for a superchron or a dynamo producing frequent geomagnetic reversals. More generally, a strong increase in VGP dispersion with latitude was not restricted to the superchrons, and a dynamo operating in a regime of high reversal frequency was evidently equally capable of producing both a strong latitude increase and a nearly latitude-invariant behavior of VGP scatter. If a relationship between the shape of VGP dispersion curve and the reversal frequency does exist, it must be much more subtle than that implied by McFadden et al. (1991). Unfortunately, the currently available PSV estimates for the Phanerozoic do not allow us to make any robust inference about that. Further efforts in assembling databases of high-quality PSV estimates for Cenozoic and Mesozoic time can potentially provide us with a clearer view on the relationship between secular variation and the reversal frequency. Presently, great care should be taken when interpreting latitude dependencies of PSV in terms of the geodynamo's tendency to reverse.

We consider a nearly latitude-invariant behavior of VGP dispersion during the Early Cretaceous-Jurassic interval of frequent polarity changes to be a robust result, which suggests that during this interval, the geodynamo could have operated in a regime characterized by a high degree of symmetry, with the magnetic energy evenly distributed between the equatorially symmetric and antisymmetric harmonics of the geomagnetic potential. Conversely, more asymmetric geodynamos implied by PSV estimates for the last 5–10 Ma, the CNS (84–126 Ma), and the PCRS (262–318 Ma) were equally capable of producing both a frequently reversing field and long intervals of stable polarity (CNS, PCRS). This implies that the propensity of the geodynamo to reverse is not controlled by the symmetry state alone and that a delicate balance in the partitioning of magnetic energy is required to force the geodynamo into the superchron regime. An integrated approach in which the statistical PSV models are paired with magnetohydrodynamic simulations may bring better understanding of the specific conditions needed for a superchron geodynamo.

Acknowledgments
The data used in this study are provided in the supporting information. This paper is an output of the 8th Nordic Paleomagnetism Workshop, held in Leirubakki, Iceland, from 30 September to 7 October 2017. We thank Tobias Rolf, Nicholas Swanson-Hysell, and Luke Fairchild for the help with compiling data; Courtney Sprain and Louise Hawkins for the help with data analysis software; and Geoffrey Cromwell for providing PSV estimates from the PSV10 database. We gratefully acknowledge the insightful reviews of Maxwell Brown and an anonymous reviewer, as well as editorial handling by Joshua Feinberg. P.D. and E.K. appreciate support from the Research Council of Norway through its Centres of Excellence funding scheme, project 646 number 223272 (CEED). T.V. acknowledges support from Otto A. Malm Foundation, Finland. L.P. appreciates support from Letterstedtska föreningens finländska avdelning (Finland). E.P acknowledges funding from IUGG. A.S. acknowledges travel support from the Centre for Earth Evolution and Dynamics, University of Oslo, Norway. S.O. acknowledges financing from Estonian Research Council research grant IUT20-34. A.B. acknowledges NERC Standard grant NE/P00170X/1 and the Leverhulme Trust Research Leadership award RL-2016-080.

References

Aubert, J., Tarduno, J. A., & Johnson, C. L. (2010). Observations and models of the long-term evolution of Earth's magnetic field. *Space Science Reviews*, *155*(1–4), 337–370. https://doi.org/10.1007/s11214-010-9684-5

Beutel, E. K., Nomade, S., Fronabarger, A. K., & Renne, P. R. (2005). Pangea's complex breakup: A new rapidly changing stress field model. *Earth and Planetary Science Letters*, *236*(1–2), 471–485. https://doi.org/10.1016/j.epsl.2005.03.021

Biggin, A. J., Piispa, E. J., Pesonen, L. J., Holme, R., Paterson, G. A., Veikkolainen, T., & Tauxe, L. (2015). Palaeomagnetic field intensity variations suggest Mesoproterozoic inner-core nucleation. *Nature*, *526*, 245–248. https://doi.org/10.1038/nature15523

Biggin, A. J., Steinberger, B., Aubert, J., Suttie, N., Holme, R., Torsvik, T. H., et al. (2012). Possible links between long-term geomagnetic variations and whole-mantle convection processes. *Nature Geoscience*, *5*, 526–533. https://doi.org/10.1038/ngeo1521

Biggin, A. J., Strik, G. H. M. A., & Langereis, C. G. (2008). Evidence for a very-long-term trend in geomagnetic secular variation. *Nature Geoscience*, *1*, 395–398. https://doi.org/10.1038/ngeo181

Biggin, A. J., van Hinsbergen, D. J. J., Langereis, C. G., Straathof, G. B., & Deenen, M. H. L. (2008). Geomagnetic secular variation in the Cretaceous Normal Superchron and in the Jurassic. *Physics of the Earth and Planetary Interiors*, *169*(1–4), 3–19. https://doi.org/10.1016/j.pepi.2008.07.004

Böhnel, H., Delgado-Argote, L. A., & Kimbrough, D. L. (2002). Discordant paleomagnetic data for Middle-Cretaceous intrusive rocks from northern Baja California: Latitude displacement, tilt, or vertical axis rotation? *Tectonics*, *21*(5), 1049. https://doi.org/10.1029/2001TC001298

Bucker, C., Schult, A., Bloch, W., & Guerreiro, S. D. C. (1986). Rock magnetism and palaeomagnetism of an Early Cretaceous/Late Jurassic dike swarm in Rio Grande de Norte, Brazil. *Journal of Geophysics*, *60*(2), 129–135.

Butler, R. F., Hervé, F., Munizaga, F., Beck, M. E. Jr., Burmester, R. F., & Oviedo, E. S. (1991). Paleomagnetism of the Patagonian plateau basalts, southern Chile and Argentina. *Journal of Geophysical Research*, *96*(B4), 6023–6034. https://doi.org/10.1029/90JB02698

Chen, W., Zhang, S., Ding, J., Zhang, J., Zhao, X., Zhu, L., et al. (2017). Combined paleomagnetic and geochronological study on Cretaceous strata of the Qiangtang terrane, central Tibet. *Gondwana Research*, *41*, 373–389. https://doi.org/10.1016/j.gr.2015.07.004

Chi, C. T., & Dorobek, S. L. (2004). Cretaceous palaeomagnetism of Indochina and surrounding regions: Cenozoic tectonic implications. *Geological Society, London, Special Publications*, *226*, 273–287. https://doi.org/10.1144/GSL.SP.2004.226.01.15

Coe, R. S., & Glatzmaier, G. A. (2006). Symmetry and stability of the geomagnetic field. *Geophysical Research Letters*, *33*, L21311. https://doi.org/10.1029/2006GL027903

Coffin, M. F., Pringle, M. S., Duncan, R. A., Gladczenko, T. P., Storey, M., Müller, R. D., & Gahagan, L. A. (2002). Kerguelen hotspot magma output since 130 Ma. *Journal of Petrology*, *43*, 1121–1137. https://doi.org/10.1093/petrology/43.7.1121

Constable, C. G., & Johnson, C. L. (1999). Anisotropic paleosecular variation models: Implications for geomagnetic field observables. *Physics of the Earth and Planetary Interiors*, *115*(1), 35–51. https://doi.org/10.1016/S0031-9201(99)00065-5

Constable, C. G., & Parker, R. L. (1988). Statistics of the geomagnetic secular variation for the past 5 m.y. *Journal of Geophysical Research*, *93*(B10), 11,569–11,581. https://doi.org/10.1029/JB093iB10p11569

Cox, A. (1969). Confidence limits for the precision parameter k. *Geophysical Journal of the Royal Astronomical Society*, *17*(5), 545–549. https://doi.org/10.1111/j.1365-246X.1969.tb00257.x

Cox, A. (1970). Latitude dependence of the angular dispersion of the geomagnetic field. *Geophysical Journal of the Royal Astronomical Society*, *20*(3), 253–269. https://doi.org/10.1111/j.1365-246X.1970.tb06069.x

Cromwell, G., Constable, C. G., Staudigel, H., Tauxe, L., & Gans, P. (2013). Revised and updated paleomagnetic results from Costa Rica. *Geochemistry, Geophysics, Geosystems*, *14*, 3379–3388. https://doi.org/10.1002/ggge.20199

Cromwell, G., Johnson, C. L., Tauxe, L., Constable, C. G., & Jarboe, N. A. (2018). PSV10: A global data set for 0–10 Ma time-averaged field and paleosecular variation studies. *Geochemistry, Geophysics, Geosystems*, *19*, 1533–1558. https://doi.org/10.1002/2017GC007318

Cucciniello, C., Langone, A., Melluso, L., Morra, V., Mahoney, J. J., Meisel, T., & Tiepolo, M. (2010). U–Pb ages, Pb–Os isotope ratios, and platinum–group element (PGE) composition of the west-central Madagascar flood basalt province. *Journal of Geology*, *118*(5), 523–541. https://doi.org/10.1086/655012

de Oliveira, W. P., Franco, D. R., Brandt, D., Ernesto, M., da Ponte Neto, C. F., Zhao, X., et al. (2018). Behavior of the paleosecular variation during the Permian-Carboniferous reversed Superchron and comparisons to the low reversal frequency intervals since Precambrian times. *Geochemistry, Geophysics, Geosystems*, *19*, 1035–1048. https://doi.org/10.1002/2017GC007262

Diehl, J. F. (1991). The Elkhorn Mountains revisited: New data for the Late Cretaceous paleomagnetic field of North America. *Journal of Geophysical Research*, *96*(B6), 9887–9894. https://doi.org/10.1029/91JB00959

Dodd, S. C., Mac Niocaill, C., & Muxworthy, A. R. (2015). Long duration (>4 Ma) and steady-state volcanic activity in the Early Cretaceous Paraná-Etendeka large Igneous Province: New palaeomagnetic data from Namibia. *Earth and Planetary Science Letters*, *414*, 16–29. https://doi.org/10.1016/j.epsl.2015.01.009

Doh, S.-J., Kim, W., Suk, D., Park, Y.-H., & Cheong, D. (2002). Palaeomagnetic and rock-magnetic studies of Cretaceous rocks in the Gongju Basin, Korea: Implication of clockwise rotation. *Geophysical Journal International*, *150*(3), 737–752. https://doi.org/10.1046/j.1365-246X.2002.01726.x

Duncan, R. A., Hooper, P. R., Rehacek, J., Marsh, J. S., & Duncan, A. R. (1997). The timing and duration of the Karoo igneous event, southern Gondwana. *Journal of Geophysical Research*, *102*, 18,127–18,138. https://doi.org/10.1029/97JB00972

Ernesto, M., Pacca, I. G., Hiodo, F. Y., & Nardy, A. J. R. (1990). Palaeomagnetism of the Mesozoic Serra Geral Formation, southern Brazil. *Physics of the Earth and Planetary Interiors*, *64*(2–4), 153–175. https://doi.org/10.1016/0031-9201(90)90035-V

Ernesto, M., Raposo, M. I. B., Marques, L. S., Renne, P. R., Diogo, L. A., & de Min, A. (1999). Paleomagnetism, geochemistry and $^{40}Ar/^{39}Ar$ dating of the north-eastern Paraná Magmatic Province: Tectonic implications. *Journal of Geodynamics*, *28*(4–5), 321–340. https://doi.org/10.1016/S0264-3707(99)00013-7

Fisher, R. (1953). Dispersion on a sphere. *Proceedings of the Royal Society of London A*, *217*(1130), 295–305. https://doi.org/10.1098/rspa.1953.0064

Fisher, N. I. (1985). Spherical medians. *Journal of the Royal Statistical Society, Series B*, *47*(2), 342–348.

Font, E., Ernesto, M., Silva, P. F., Correia, P. B., & Nascimento, M. A. L. (2009). Palaeomagnetism, rock magnetism and AMS of the Cabo Magmatic Province, NE Brazil, and the opening of South Atlantic. *Geophysical Journal International*, *179*(2), 905–922. https://doi.org/10.1111/j.1365-246X.2009.04333.x

Gilbert, J. C., & Lawton, T. F. (2012). Contrasting detrital zircon assemblages and provenance of Upper Jurassic and Lower Cretaceous strata, southeast Arizona and southwest New Mexico. *Geological Society of America Abstracts with Programs*, *44*(6), 82.

Glatzmaier, G. A., Coe, R. S., Hongre, L., & Roberts, P. H. (1999). The role of the Earth's mantle in controlling the frequency of geomagnetic reversals. *Nature*, *401*, 885–890. https://doi.org/10.1038/44776

Glatzmaier, G. A., & Roberts, P. H. (1995). A three-dimensional self-consistent computer simulation of a geomagnetic field reversal. *Nature*, *377*, 203–209. https://doi.org/10.1038/377203a0

Gradstein, F. M., Ogg, J. G., Schmitz, M., & Ogg, G. (2012). *The geologic time scale*. Boston, MA: Elsevier.

Gregor, C. B., Mertzman, S., Nairn, A. E. M., & Negendank, J. (1974). Paleomagnetism and the alpine tectonics of Eurasia V: The paleomagnetism of some Mesozoic and Cenozoic volcanic rocks from the Lebanon. *Tectonophysics*, *21*(4), 375–395. https://doi.org/10.1016/0040-1951(74)90004-3

Gromme, S., Mankinen, E. A., & Prévot, M. (2010). Time-averaged paleomagnetic field at the equator: Complete data and results from the Galapagos Islands. *Ecuador, Geochemistry Geophysics Geosystems*, *11*, Q11009. https://doi.org/10.1029/2010GC003090

Gubbins, D. (1994). Geomagnetic polarity reversals: A connection with secular variation and core-mantle interaction? *Reviews of Geophysics*, *32*(1), 61–83. https://doi.org/10.1029/93RG02602

Gunderson, J. A., & Sheriff, S. D. (1991). A new Late Cretaceous paleomagnetic pole from the Adel Mountains, west central Montana. *Journal of Geophysical Research*, *96*(B1), 317–326. https://doi.org/10.1029/90JB01963

Hankard, F., Cogné, J.-P., Quidelleur, X., Bayasgalan, A., & Lkhagvadorj, P. (2007). Palaeomagnetism and K-Ar dating of Cretaceous basalts from Mongolia. *Geophysical Journal International*, *169*(3), 898–908. https://doi.org/10.1111/j.1365-246X.2007.03292.x

Hargraves, R. B., Rehacek, J., & Hooper, P. R. (1997). Palaeomagnetism of the Karoo igneous rocks in southern Africa. *South African Journal of Geology*, *100*(3), 195–212.

Harlan, S. S., Snee, L. W., Reynolds, M. W., Mehnert, H. H., Schmidt, R. G., Sheriff, S. D., & Irving, A. J. (2005). $^{40}Ar/^{39}Ar$ and K-Ar geochronology and tectonic significance of the Upper Cretaceous Adel Mountain Volcanics and spatially associated tertiary igneous rocks, northwestern Montana. *U.S. Geological Survey Professional Paper, 1696*. Reston, VA: U.S. Geological Survey.

Harrison, C. G. A. (2009). Latitudinal signature of Earth's magnetic field variation over the last 5 million years. *Geochemistry, Geophysics, Geosystems*, *10*, Q02012. https://doi.org/10.1029/2008GC002298

Henthorn, D. I. (1981). The magnetostratigraphy of the Lebombo Group along the Olifants River, Kruger National Park. *Annals of the Geological Survey of South Africa*, *15*, 1–10.

Huang, S., Pan, Y. X., & Zhu, R. X. (2013). Paleomagnetism of the Late Cretaceous volcanic rocks of the Shimaoshan Group in Yongtai County, Fujian Province. *Science China Earth Sciences*, *56*(1), 22–30. https://doi.org/10.1007/s11430-012-4519-8

Hulot, G., & Gallet, Y. (1996). On the interpretation of virtual geomagnetic pole (VGP) scatter curves. *Physics of the Earth and Planetary Interiors*, *95*(1–2), 37–53. https://doi.org/10.1016/0031-9201(95)03106-5

Iglesia Llanos, M. P., Lanza, R., Riccardi, A. C., Geuna, S., Laurenzi, M. A., & Ruffini, R. (2003). Palaeomagnetic study of the El Quemado complex and Marifil Formation, Patagonian Jurassic igneous province, Argentina. *Geophysical Journal International*, *154*(3), 599–617. https://doi.org/10.1046/j.1365-246X.2003.01923.x

Irving, E., & Ward, M. A. (1964). A statistical model of the geomagnetic field. *Pure and Applied Geophysics*, *57-57*(1), 47–52. https://doi.org/10.1007/BF00879707

Johnson, C. L., & Constable, C. G. (1996). Palaeosecular variation recorded by lava flows over the past five million years. *Philosophical Transactions of the Royal Society of London A*, *354*(1704), 89–141. https://doi.org/10.1098/rsta.1996.0004

Johnson, C. L., Constable, C. G., Tauxe, L., Barendregt, R., Brown, L. L., Coe, R. S., et al. (2008). Recent investigations of the 0-5 Ma geomagnetic field recorded by lava flows. *Geochemistry, Geophysics, Geosystems*, *9*, Q04032. https://doi.org/10.1029/2007GC001696

Kent, D. V., Wang, H., & Rochette, P. (2010). Equatorial paleosecular variation of the geomagnetic field from 0 to 3 Ma lavas from the Galapagos Islands. *Physics of the Earth and Planetary Interiors*, *183*(3–4), 404–412. https://doi.org/10.1016/j.pepi.2010.08.010

Kirschvink, J. L. (1980). The least-squares line and plane and the analysis of palaeomagnetic data. *Geophysical Journal of the Royal Astronomical Society*, *62*, 699–718. http://doi.org/10.1111/j.1365-246X.1980.tb02601.x

Klootwijk, C. T. (1971). Palaeomagnetism of the upper Gondwana Rajmahal traps, northeast India. *Tectonophysics*, *12*(6), 449–467. https://doi.org/10.1016/0040-1951(71)90045-X

Kluth, C. F., Butler, R. F., Harding, L. E., Shafiqullah, M., & Damon, P. E. (1982). Paleomagnetism of Late Jurassic rocks in the northern Canelo Hills, southeastern Arizona. *Journal of Geophysical Research*, *87*(B8), 7079–7086. https://doi.org/10.1029/JB087iB08p07079

Kosterov, A. A., & Perrin, M. (1996). Paleomagnetism of the Lesotho basalt, southern Africa. *Earth and Planetary Science Letters*, *139*(1–2), 63–78. https://doi.org/10.1016/0012-821X(96)00005-2

Kulakov, E. V., Smirnov, A. V., Biggin, A. J., Hawkins, L., Sprain, C., Paterson, G. A., & Fairchild, L. (2018). The long-term history of the Mesozoic geodynamo: A paleointensity perspective. Geophysical Research Abstracts (Vol. 20, EGU2018–7459), EGU General Assembly 2018, Vienna, Austria.

Lanza, R., & Zanella, E. (1993). Palaeomagnetism of the Ferrar dolerite in the northern Prince Albert Mountains (Victoria Land, Antarctica). *Geophysical Journal International*, *114*(3), 501–511. https://doi.org/10.1111/j.1365-246X.1993.tb06983.x

Lemna, O. S., Bachtadse, V., Kirscher, U., Rolf, C., & Petersen, N. (2016). Paleomagnetism of the Jurassic Transantarctic Mountains revisited—Evidence for large dispersion of apparent polar wander within less than 3 Myr. *Gondwana Research*, *31*, 124–134. https://doi.org/10.1016/j.gr.2015.01.002

Lhuillier, F., Gilder, S. A., Wack, M., He, K., Petersen, N., Singer, B. S., et al. (2016). More stable yet bimodal geodynamo during the Cretaceous superchron? *Geophysical Research Letters*, *43*, 6170–6177. https://doi.org/10.1002/2016GL069303

Linder, J., & Gilder, S. A. (2012). Latitude dependency of the geomagnetic secular variation S parameter: A mathematical artifact. *Geophysical Research Letters*, *39*, L02308. https://doi.org/10.1029/2011GL050330

Løvlie, R. (1979). Mesozoic palaeomagnetism in Vestfjella, Dronning Maud Land, Antarctica. *Geophysical Journal of the Royal Astronomical Society*, *59*, 529–537. https://doi.org/10.1111/j.1365-246X.1979.tb02571.x

Lowrie, W., & Kent, D. V. (2004). Geomagnetic polarity timescales and reversal frequency regimes. In J. Channell, D. Kent, W. Lowrie, & J. Meert (Eds.), *Timescales of the paleomagnetic fieldGeophysical Monograph Series* (Vol. 145, pp. 117–129). Washington, DC: American Geophysical Union. https://doi.org/10.1029/145GM09

Luttinen, A. V., Heinonen, J. S., Kurhila, M., Jourdan, F., Mänttäri, I., Vuori, S. K., & Huhma, H. (2015). Depleted mantle-sourced CFB magmatism in the Jurassic Africa-Antarctica rift: Petrology and $^{40}Ar/^{39}Ar$ and U/Pb chronology of the Vestfjella dyke swarm, Dronning Maud Land, Antarctica. *Journal of Petrology*, *56*(5), 919–952. https://doi.org/10.1093/petrology/egv022

Ma, Y., Yang, T., Bian, W., Jin, J., Zhang, S., Wu, H., & Li, H. (2016). Early Cretaceous paleomagnetic and geochronologic results from the Tethyan Himalaya: Insights into the Neotethyan paleogeography and the India-Asia collision. *Scientific Reports*, *6*(1). https://doi.org/10.1038/srep21605

Ma, Y., Yang, T., Yang, Z., Zhang, S., Wu, H., Li, H., et al. (2014). Paleomagnetism and U-Pb zircon geochronology of Lower Cretaceous lava flows from the western Lhasa terrane: New constraints on the India-Asia collision process and intracontinental deformation within Asia. *Journal of Geophysical Research: Solid Earth*, *119*, 7404–7424. https://doi.org/10.1002/2014JB011362

McElhinny, M. W., & McFadden, P. L. (1997). Palaeosecular variation over the past 5 Myr based on a new generalized database. *Geophysical Journal International*, *131*(2), 240–252. https://doi.org/10.1111/j.1365-246X.1997.tb01219.x

McElhinny, M. W., & McFadden, P. L. (2000). *Paleomagnetism: Continents and Oceans*. San Diego, CA: Academic Press.

McFadden, P. L. (1980). The best estimate of Fisher's precision parameter k. *Geophysical Journal of the Royal Astronomical Society*, *60*(3), 397–407. https://doi.org/10.1111/j.1365-246X.1980.tb04816.x

McFadden, P. L., & McElhinny, M. W. (1984). A physical model for palaeosecular variation. *Geophysical Journal of the Royal Astronomical Society*, *78*(3), 809–830. https://doi.org/10.1111/j.1365-246X.1984.tb05072.x

McFadden, P. L., Merrill, R. T., & McElhinny, M. W. (1988). Dipole/quadrupole family modeling of paleosecular variation. *Journal of Geophysical Research*, *93*(B10), 11,583–11,588. https://doi.org/10.1029/JB093iB10p11583

McFadden, P. L., Merrill, R. T., McElhinny, M. W., & Lee, S. (1991). Reversals of the Earth's magnetic field and temporal variations of the dynamo families. *Journal of Geophysical Research*, *96*(B3), 3923–3933. https://doi.org/10.1029/90JB02275

Mena, M., Goguitchaichvili, A., Solano, M. C., & Vilas, J. F. (2011). Paleosecular variation and absolute geomagnetic paleointensity records retrieved from the Early Cretaceous Posadas Formation (Misiones, Argentina). *Studia Geophysica et Geodaetica*, *55*, 279–309. https://doi.org/10.1007/s11200-011-0016-3

Mendía, J. E. (1978). Palaeomagnetism of alkaline lava flows from El Salto-Almafuerte, Córdoba Province, Argentina. *Geophysical Journal of the Royal Astronomical Society*, *54*(3), 539–546. https://doi.org/10.1111/j.1365-246X.1978.tb05493.x

Merrill, R. T., McElhinny, M. W., & McFadden, P. L. (1998). *The magnetic field of the Earth: Paleomagnetism, the core, and the deep mantle*. London, UK: Academic Press.

Merrill, R. T., & McFadden, P. L. (1988). Secular variation and the origin of geomagnetic field reversals. *Journal of Geophysical Research*, *93*(B10), 11,589–11,597. https://doi.org/10.1029/JB093iB10p11589

Metelkin, D. V., Gordienko, I. V., & Klimuk, V. S. (2007). Paleomagnetism of Upper Jurassic basalts from Transbaikalia: New data on the time of closure of the Mongol-Okhotsk Ocean and Mesozoic intraplate tectonics of Central Asia. *Russian Geology and Geophysics*, *48*(10), 825–834. https://doi.org/10.1016/j.rgg.2007.09.004

Metelkin, D. V., Kazansky, A. Y., Bragin, V. Y., Tsel'movich, V. A., Lavrenchuk, A. V., & Kungurtsev, L. V. (2007). Paleomagnetism of the Late Cretaceous intrusions from the Minusa trough (southern Siberia). *Russian Geology and Geophysics*, *48*(2), 185–198. https://doi.org/10.1016/j.rgg.2006.03.001

Metelkin, D. V., Vernikovsky, V. A., Kazansky, A. Y., & Wingate, M. T. D. (2010). Late Mesozoic tectonics of central Asia based on paleomagnetic evidence. *Gondwana Research*, *18*(2–3), 400–419. https://doi.org/10.1016/j.gr.2009.12.008

Moreira Florisbal, L., Heaman, L. M., de Assis Janasi, V., & de Fatima Bitencourt, M. (2014). Tectonic significance of the Florianópolis Dyke Swarm, Paraná–Etendeka Magmatic Province: A reappraisal based on precise U–Pb dating. *Journal of Volcanology and Geothermal Research*, *289*, 140–150. https://doi.org/10.1016/j.jvolgeores.2014.11.007

Ogg, J. G. (2012). Geomagnetic polarity time scale. In F. M. Gradstein, J. G. Ogg, M. G. Schmitz, & G. M. Ogg (Eds.), *The geologic time scale* (pp. 85–113). Boston, MA: Elsevier. https://doi.org/10.1016/B978-0-444-59425-9.00005-6

Opdyke, N. D., & Channell, J. E. T. (1996). *Magnetic stratigraphy*. London, UK: Academic Press.

Opdyke, N. D., Hall, M., Meija, V., Huang, K., & Foster, D. A. (2006). The time averaged field at the equator: Results from Ecuador. *Geochemistry, Geophysics, Geosystems*, *7*, Q11005. https://doi.org/10.1029/2005GC001221

Opdyke, N. D., Kent, D. V., Foster, D. A., & Huang, K. (2015). Paleomagnetism of Miocene volcanics on Sao Tome: Paleosecular variation at the Equator and a comparison to its latitudinal dependence over the last 5 Myr. *Geochemistry, Geophysics, Geosystems*, *16*, 3870–3882. https://doi.org/10.1002/2015GC005901

Opdyke, N. D., Kent, D. V., Huang, K., Foster, D. A., & Patel, J. P. (2010). Equatorial paleomagnetic time-averaged field results from 0–5 Ma lavas from Kenya and the latitudinal variation of angular dispersion. *Geochemistry, Geophysics, Geosystems*, *11*, Q05005. https://doi.org/10.1029/2009GC002863

Palmer, H. C., Hayatsu, A., & MacDonald, W. D. (1980). The Middle Jurassic Camaraca Formation, Arica, Chile: Palaeomagnetism, K-Ar age dating and tectonic implications. *Geophysical Journal of the Royal Astronomical Society*, *62*(1), 155–172. https://doi.org/10.1111/j.1365-246X.1980.tb04849.x

Piper, J. D. A. (1975). A palaeomagnetic study of the coast-parallel Jurassic dyke swarm in southern Greenland. *Physics of the Earth and Planetary Interiors*, *11*(1), 36–42. https://doi.org/10.1016/0031-9201(75)90073-4

Pivarunas, A., Meert, J., & Miller, S. (2018). Assessing the intersection/remagnetization puzzle with synthetic apparent polar wander paths. *Geophysical Journal International*, *214*(2), 1164–1172. https://doi.org/10.1093/gji/ggy216

Poornachandra Rao, G. V. S., & Mallikharjuna Rao, J. (1996). Palaeomagnetism of the Rajmahal traps of India: Implication to the reversal in the Cretaceous Normal Superchron. *Journal of Geomagnetism and Geoelectricity*, *48*(7), 993–1000. https://doi.org/10.5636/jgg.48.993

Press, W. H., Teukolsky, S. A., Vetterling, W. T., & Flannery, B. P. (1992). *Numerical Recipes in FORTRAN 77: The Art of Scientific Computing* (2nd ed.). Cambridge, UK: Cambridge University Press.

Raposo, M. I. B., & Ernesto, M. (1995). An Early Cretaceous paleomagnetic pole from Ponta Grossa dikes (Brazil): Implications for the South American Mesozoic apparent polar wander path. *Journal of Geophysical Research*, *100*(B10), 20,095–20,109. https://doi.org/10.1029/95JB01681

Raposo, M. I. B., Ernesto, M., & Renne, P. R. (1998). Paleomagnetism and $^{40}Ar/^{39}Ar$ dating of the Early Cretaceous Florianópolis dike swarm (Santa Catarina Island), southern Brazil. *Physics of the Earth and Planetary Interiors*, *108*(4), 275–290. https://doi.org/10.1016/S0031-9201(98)00102-2

Ren, Q., Zhang, S., Wu, H., Liang, Z., Miao, X., Zhao, H., et al. (2016). Further paleomagnetic results from the ~ 155 Ma Tiaojishan Formation, Yanshan Belt, North China, and their implications for the tectonic evolution of the Mongol-Okhotsk suture. *Gondwana Research*, *35*, 180–191. https://doi.org/10.1016/j.gr.2015.05.002

Riisager, J., Perrin, M., Riisager, P., & Vandamme, D. (2001). Palaeomagnetic results and palaeointensity of Late Cretaceous Madagascan basalt. *Journal of African Earth Sciences*, *32*(3), 503–518. https://doi.org/10.1016/S0899-5362(01)90111-3

Riley, T. L., & Knight, K. B. (2001). Age of pre-break-up Gondwana magmatism. *Antarctic Science*, *13*, 99–110. https://doi.org/10.1017/S0954102001000177

Riley, T. R., Milar, L., Watkeys, M. K., Curtis, M. L., Leat, P. T., Klausen, M. B., & Fanning, C. M. (2004). U-Pb zircon (SHRIMP) ages for the Lebombo rhyolites, South Africa: Refining the duration of Karoo volcanism. *Journal of the Geological Society, London*, *161*(4), 547–550. https://doi.org/10.1144/0016-764903-181

Ron, H., Nur, A., & Hofstetter, A. (1990). Late Cenozoic and recent strike slip tectonics in Mt. Carmel northern Israel. *Annales Tectonicae*, *4*(2), 70–80.

Schult, A., & Guerreiro, S. D. C. (1980). Palaeomagnetism of Upper Cretaceous volcanic rocks from Cabo de Sto. Agostinho, Brazil. *Earth and Planetary Science Letters*, *50*(1), 311–315. https://doi.org/10.1016/0012-821X(80)90141-7

Schult, A., Hussain, A. G., & Soffel, H. C. (1981). Palaeomagnetism of Upper Cretaceous volcanics and Nubian sandstones of Wadi Natash, SE Egypt and implications for the polar wander path for Africa in the Mesozoic. *Journal of Geophysics*, *50*(1), 16–22.

Segev, A., Sass, E., Ron, H., Lang, B., Kolodny, Y., & McWilliams, M. (2002). Stratigraphic, geochronologic, and paleomagnetic constraints on Late Cretaceous volcanism in northern Israel. *Israel Journal of Earth Sciences*, *51*(3–4), 297–309. https://doi.org/10.1560/VUTP-RNR5-UU08-Y7WT

Sherwood, G., Shaw, J., Baer, G., & Basu Mallik, S. (1993). The strength of the geomagnetic field during the Cretaceous Quiet Zone: Palaeointensity results from Israeli and Indian lavas. *Journal of Geomagnetism and Geoelectricity*, *45*(4), 339–360. https://doi.org/10.5636/jgg.45.339

Shibuya, H., Cassidy, J., Smith, I. E. M., & Itaya, T. (1995). Paleomagnetism of young New Zealand basalts and longitudinal distribution of paleosecular variation. *Journal of Geomagnetism and Geoelectricity*, *47*(10), 1011–1022. https://doi.org/10.5636/jgg.47.1011

Smirnov, A. V., Kulakov, E. V., Foucher, M. S., & Bristol, K. E. (2017). Intrinsic paleointensity bias and the long-term history of the geodynamo. *Science Advances*, *3*(2), e1602306. https://doi.org/10.1126/sciadv.1602306

Smirnov, A. V., & Tarduno, J. A. (2004). Secular variation of the Late Archean-Early Proterozoic geodynamo. *Geophysical Research Letters*, *31*, L16607. https://doi.org/10.1029/2004GL020333

Smirnov, A. V., Tarduno, J. A., & Evans, D. A. D. (2011). Evolving core conditions ca. 2 billion years ago detected by paleosecular variation. *Physics of the Earth and Planetary Interiors*, *187*(3–4), 225–231. https://doi.org/10.1016/j.pepi.2011.05.003

Smith, W. A. (1987). Paleomagnetic results from a crosscutting system of northwest and north-south trending diabase dikes in the North Carolina Piedmont. *Tectonophysics*, *136*(1–2), 137–150. https://doi.org/10.1016/0040-1951(87)90336-2

Solano, M. C., Goguitchaichvili, A., Bettucci, L. S., Ruiz, R. C., Calvo-Rathert, M., Ruiz-Martinez, V. C., et al. (2010). Paleomagnetism of Early Cretaceous Arapey Formation (northern Uruguay). *Studia Geophysica et Geodaetica*, *54*(4), 533–546. https://doi.org/10.1007/s11200-010-0032-8

Sprain, C. J., Feinberg, J. M., Geissman, J. W., Strauss, B., & Brown, M. C. (2016). Paleointensity during periods of rapid reversal: A case study from the Middle Jurassic shamrock batholith, western Nevada. *GSA Bulletin*, *128*(1–2), 223–238. https://doi.org/10.1130/B31283.1

Suttie, N., Biggin, A., & Holme, R. (2015). Robust estimators of palaeosecular variation. *Geophysical Journal International*, *200*(2), 1046–1051. https://doi.org/10.1093/gji/ggu443

Swenson, P., & McWilliams, M. (1989). Paleomagnetic results from the Upper Cretaceous Maudlow and Livingston Formations, Southwest Montana. *Geophysical Research Letters*, *16*(7), 669–672. https://doi.org/10.1029/GL016i007p00669

Tan, X., Gilder, S., Kodama, K. P., Jiang, W., Han, Y., Zhang, H., et al. (2010). New paleomagnetic results from the Lhasa block: Revised estimation of latitudinal shortening across Tibet and implications for dating the India-Asia collision. *Earth and Planetary Science Letters*, *293*(3–4), 396–404. https://doi.org/10.1016/j.epsl.2010.03.013

Tarduno, J. A., & Cottrell, R. D. (2005). Dipole strength and variation of the time-averaged reversing and nonreversing geodynamo based on Thellier analyses of single plagioclase crystals. *Journal of Geophysical Research*, *110*, B11101. https://doi.org/10.1029/2005JB003970

Tarduno, J. A., Cottrell, R. D., & Smirnov, A. V. (2001). High geomagnetic intensity during the mid-Cretaceous from Thellier analyses of single plagioclase crystals. *Science*, *291*(5509), 1779–1783. https://doi.org/10.1126/science.1057519

Tarduno, J. A., Cottrell, R. D., & Smirnov, A. V. (2002). The Cretaceous superchron geodynamo: Observations near the tangent cylinder. *Proceedings of the National Academy of Sciences of the United States of America*, *99*(22), 14,020–14,025. https://doi.org/10.1073/pnas.222373499

Tauxe, L., Constable, C., Johnson, C. L., Koppers, A. A. P., Miller, W. R., & Staudigel, H. (2003). Paleomagnetism of the southwestern U.S.A. recorded by 0-5 Ma igneous rocks. *Geochemistry, Geophysics, Geosystems*, *4*(4), 8802. https://doi.org/10.1029/2002GC000343

Tauxe, L., & Kent, D. V. (2004). A simplified statistical model for the geomagnetic field and the detection of shallow bias in paleomagnetic inclinations: Was the ancient magnetic field dipolar? In J. Channell, D. Kent, W. Lowrie, & J. Meert (Eds.), *Timescales of the paleomagnetic field*, *Geophysical Monograph Series* (Vol. 145, pp. 101–115). Washington, DC: American Geophysical Union. https://doi.org/10.1029/145GM08

Tauxe, L., & Staudigel, H. (2004). Strength of the geomagnetic field in the Cretaceous Normal Superchron: New data from submarine basaltic glass of the Troodos Ophiolite. *Geochemistry, Geophysics, Geosystems*, *5*, Q02H06. https://doi.org/10.1029/2003GC000635

Van der Voo, R. (1990). The reliability of paleomagnetic data. *Tectonophysics*, *184*(1), 1–9. https://doi.org/10.1016/0040-1951(90)90116-P

van Dongen, P. G., van der Voo, R., & Raven, T. (1967). Paleomagnetism and the alpine tectonics of Evrasia III: Paleomagnetic research in the Central Lebanon Mountains and in the tartous area (Syria). *Tectonophysics*, *4*(1), 35–53. https://doi.org/10.1016/0040-1951(67)90057-1

van Hinsbergen, D. J. J., Straathof, G. B., Kuiper, K. F., Cunningham, W. D., & Wijbrans, J. (2008). No vertical axis rotations during Neogene transpressional orogeny in the NE Gobi Altai: Coinciding Mongolian and Eurasian Early Cretaceous apparent polar wander paths. *Geophysical Journal International*, *173*(1), 105–126. https://doi.org/10.1111/j.1365-246X.2007.03712.x

Vandamme, D. (1994). A new method to determine paleosecular variation. *Physics of the Earth and Planetary Interiors*, *85*(1–2), 131–142. https://doi.org/10.1016/0031-9201(94)90012-4

Veikkolainen, T., Evans, D. A. D., Korhonen, K., & Pesonen, L. J. (2014). On the low-inclination bias of the Precambrian geomagnetic field. *Precambrian Research*, *244*, 23–32. https://doi.org/10.1016/j.precamres.2013.09.004

Veikkolainen, T., & Pesonen, L. J. (2014). Palaeosecular variation, field reversals and the stability of the geodynamo in the Precambrian. *Geophysical Journal International*, *199*(3), 1515–1526. https://doi.org/10.1093/gji/ggu348

Yang, T., Ma, Y., Zhang, S., Bian, W., Yang, Z., Wu, H., et al. (2015). New insights into the India-Asia collision process from Cretaceous paleomagnetic and geochronologic results in the Lhasa terrane. *Gondwana Research*, *28*(2), 625–641. https://doi.org/10.1016/j.gr.2014.06.010

Yi, Z., Huang, B., Yang, L., Tang, X., Yan, Y., Qiao, Q., et al. (2015). A quasi-linear structure of the southern margin of Eurasia prior to the India-Asia collision: First paleomagnetic constraints from Upper Cretaceous volcanic rocks near the western syntaxis of Tibet. *Tectonics*, *34*, 1431–1451. https://doi.org/10.1002/2014TC003571

Zhao, X., Coe, R. S., Zhou, Y., Wu, H., & Wang, J. (1990). New paleomagnetic results from northern China: Collision and suturing with Siberia and Kazakhstan. *Tectonophysics*, *181*(1–4), 43–81. https://doi.org/10.1016/0040-1951(90)90008-V

Zhu, R., Pan, Y., He, H., Qin, H., & Ren, S. (2008). Palaeomagnetism and $^{40}Ar/^{39}Ar$ age from a Cretaceous volcanic sequence, Inner Mongolia, China: Implications for the field variation during the Cretaceous normal superchron. *Physics of the Earth and Planetary Interiors*, *169*(1–4), 59–75. https://doi.org/10.1016/j.pepi.2008.07.025